Design, active sites and performance of unconventional ZrO_2-based catalysts for non-oxidative dehydrogenation of $C_3 – C_4$ alkanes

Dissertation

zur Erlangung des akademischen Grades
Doctor rerum naturalium
(Dr. rer. nat.)

der Matematisch-Naturwissenschaftlichen Fakultät
der Universität Rostock

vorgelegt von

Diplom-Chemikerin Tatiana Otroshchenko

geboren am 09. Juni 1990 in Nikolaew, Ukraine

Rostock 2018

urn:nbn:de:gbv:28-diss2018-0033-0

Gutachter

1. Gutachter:

   PD Dr. habil. Evgenii V. Kondratenko
   Leibniz-Institut für Katalyse e.V. an der Universität Rostock (Deutschland)

2. Gutachter:

   Prof. Bert M. Weckhuysen
   Universität Utrecht (Niederlande)

Tag der Einreichung: 29. September 2017

Tag der mündlichen Prüfung: 30. Januar 2018

Zusammenfassung

Die katalytische nicht-oxidative Dehydrierung (DH) von C_3-C_4-Alkanen gewinnt aufgrund steigender Nachfrage nach den entsprechenden Olefinen zunehmend an Bedeutung. Kommerzielle geträgerte Katalysatoren mit aktiven CrO_x- oder Pt-Sn-Spezies haben jedoch Nachteile, da sie toxisch oder nur begrenzt verfügbar sind. Vor diesem Hintergrund konzentrierte sich die vorliegende Arbeit auf die Entwicklung alternativer DH-Katalysatoren auf Basis von Metalloxiden. Die Hypothese war, dass Gitterdefekte auf der Oberfläche dieser Oxide katalytisch aktive Zentren sein können. Diese Metalloxide zeichnen sich durch den meist unveränderlichen Oxidationszustand des Metalls und ihre Fähigkeit zur Abgaben von Gittersauerstoff aus.

Zur Überprüfung der Hypothese wurden verschiedene kommerziell verfügbare Metalloxide für die Propan-DH getestet. Lanthan dotiertes ZrO_2 wurde als geeigneter Kandidat identifiziert. Um das Potenzial von ZrO_2-basierten Katalysatoren weiter zu untersuchen, wurden die Auswirkungen verschiedener Dotierungen (Li_2O, MgO, CaO, La_2O_3, Sm_2O_3, Y_2O_3 oder CrO_3), die Vorbehandlung der Katalysatoren und die Anwesenheit von geträgerten hydrierungsaktiven Metallen (Ru, Cu, Ni oder Co) auf die Katalysatoraktivität und -selektivität bei der DH von Propan, Isobutan und n-Butan detailliert untersucht. Die Charakterisierung der Katalysatoren durch komplementäre Techniken (XRD, XPS, TEM, Raman-Spektroskopie, NH_3 temperaturprogrammierte Desorption, IR-Spektroskopie und O_2-Titrationsexperimente) zeigte, dass koordinativ ungesättigtes Zirkonium(IV)-Kation (Zr_{cus}) und benachbarter Gittersauerstoff an der Aktivierung der C-H-Bindung in Alkanen beteiligt sind. Die Zr_{cus}-Zentren entstehen, wenn Gittersauerstoff bei reduktiver Katalysatorbehandlung aus ZrO_2 entfernt wird. Die Anwesenheit von hydrierungsaktiven Metallen auf der Oberfläche von ZrO_2 begünstigte die Bildung von Zr_{cus}. Außerdem wurde festgestellt, dass die Dotierung des ZrO_2 einen Einfluss auf die Bildung/Stabilisierung von Zr_{cus} während der reduktiven Behandlung des Katalysators hat. Darüber hinaus beeinflusst die Dotierung die intrinsische Aktivität von Zr_{cus} und hemmt die unerwünschte Koksbildung durch die Verminderung der Anzahl stark saurer Zentren auf der Oberfläche von ZrO_2. Die im Vergleich zu anderen Dotierungen extrem hohe DH-Aktivität der Katalysatoren auf Basis von ZrO_2 und CrO_3 wurde auf einen Synergieeffekt zwischen katalytisch aktiven CrO_x- und Zr_{cus}-Spezies zurückgeführt. Die Aktivität solcher Katalysatoren hängt auch davon ab, ob sich CrO_x in geträgerter Form auf der Oberfläche oder in Kationenpositionen innerhalb des ZrO_2-Gitters befindet.

Die praktische Relevanz neuartiger Katalysatoren auf ZrO_2-Basis für die Propan- und Isobutan-DH wurde unter industrienahen Bedingungen demonstriert. Ihre Aktivitäten, Selektivitäten und Haltbarkeiten sind vergleichbar mit denen industriell relevanter CrO_x- und Pt-basierter Katalysatoren.

Abstract

Catalytic non-oxidative dehydrogenation (DH) of C_3 – C_4 alkanes is of increasing importance due to the growing demand for the corresponding olefins. Commercial catalysts with supported CrO_x or Pt-Sn species have, however, shortcomings of being toxic or limited availability. Against this background, the present thesis was focused on the development of alternative DH catalysts on the basis of metal oxides with usually unchangeable metal oxidation state but with high ability for lattice oxygen removal. The working hypothesis was that catalytically active sites can be lattice defects on the surface of such materials.

On the basis of primary screening of catalytic activity of various commercial metal oxides in propane DH, lanthanum-doped ZrO_2 was identified as a promising candidate. To further explore the potential of ZrO_2-based catalysts, the effects of dopant (Li_2O, MgO, CaO, La_2O_3, Sm_2O_3, Y_2O_3, or CrO_3), catalyst treatment and the presence of supported metal (Ru, Cu, Ni or Co) on catalyst activity and selectivity in DH of propane, isobutane and n-butane were investigated in detail. The characterization of the catalysts by complementary techniques (XRD, XPS, TEM, Raman spectroscopy, NH_3 temperature-programmed desorption, IR spectroscopy and O_2 titration experiments) enabled to conclude that coordinatively unsaturated zirconium (IV) cations (Zr_{cus}) and neighboring lattice oxygen participate in the C-H bond activation in alkanes. Such defect sites are formed when surface lattice oxygen of ZrO_2 is removed during reductive treatment. The presence of hydrogenation-active metal was shown to promote formation of Zr_{cus} sites too. It was also established that different dopants for ZrO_2 have different ability to generate/stabilize Zr_{cus} sites during reductive treatment of the catalyst. Moreover, the dopant has an influence on the intrinsic activity of Zr_{cus} sites and inhibits non-desired coke formation due to reducing concentration of strong acidic sites on the surface of ZrO_2. In comparison with other dopants, the extremely high DH activity of the catalysts on the basis of ZrO_2 and CrO_3 was referred to a synergy effect between two types of active sites, i.e. CrO_x and Zr_{cus}. The performance of such catalysts was also shown to depend on the kind of chromium species, i.e. supported CrO_x versus Cr located in cation positions inside the lattice of ZrO_2.

Practical relevance of novel ZrO_2-based catalysts was demonstrated in propane and isobutane DH under industrially relevant conditions. Their activity, selectivity, and durability were established to be comparable with those of analogues of industrial CrO_x- and Pt-based catalysts.

Eidesstattliche Versicherung

Hiermit versichere ich, Tatiana Otroshchenko, dass ich die vorliegende Dissertation selbständig verfasst habe. Die benutzten Hilfsmittel wurden in der Arbeit aufgeführt.

Die vorliegende Arbeit wurde am Leibniz-Institut für Katalyse e.V. (LIKAT) an der Universität Rostock im Forschungsbereich „Katalysatorenentwicklung und Reaktionstechnik“ (Leiter Dr. David Linke) unter der Betreuung von PD Dr. habil. Evgenii V. Kondratenko (Leiter der Themengruppe „Reaktionsmechanismen“) angefertigt. Die Durchführung der experimentellen Arbeiten fand von Oktober 2014 bis Juli 2017 am LIKAT in Rostock statt.

Danksagung

Herrn PD Dr. habil. Evgenii V. Kondratenko danke ich vielmals für die Möglichkeit zur Durchführung dieser Arbeit, seine Motivation, sein fortwährendes Interesse und seine Unterstützung bei der Erstellung dieser Arbeit sowie die vielen anregenden Diskussionen.

Herrn Dr. David Linke, Leiter des Bereichs „Katalysatorentwicklung und Reaktionstechnik“ am LIKAT, danke ich für die freundliche Aufnahme in den Arbeitskreis.

Weiterhin möchte ich mich bei Dr. Marga-Martina Pohl, Dr. Jörg Radnik und Benjamin Paul für Messungen mittels Transmissionselektronenmikroskopie (TEM), Röntgenphotoemissionsspektroskopie (XPS) und Rasterelektronenmikroskopie (SEM) bedanken. Ich danke vielmals Dr. Vita A. Kondratenko für Messungen im TAP Reaktor, Dr. Matthias Schneider und Dr. Henrik Lund für Messungen mittels Röntgendiffraktometrie (XRD), Dr. Ursula Bentrup und Dr. Nils Rockstroh für Messungen mittels Ramanspektroskopie, Dr. Jacqueline Priebe und Ulrich Marx für Elektronenspinresonanz-Experimente (EPR).

Weiterer Dank gilt meinen Kollegen für ihre großzügige Hilfsbereitschaft und die freundschaftliche Arbeitsatmosphäre. Ich danke vielmals Dr. Stefan Josef Ahlers, Dr. Martin Holena, Dr. Martin Fait, Dr. Mariana Stoyanova, Dr. Uwe Rodemerck, Dr. Sergey Sokolov, Dr. Andrea Malmusi, Dr. Olga Bulavchenko, Matthias Albrecht, Sebastian Smyczek, Andreas Schröder, Martina Marschall, Karin Buchholz, Yaoyuan Zhang, Shanlei Han, Zeynep Aydin und Thanh Nguyen.

Ich möchte mich auch bei dem Deutschen Akademischen Austauschdienst (DAAD) und dem Ministerium für Bildung und Wissenschaft der Russischen Föderation für die finanzielle Unterstützung dieser Arbeit bedanken.

Ein besonderer Dank gilt und wird immer meiner lieben Familie gelten, die fortwährend an mich gedacht und geglaubt hat: meinen Eltern Tatiana Kirienko und Pyotr Otroshchenko, meiner Tante Elena Kirienko, meinen Großmüttern Sinaida Kirienko und Nelya Otroshchenko und meinen Brüdern Nikolay und Ivan Otroshchenko.

Table of Contents

Abbreviations and symbols

ABS	acrylonitrile-butadiene-styrene
AMU	atomic mass unit
BET	Brunauer, Emmett, and Teller
D	catalyst deactivation parameter (%)
DH	dehydrogenation
EPR	electron paramagnetic resonance
ETBE	ethyl tert-butyl ether
FID	flame ionization detector
MS	mass spectrometry
MTBE	methyl tert-butyl ether
MTO	methanol-to-olefin
NP	nanoparticles
ODH	oxidative dehydrogenation
PDH	non-oxidative propane dehydrogenation
STY	space time yield ($kg \cdot h^{-1} \cdot m^{-3}$)
TAP	temporal analysis of products
TCD	thermal conductivity detector
TEM	transmission electron microscopy
TOF	turn over frequency (s^{-1})
TPD	temperature-programmed desorption
TPO	temperature-programmed oxidation
TPR	temperature-programmed reduction
UV-vis	ultra-violet – visible region
XRD	X-ray diffraction
XPS	X-ray photoelectron spectroscopy
c-ZrO_2	cubic phase of ZrO_2
E_a	apparent activation energy ($kJ \cdot mol^{-1}$)
F	single oxygen vacancy with two trapped electrons
F^+	single oxygen vacancy with one trapped electron
F_{feed}	volume flow rate of feed gas ($ml \cdot min^{-1}$)
$F(R_{rel})$	Kubelka-Munk function
H	numbers of moles of hydrogen related to the number of moles of alkane in the feed
ΔH_{298}^0	enthalpy of reaction ($kJ \cdot mol^{-1}$)
HZ	Brønsted acidic site
I	number of moles of inert gas related to the number of moles of alkane in the feed
K_p	equilibrium constant
L^+	Lewis acidic site
$m_{catalyst}$	catalyst amount (g)
$m(C_nH_{2n})$	overall amount of alkene produced within one catalytic cycle over used catalyst amount (g)
$m_g(C_nH_{2n})$	overall amount of alkene produced within one catalytic cycle over 1 g of catalyst ($g \cdot g^{-1}_{catalyst}$)

$m_{m^3}(C_nH_{2n})$	overall amount of alkene produced within one catalytic cycle over 1 m^3 of catalyst ($kg \cdot m^{-3}$)
$M(C_nH_{2n})$	molar weight of alkene ($g \cdot mol^{-1}$)
m-ZrO_2	monoclinic phase of ZrO_2
$\dot{n}_i$	molar flow of gas-phase component ($mol \cdot min^{-1}$)
N_A	Avogadro constant ($N_A = 6.02 \cdot 10^{23}\ mol^{-1}$)
$N(O_{consumed})$	amount of oxygen atoms consumed by 1 g of catalyst during O_2-pulse titration experiment ($atoms \cdot g^{-1}$)
$N(Ru_{surf}\ or\ Cr_{surf})$	amount of surface atoms of Ru or Cr per 1 g of catalyst (g^{-1})
P	total pressure (bar)
$\rho_{catalyst}$	catalyst density ($g \cdot ml^{-1}$)
$r(C_nH_{2n})$	rate of alkene formation ($mol_{CnH2n} \cdot g^{-1}_{catalyst} \cdot min^{-1}$)
R_{rel}	relative reflectance
S	selectivity
S_{BET}	specific surface area ($m^2 \cdot g^{-1}$)
T	temperature (°C)
T_{maxCO2}	temperature of maximum of CO_2 release (°C)
T_{maxH2}	temperature of maximal consumption of hydrogen (°C)
t-ZrO_2	tetragonal phase of ZrO_2
V_m	molar volume ($V_m = 22400\ ml \cdot mol^{-1}$)
X	conversion
Zr_{cus}	coordinatively unsaturated Zr cation
θ	Bragg diffraction angle (°)
λ	wavelength (nm)
v_i	reciprocal stoichiometric coefficient
x_i	molar fraction of product *i*
$\omega(Cr_2O_3)$	weight concentration of Cr_2O_3 (wt. %)

1. Introduction

1.1. Usage of light olefins

Light olefins such as ethylene, propene, n-butenes and isobutylene are important building blocks in the chemical industry.[1] Ethylene is the most demanded petrochemical in the world with an annual production of about 155 million tons in 2015.[2] Approximately 61% of the total amount of manufactured ethylene is consumed for the production of polyethylene used in packaging and textile industry. Other part of ethylene is used for the production of various chemical intermediates such as ethylene oxide, ethylene dichloride and ethylbenzene (see ethylene products chain in Figure A-1 (a) in Appendix).[3]

Propene is the second largest-volume olefin with a global annual production of about 100 million tons.[3] A major part of propene (more than 55%) is used for the production of polypropylene. About 13% of propene is consumed for the manufacture of propylene oxide used as a precursor for the synthesis of polyether polyols and propylene glycol. Other main substances produced from propene are cumene, acrylonitrile and acrylic acid. Cumene is formed by alkylating benzene with propene and is an initial substance for producing acetone and phenol. Acrylonitrile is formed through oxidation of propene in presence of ammonia and used as a main component in the production of acrylic fiber and ABS (acrylonitrile-butadiene-styrene) resins.[4] Acrylic acid finds its application in the manufacturing of polymeric products (see propene products chain in Figure A-1 (b) in Appendix).[5]

Butenes are basically used for the production of 2-butanol, 1,3-butadiene and propene (see n-butenes products chain in Figure A-1 (c) in Appendix). Isobutylene finds its application in the production of methacrolein and methacrylic acid, synthesis of isooctane by dimerization and subsequent hydrogenation, and in the production of MTBE (methyl tert-butyl ether) and ETBE (ethyl tert-butyl ether), which are used as octane enhancers (see isobutylene products chain in Figure A-1 (d) in Appendix).[3, 4]

1.2. Production of light olefins from crude oil

Today, the major amount of light olefins is produced through cracking of various fractions of crude oil. The cracking process implies breaking down long-chain saturated hydrocarbons into

lower hydrocarbons. *Steam cracking (or thermal cracking)* is still the main route for the production of light olefins and currently supplies about 95% of the world's ethylene and 60% of the world's propene.[2] In such process, naphtha feed (fraction of crude oil, which distills below 240°C[6]) is mixed with steam and fed into a tubular reactor located in a furnace. The use of steam is necessary to dilute the heavy feedstock, to increase feed temperature, and to decrease the pressure drop which can be caused by coke formation inside the reactor when operating without steam. The reaction typically occurs at around 850 – 900°C. The residence time of hydrocarbons in the hot reactor zone is shorter than one second. After passing through this zone the non-converted feed and reaction products are quickly cooled down in a transfer line of heat exchanger to inhibit undesired conversion of produced olefins into coke.[7] From a mechanistic viewpoint [8-10], product formation occurs though a free-radical chain mechanism including chain-initiation reactions, propagation reactions and termination reactions (equations (1.1) – (1.5)).

Chain initiation

$$C_nH_{2n+2} \rightarrow C_mH_{2m+1}\cdot + C_kH_{2k+1}\cdot \quad (1.1)$$

Propagation

$$C_mH_{2m+1}\cdot + C_nH_{2n+2} \rightarrow C_mH_{2m+2} + C_nH_{2n+1}\cdot \quad (1.2)$$

$$C_nH_{2n+1}\cdot \rightarrow C_mH_{2m} + C_kH_{2k+1}\cdot \quad (1.3)$$

Termination

$$C_mH_{2m+1}\cdot + C_kH_{2k+1}\cdot \rightarrow C_nH_{2n+2} \quad (1.4)$$

$$C_mH_{2m+1}\cdot + C_kH_{2k+1}\cdot \rightarrow C_mH_{2m} + C_kH_{2k+2} \quad (1.5)$$

Due to the high temperature required for thermal cracking, difficulty in controlling of the selectivity to certain light olefins and low yield of ethylene and propene (approximately 25% and 13%, respectively), much attention has been given to the development of more efficient processes to produce these olefins.[11] Catalytic cracking is an alternative route to produce light olefins at lower temperature and with higher ethylene and propene yields. For example, *fluid catalytic cracking* is performed at about 315 – 650°C over zeolite-based catalysts.[12] It is generally assumed that both Lewis (L^+) and Brønsted (HZ) acidic sites participate in the reaction.[13] On the one hand, Lewis centers are very strong aprotic acidic species with vacant orbitals, which are capable to subtract H^- from alkane molecules converting them into carbenium ions $C_nH_{2n+1}^+$ (equation 1.6). On the other hand, Brønsted centers are strong protic acidic species which either protonate alkane molecules to carbonium ions $C_nH_{2n+3}^+$ (equation 1.7) or directly protolyze C-C bonds in alkanes resulting in the formation of lower alkanes and carbenium ions (equation 1.8). The carbocations obtained undergo processes of chain rearrangement and hydrogen transfer which lead to the formation of desired products.[14-18]

H abstraction	$C_nH_{2n+2} + L^+ \rightarrow C_nH_{2n+1}^+ + HL$	(1.6)
Protonation	$C_nH_{2n+2} + HZ \rightarrow C_nH_{2n+3}^+ + Z^-$	(1.7)
Protolysis	$C_nH_{2n+2} + HZ \rightarrow C_mH_{2m+2} + C_kH_{2k+1}^+ + Z^-$	(1.8)

Ethylene and gasoline are the main products obtained from steam cracking and fluid catalytic cracking, while propene and butenes are produced in significantly lower amounts.[1] Currently, the demand for light olefins, in particular for propene, is evidently increasing but cracking processes cannot completely supply the required amount of these important building blocks of the chemical industry (Figure 1-1). Moreover, several drawbacks of the cracking processes such as consumption of large amount of energy, low selectivity to $C_3 - C_4$ alkenes and production of large amounts of greenhouse gases (CO_2, CH_4) force petrochemical industry to search for alternative technologies for on-purpose production of these alkenes.

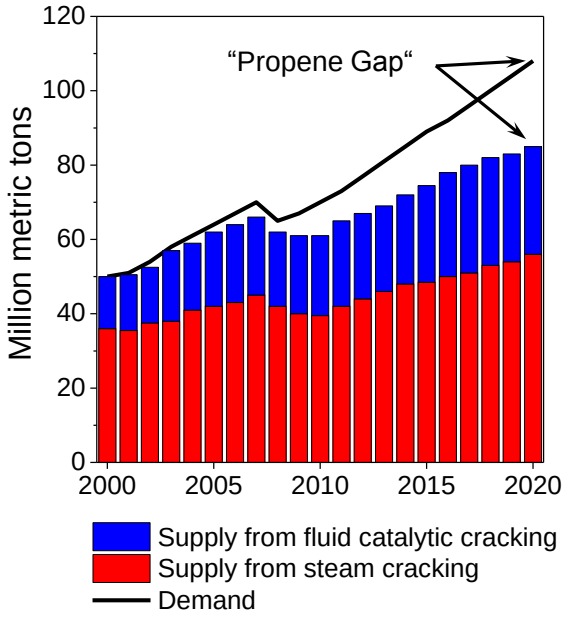

Figure 1-1 Propene supply and demand.[1]

1.3. On-purpose production of light olefins

The most promising technologies for on-purpose production of light olefins are methanol-to-olefins (MTO) and methanol-to-propylene (MTP) processes, metathesis of ethylene with 2-butenes (for propene production), and dehydrogenation of light alkanes.[4] A brief description of each technology is given below.

The *MTO process* developed by UOP and Norsk Hydro (now INEOS) over acidic zeolite catalysts such as SAPO-34 (silicon, aluminum and phosphorous based molecular sieve) is performed in a fluidized-bed reactor at about 340 – 540°C. The small (about 4 Å) pore size of SAPO-34 prevents formation of heavy and/or branched hydrocarbons thus leading to high selectivity to the desired low linear olefins.[19, 20] Since methanol can be easily produced from natural gas and coal, which are more abundant than crude oil, the MTO process is of high interest for the chemical industry.[21] The selectivity to ethylene and propene may exceed 80%. In order to increase the selectivity, the MTO process can be combined with an olefin cracking process (OCP). A schematic illustration of the integrated unit consisting of both MTO process and OCP developed jointly by Total Petrochemicals and UOP is shown in Figure A-2.[20] From a mechanistic point of view, methanol is initially dehydrated to dimethyl ether which then reacts further to form light olefins (equation (1.9)).[22] These two stages occur in the same reactor.

$$2CH_3OH \leftrightarrow CH_3OCH_3 \rightarrow \text{light olefins} \qquad (1.9)$$

The *MTP process* developed by Lurgi operates in parallel fixed-bed reactors at atmospheric or close to atmospheric pressure and in the temperature range of 350 – 500°C.[21] The reaction proceeds according to equation (1.9). It is, however, worth mentioning that the synthesis of dimethyl ether and the formation of olefins occur in different reactors. The process is mainly focused on maximizing propene yield and propene/ethylene ratio using zeolite catalysts (highly siliceous aluminosilicate H-ZSM-5). Apart from propene as a main product, there are some side products, such as ethene, and butenes, which are recycled after propene extraction (see a scheme of the MTP process in Figure A-3).[20]

The *Metathesis of ethylene with 2-butenes* (equation (1.10)) was adapted as a licensed olefins conversion technology (OCT) by ABB Lummus Global, Houston (USA) for the production of propene.[23] This process, known as the Phillips triolefin process, was originally developed by Phillips Petroleum Co. (USA), and operated from 1966 to 1972 in the reverse direction, i.e. for the conversion of propene into ethylene and butene due to lower propene demand at that time. Nowadays, propene demand is much higher, so that, the metathesis of 2-butene and ethylene is used for on-purpose propene production.

$$CH_2{=}CH_2 + CH_3CH{=}CHCH_3 \rightarrow 2CH_3CH{=}CH_2 \qquad (1.10)$$

Three main types of heterogeneous catalysts are now commercially available: tungsten oxide supported on silica (WO_x/SiO_2), molybdenum oxide supported on alumina (MoO_x/Al_2O_3) and rhenium oxide supported on alumina (ReO_x/Al_2O_3). [24-26] The WO_x/SiO_2 system is the most common in industry due to its low cost and high poison resistance. The reaction over WO_x/SiO_2 catalyst is performed at 300 – 550°C. Generally, it is assumed that the key stage of the reaction involves the formation of W-carbenes from surface WO_x-species. The carbenes react further with olefin molecule to form a metallacyclobutane. The latter yields a new olefin and a new metallocarbene (Figure 1-2).[25-27] The proposed mechanism is also valid for MoO_x- and ReO_x-based catalysts.

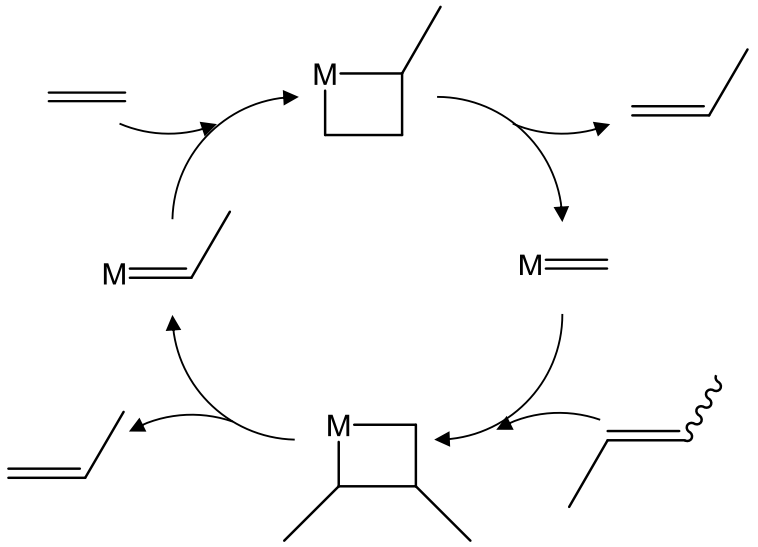

Figure 1-2 Mechanism for the metathesis of ethylene with 2-butenes proposed by Hérisson and Chauvin.[27]

Dehydrogenation of light alkanes proceeds through either oxidative or non-oxidative routes. The latter approach will be discussed in a separate chapter (section 1.4) in detail because it was the topic of the present work. The below discussion is devoted to the oxidative dehydrogenation (ODH) of alkanes. This reaction takes place in the presence of an oxidizing agent such as molecular oxygen. The corresponding alkenes and water are the reaction products (equation (1.11)).[28]

$$C_nH_{2n+2} + ½O_2 \rightarrow C_nH_{2n} + H_2O \qquad \Delta H^0 < 0 \qquad (1.11)$$

ODH is an attractive process in terms of thermodynamics since the reaction is exothermic and can be carried out at low temperatures. Moreover, the risk of catalyst deactivation through

coke formation is also minimized. However, ODH is not currently used as an industrial method because the selectivity to the desired products is quite low. This is due to the fact that the olefins formed are more reactive than the corresponding alkanes and can participate in further oxidation reactions which are thermodynamically favored.[29, 30] The most active and selective oxidative dehydrogenation catalysts described in literature contain reducible transition metal oxides (V_2O_5, MoO_3, Cr_2O_3, NiO), alkali and alkaline earth ions and oxides (CaO, MgO, Li^+/MgO), rare earth metal oxides (CeO_2/CeF_3, Sm_2O_3/CeF_3, Nd_2O_3/CeF_3, Y_2O_3/CeF_3), or noble metals (Pt, Pd).[31, 32] The reaction mechanism of ODH depends on the type of the catalyst. According to [32], the main stages of ODH can be summarized as follows.

1. Weak/physical adsorption of alkane on catalyst surface.
2. Breaking the C–H bond with the formation of the alkyl species.
3. Reaction of the alkyl species with oxygen and formation of alkene.
4. Catalyst cyclic reduction/reoxidation.

It was found that the ODH reaction over catalysts on the basis of oxides of reducible metals (Ce, Co, Cr, Cu, Fe, Mo, Ni, ,Ti, V, W, etc.) proceeds though a Mars-van Krevelen mechanistic scheme [33, 34] According to this mechanism, oxygen for the reaction comes from the lattice of the oxide catalyst. The reduced catalyst is then reoxidized by gaseous oxygen.[29, 32] Thus, according to [29], propane ODH over such metal oxides (MO_x) can be described by a sequence of overall reaction pathways shown in equations (1.12) – (1.16).

C_3H_8 adsorption	$C_3H_8 + O^* \rightarrow C_3H_8O^*$	(1.12)
C-H cleavage	$C_3H_8O^* + O^* \rightarrow C_3H_7O^* + HO^*$	(1.13)
C_3H_6 desorption	$C_3H_7O^* \rightarrow C_3H_6 + HO^*$	(1.14)
Recombination of OH groups	$HO^* + HO^* \rightarrow H_2O + O^* + *$	(1.15)
Reoxidation of the catalyst	$O_2 + * + * \rightarrow O^* + O^*$	(1.16)

Here, O* represents lattice oxygen of MO_x, OH* is a hydroxyl group formed on the surface of metal oxide (M-O-H), $C_3H_7O^*$ is an adsorbed propoxide bonded to M (M-O-C_3H_7), and * is a surface oxygen vacancy associated with metal cation.

1.4. Non-oxidative catalytic dehydrogenation of light alkanes

1.4.1. Thermodynamics of non-oxidative propane dehydrogenation

Non-oxidative catalytic dehydrogenation (DH) of light alkanes for the production of corresponding olefins has been in use since the late 1930s. During World War II, the main interest was devoted to the dehydrogenation of butanes to butenes, which were then dimerized to octenes and hydrogenated to octanes to yield high-octane aviation fuel.[35, 36] Nowadays, the dehydrogenation of propane and isobutane has become more important.[37] Non-oxidative catalytic dehydrogenation is a thermodynamically limited reaction resulting in the formation of alkene and hydrogen from the corresponding alkane (equation (1.17)).[4]

$$C_nH_{2n+2} \rightarrow C_nH_{2n} + H_2 \quad (1.17)$$

The process is endothermic and, in accordance with the Le Chatelier's principle, requires relatively high temperatures (550 – 750°C) and low partial pressure of alkane to achieve high alkane conversion and alkene yield. Accoring to Ref. [38], the equilibrium conversion can be easily calculated from equation (1.18) if the reaction feed consists of alkane only. In the presence of any diluting agent (e.g inert gas or co-fed hydrogen) this equation is transformed into equation (1.19) [39]. A detailed derivation of the latter formula is given in Appendix (equations (A.1) – (A.11)).

$$K_p = \frac{X^2 \times P}{1 - X^2} \quad (1.18)$$

$$K_p = \frac{X \times P \times (X + H)}{(1 - X) \times (1 + X + I + H)} \quad (1.19),$$

where X is the equilibrium conversion, P is the total pressure and K_p is the equilibrium constant. I and H stand for the number of moles of inert gas and hydrogen in the feed related to the number of moles of alkane in the feed, respectively.

The enthalpy required for dehydrogenation of alkanes decreases with increasing the length of alkane chain (ΔH^0_{298} = 137.0 kJ·mol^{-1} for C_2H_6, 124.3 kJ·mol^{-1} for C_3H_8, and 117.6 kJ·mol^{-1} for iso-C_4H_{10}). Thus, an equilibrium conversion of 50% is achieved for lighter alkanes at higher temperatures (Figure 1-3 (a)).[37] Increasing the pressure leads to a rise in the temperature required to reach this conversion level (Figure 1-3 (b)).

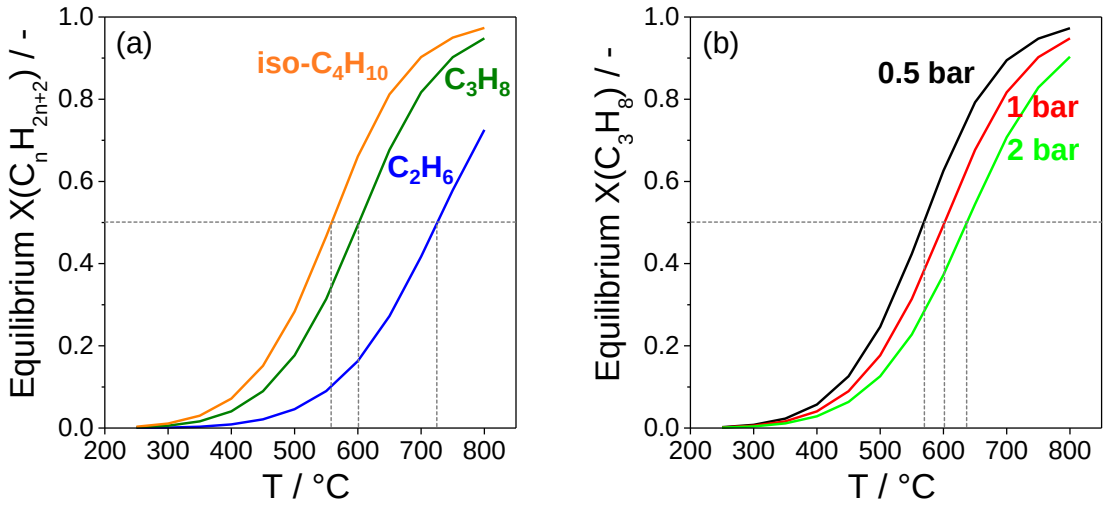

Figure 1-3 (a) Equilibrium conversion of C_2H_6, C_3H_8, iso-C_4H_{10} to the corresponding olefins as a function of temperature at 1 bar of each gas; (b) influence of C_3H_8 partial pressure on the equilibrium conversion. Calculations were made based on the thermodynamic data (see equations (A.12) – (A.15) and Table A-1 in Appendix).

Generally, the C-H bonds of alkanes and olefins are more reactive than the C-C bonds. However, as olefins are considerably more reactive than the corresponding alkanes, they can further participate in undesired secondary reactions such as hydrogenolysis (the addition of hydrogen into a C-C bond of hydrocarbon with the formation of two smaller hydrocarbon molecules), cracking, isomerization and coke formation.[4, 40] Moreover, high temperatures used for alkane dehydrogenation promote formation of coke causing catalyst deactivation.

In order to perform alkane dehydrogenation in industry at high levels of olefin yield, several technologies for dehydrogenation of light alkanes were developed. They are Oleflex (UOP) and STAR (Krupp-Uhde), which use Pt-based catalysts, and Catofin (Lummus) and Snamprogetti/Yarsintez, which utilize CrO_x-based catalysts. Among all the technologies, the most used and well-known processes are Oleflex and Catofin.[4, 40] These processes are described in sections 1.4.2 and 1.4.3, respectively.

1.4.2. Oleflex process

The Oleflex process of UOP was firstly introduced for propane and isobutane dehydrogenation in Thailand in 1990.[41] Nowadays, an annual production of light olefins by the Oleflex process is over 12 million metric tons.[42] The applied technology consists of three sections: reactor section, catalyst regeneration section (continuous catalyst regeneration (CCR)

unit) and product recovery section.[36] Figure 1-4 shows a scheme of the Oleflex process, and the main characteristics of the process are summarized in Table A-2 in Appendix. The reactor section consists of several adiabatic radial-flow (moving bed) reactors connected in a series and preheaters located between the reactors. The alkane dehydrogenation reaction is performed at temperatures between 525 and 705°C and pressures of 1 – 3 bars. The catalyst slowly moves through the reactors from top to bottom, while the reaction mixture flows through the reactors radially from inside to the outside. The transport of the catalyst from one reactor to the next one and to the CCR is ensured by a lock hopper system and transfer lines. Hydrogen used as the lift gas for catalyst transfer has an additional function to reduce coke deposits on the catalyst. After the catalyst passes the last reactor, it goes to the CCR unit. Nitrogen is used as the lift gas for the catalyst transfer. In the CCR, coke deposits are burned off from the catalyst surface with air, while the active component (platinum) is redispersed on the support material by treating the catalyst with a chlorine-air mixture. Then the catalyst is pre-reduced with hydrogen and transferred back to the reactors.[4, 43] The total circulation time of the catalyst through the reactor–regenerator loop is 5 – 10 days. Separation of the products occurs in product recovery section. Outlet gas mixture is cooled down, compressed and dried. Hydrogen is separated from hydrocarbons cryogenically. Then, hydrocarbon feed goes through hydrogenation unit to remove diolefins and athetilenes, then through de-ethanizer and propane-propene splitter.[40]

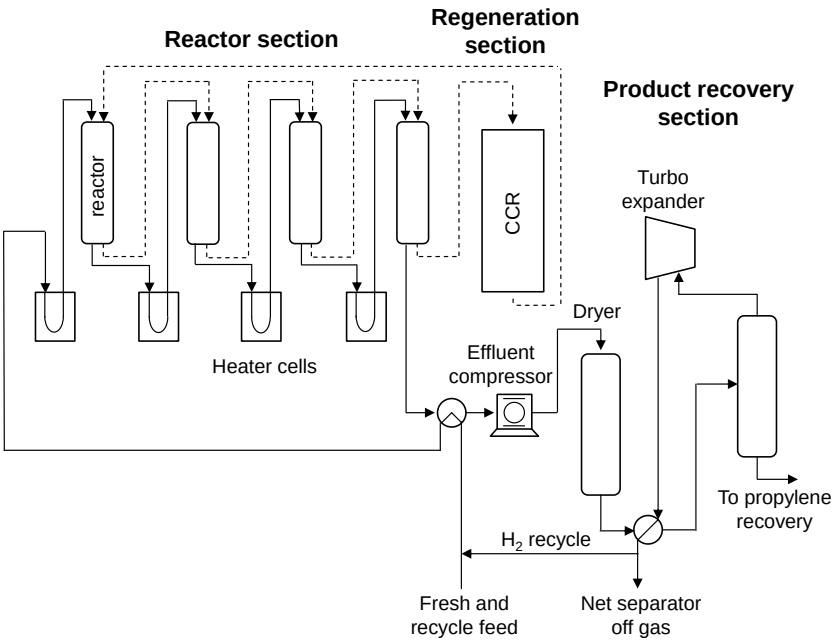

Figure 1-4 Schematic illustration of Oleflex dehydrogenation unit.[36]

Catalysts used in the Oleflex process contain platinum as an active component supported on a thermally stable support such as alumina.[43] The use of platinum is caused by its great ability for the activating C-H bonds and low activity for the cleavage of C-C bonds.[44] Earlier generation catalysts (catalysts DeH-6, DeH-8) possessed 0.75 wt.% of platinum and had a lifetime of about 1 year, while those of newer generation (e.g. DeH-14) possess only 0.45 wt.% of platinum and demonstrate an improved lifetime of about 3 years.[43] Typically besides Pt the catalysts contain up to 1.5 wt.% of Sn.

The reaction mechanism of propane dehydrogenation catalyzed by Pt-based catalysts can be described by equations (1.20) – (1.24) (Pt means Pt-site).[45]

Adsorption of propane	$C_3H_8 + Pt \rightarrow C_3H_8Pt$	(1.20)
First C-H activation	$C_3H_8Pt + Pt \rightarrow C_3H_7Pt + HPt$	(1.21)
Second C-H activation	$C_3H_7Pt + Pt \rightarrow C_3H_6Pt + HPt$	(1.22)
Desorption of propene	$C_3H_6Pt \rightarrow C_3H_6 + Pt$	(1.23)
Desorption of hydrogen	$2HPt \rightarrow H_2 + 2Pt$	(1.24)

Propane molecule is firstly physisorbed on platinum surface and then surface reactions of first and second activation of C-H bond take place. Final stage is desorption of propene and hydrogen. Besides the desired dehydrogenation reaction, some other side reactions such as formation of coke, isomerization (in case of dehydrogenation of C_4 alkanes) and hydrogenolysis may take place on platinum and acidic sites of the support (Figure 1-5).[36] To increase the selectivity to the dehydrogenation products, the catalyst should be modified with proper additives. Thus, some additives such as Sn, Zn, In and Ga are used in order to prevent formation of large Pt ensembles.[46-49] Since side reactions, which can occur over Pt sites, are structure-sensitive and catalyzed by large Pt ensembles, increasing dispersion of platinum results in inhibiting such reactions. Moreover, the dehydrogenation reaction is believed to be structure-insensitive, i.e. all platinum sites catalyze the cleavage of C-H bond. Since large Pt ensembles are not required for alkane dehydrogenation, and only amount of available active species is important, increasing dispersion of platinum also leads to an increase in catalyst dehydrogenation activity. Therefore, modified Pt-based catalysts demonstrate higher selectivity towards desired products as well as higher activity compared to unmodified counterparts.[50]

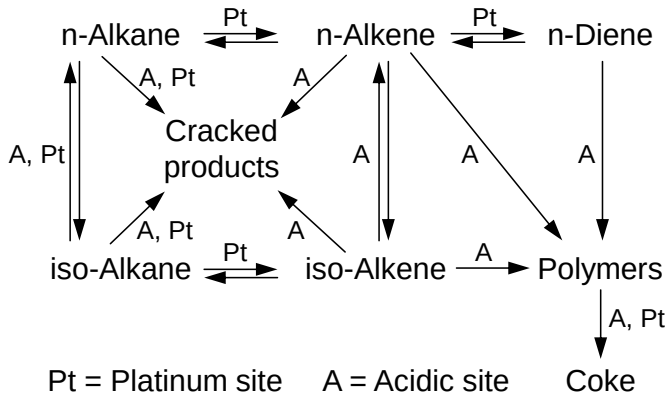

Figure 1-5 Reactions catalyzed by platinum and acidic sites which can happen during light alkane dehydrogenation over Pt-based unmodified catalysts.[36]

Tin is considered to be one of the most efficient promoters for Pt-based catalysts. It is assumed that the presence of Sn leads to both geometric and electronic effects on Pt propertries. Due to the geometric effect the size of platinum ensembles decreases. On the other hand, modification of catalytic properties of platinum by electronic effect implies that electrons from metallic Sn or Sn^{2+} species might transfer to the 5d band of platinum resulting in a decrease of the interaction of hydrocarbons with platinum, thus lowering the contribution of hydrogenolysis and coke formation.[4, 51] This leads to a change in the heat of adsorption of hydrocarbons participating in the reaction. Another important role of tin is promoting migration of coke from Pt species to the support resulting in increase in catalyst stability.[52] Moreover, tin decreases support acidity and thus suppresses side reactions catalyzed by acidic sites (skeletal isomerization, cracking, polymerization, and coke formation).

1.4.3. Catofin process

The Catofin dehydrogenation process technology is currently owned by Süd-Chemie and is offered for license by ABB Lummus.[35] The process uses an adiabatic fixed-bed reactor system consisting of 5 – 8 reactors operating in alternating modes. Besides of the catalyst, inert materials, such as, alumina or silica balls are located in the reactors below and above the catalyst bed to fix the catalyst and to fill up the reactors.[36] Figure 1-6 shows schematic illustration of the Catofin process, and Table A-2 in Appendix summarizes the main characteristics of the process.

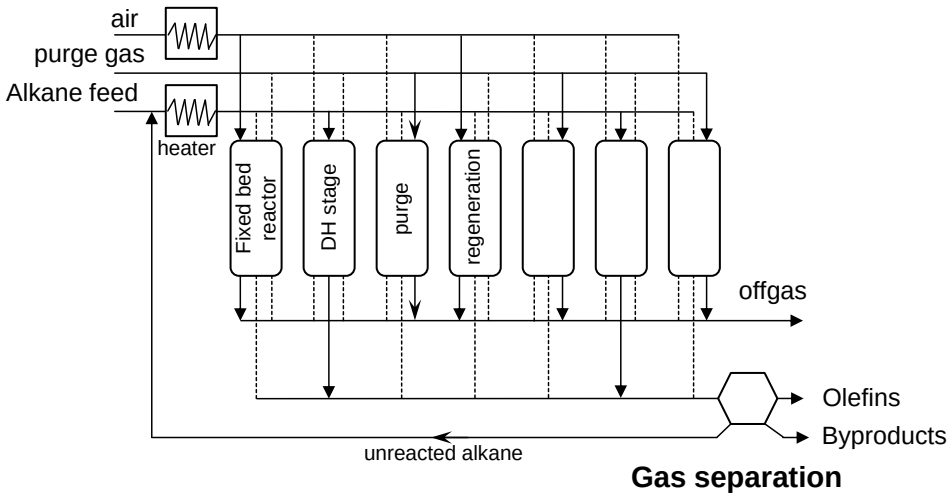

Figure 1-6 Schematic illustration of Catofin dehydrogenation unit.[40]

The reactors undergo cyclic operation where dehydrogenation, regeneration and purge stages alternate. The reactor operation modes are automatically switched. While some reactors perform dehydrogenation stage, other reactors are in regeneration (coke burning) or in a purge modes, so that, a constant flow of reaction products can be achieved. Part of the heat generated during regeneration of the spent catalyst due to burning of coke is used for the dehydrogenation reaction. The dehydrogenation stage operates at low pressure (0.2 – 0.5 bar) in order to shift reaction equilibrium to reaction products and to achieve higher alkane conversion according to the Le Chatelier's principle. The reaction is performed at about 575°C. The total duration of one cycle consisting of DH stage, purge, regeneration, and again purge is limited by the amount of heat available and usually does not exceed 30 min. [36, 40, 43]

The dehydrogenation reaction in the Catofin process is carried out over chromia-based catalysts with a lifetime of about 2 – 3 years.[36] The industrial catalysts mostly consist of 10 – 20 wt.% of chromium oxide supported on the surface of alumina doped with potassium (up to 2 wt.%) as a promoter.[37, 43, 53] Despite of thorough studies of such catalysts, there are still a lot of discussions about the nature of active sites and their contribution to the total catalytic activity. Different authors suggest the presence of a number of chromium-containing sites on the surface of freshly-prepared catalyst. They are amorphous and crystalline Cr_2O_3 clusters, isolated Cr^{3+} and Cr^{5+} species, water soluble Cr^{6+} and grafted Cr^{6+} species chemically bonded with alumina in form of mono- and poly- chromates, aluminum-chromium-chromate (Cr^{6+}) species coupled with Cr_2O_3 clusters.[37, 53-56] Fridman et al.[53] postulated that the fresh catalyst undergoes complete

surface restructuring of unstable chromium species under dehydrogenation conditions. Thus, isolated aluminum-chromate species disappear, and total amount of Cr^{6+} species decreases during initial stages of dehydrogenation process due to the transformation of Cr^{6+} into Cr^{3+} species. Weakly bonded small (less than 300Å) amorphous Cr_2O_3 clusters agglomerate forming relatively stable Cr_2O_3 clusters of larger size. Crystalline Cr_2O_3 clusters were found to be the most stable species. Some authors consider that reduction of CrO_x/Al_2O_3 catalyst leads to the formation of Cr^{2+} species which are active in dehydrogenation reaction. However, there is still no direct evidence of this theory.[57, 58] Nowadays, most authors believe that coordinatively unsaturated Cr^{3+} sites are active in alkane dehydrogenation.[40, 59] Neighboring O^{2-} ions are considered to be involved in the reaction as well.[60] The possible route of dehydrogenation may proceed through the dissociation of the alkane molecule into an alkyl group bonded to surface Cr^{3+} site and a hydrogen atom bonded to surface O^{2-} site, as shown in Figure 1-7. The surface reaction of the adsorbed alkane, i.e. the cleavage of the C-H bond, is generally viewed as the rate-determining step in the dehydrogenation of propane; while for dehydrogenation of isobutane, the adsorption of the alkane is the rate-determining step.[43]

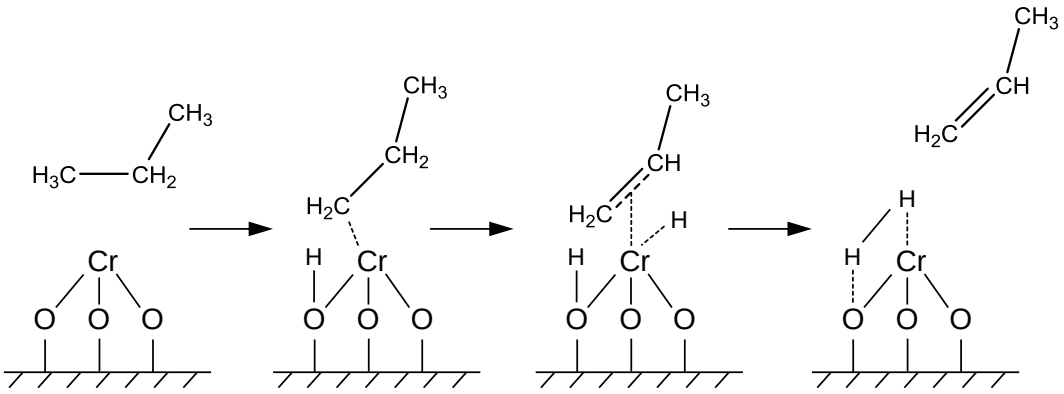

Figure 1-7 Possible pathway of non-oxidative dehydrogenation of propane over CrO_x-based catalysts.[40]

The presence of potassium as a promoter in chromia-based catalyst not only suppresses undesired side reactions by reducing acidity of support but also strongly influences catalytic properties of chromia active species. Thus, potassium forms potassium chromate and potassium dichromate, i.e. Cr(VI) complexes during oxidation treatment of the catalyst. Such complexes decompose with a formation of highly dispersed active Cr^{3+} sites under reductive conditions.[43]

1.4.4. Alternative catalysts for non-oxidative dehydrogenation of light alkanes

Despite the great performance of Pt- and CrO_x-based catalysts in dehydrogenation of light alkanes to olefins, a number of challenges, including complexity of regeneration stage and high cost of platinum, as well as environmental issues associated with chromium, have incited to search for alternatives.[4] The most promising alternative catalysts developed up to now are those containing supported metal oxides such as VO_x, GaO_x, MoO_x, etc.[40, 61-63] Reaction mechanism of dehydrogenation of light alkanes over such catalysts is similar to that proposed for chromia-based catalysts and involves participation of coordinatively unsaturated metal cations and surface oxygen atoms.[64-71]

Among the above mentioned alternative catalysts, VO_x-based systems are considered to be the most attractive because of their high activity and stable performance upon regeneration.[66] For example, Sokolov et al.[64] established that VO_x/MCM-41 catalyst was active and selective in propane dehydrogenation at 550°C and performed superior to CrO_x- and PtSn-based analogues of industrial catalysts in terms of durability in a series of dehydrogenation-regeneration cycles. Moreover, it was demonstrated that VO_x-based catalyst did not require reductive activation before catalytic reaction. Additionally, VO_x-based catalysts have lower price than Pt-based catalysts, and are less hazardous to environment than Cr-based catalysts, so that, such catalysts may be considered as great alternatives to industrial ones.[72]

It is generally accepted that VO_x-based catalysts contain vanadium ions of different oxidation stage. Nowadays, the contribution of each V site in total activity of the catalyst is not completely clear. Liu et al.[66] suggested that V^{3+}, V^{4+} and V^{5+} species exhibit different activity for propane dehydrogenation, and the V^{3+} ions are more active than V^{5+} and V^{4+} ions. Similar, Tian et al.[73] concluded that both V^{3+} and V^{4+} are active in isobutane dehydrogenation, with the former being more active. On contrary, according to Harlin et al.[65], the activity of V^{4+} species in dehydrogenation of iso- and n-butanes is higher than that of V^{3+} species.

Ga_2O_3-based catalysts also seem to be promising for dehydrogenation reaction. The first reports about high dehydrogenation activity of supported gallium oxide appeared in the late 1980s.[4] The catalysts demonstrate high activity and selectivity but low on-stream stability due to the formation of carbon deposits on catalytically active sites. In order to increase catalyst stability, CO_2 is often added to the alkane-containing feed.[69, 74] The presence of CO_2 was

reported to induce removal of surface aggregated carbon (suppressing coke formation) via the Boudouard reaction (equation 1.25). Moreover, the formation of the dehydrogenation products in a presence of CO_2 is accelerated by removal of H_2 through a reverse water-gas-shift reaction (equation 1.26).[69, 74]

$$CO_2 + C \rightarrow 2CO \quad (1.25)$$

$$CO_2 + H_2 \rightarrow CO + H_2O \quad (1.26)$$

Recently, Sattler et al. reported about a new family of Ga_2O_3-based catalysts containing minute amounts of Pt.[70] The authors assumed that in such catalysts coordinately unsaturated Ga^{3+} sites are active species and platinum is a promoter. So designed catalysts demonstrated high activity and selectivity in propane dehydrogenation and were shown to be highly resistant to coking.

With regard to MoO_x-based catalysts, the non-oxidative dehydrogenation of alkanes has been studied scarcely. In general, MoO_x-based catalysts demonstrate relatively low conversion and selectivity.[40] Moreover, such catalysts sinter rapidly compared to other dehydrogenation catalysts. That leads to their fast deactivation.[4]

2. Objectives and strategy of this thesis

2.1. Objectives

As demonstrated in the above literature overview, catalysts with supported Pt and CrO_x are applied for large-scale production of propene and isobutylene through non-oxidative dehydrogenation of the corresponding alkanes. The catalysts, however, faces challenge, which are high cost of platinum as well as toxicity of chromium (VI) compounds. Despite numerous attempts, only a limited progress has been achieved in the development of catalysts free of Pt and CrO_x. Moreover, industrial as well as most of alternative catalysts are materials with supported catalytically active metal or metal oxide species. The properties of such catalysts are largely determined by the fine structure of active supported species and their interaction with the support. However, there are often no straightforward methods to synthesize specific supported structures where atoms would be arranged in a predetermined way. Even when such structures were prepared, they were found to alter under severe reaction conditions thus resulting in a change of the catalyst performance.

To address the above challenges, this thesis elucidated the potential of metal oxides in which the dehydrogenation function is reserved to surface lattice defects such as coordinatively unsaturated (cus) metal cations. The idea behind such concept is that metal oxides with usually unchangeable metal oxidation state but with high oxygen mobility can form such defects upon removal of lattice oxygen. The specific scientific aims were:

I. to verify this concept experimentally through determining propane DH activity of metal oxides differing in their oxygen mobility. ZrO_2-based materials with relatively weak metal-oxygen bond are to be studied in detail.

II. to identify the nature of active sites in ZrO_2-based unconventional catalysts and to determine factors affecting their formation. To this end, doped and undoped materials additionally possessing tiny amounts of supported metals are to be synthesized and characterized by complementary *ex situ* and *in situ* techniques as well as tested for their activity for alkane DH.

III. to elucidate reaction pathways leading to selective and non-selective products and to identify catalyst physico-chemical properties influencing these routes.

IV. to investigate if there is a synergy effect between two types (CrO_x and Zr_{cus}) of active sites in bulk binary $CrZrO_x$ or supported $CrO_x/LaZrO_x$ catalysts in terms of their DH activity.

The final objective of this thesis was to demonstrate practical relevance of ZrO_2-based catalysts. For this purpose, several Cr-free and Cr-containing ZrO_2-based catalysts are to be tested in a series of cycles consisting of propane or isobutane DH and oxidative regeneration stages. Their activity, selectivity, and durability are to be compared with those of analogues of CrO_x- and Pt-Sn-based industrial catalysts. Additionally, effect of hydrogen co-feeding on selectivity and catalyst stability in propane DH is to be studied.

2.2. Strategy and outline

The strategy for achieving the above objectives is introduced below. In **Section 4.1**, the feasibility of a new concept for designing alkane dehydrogenation catalysts was investigated. To this end, several metal oxides differing in their oxygen mobility were chosen for determining their activity in propane dehydrogenation. The most active $LaZrO_x$-containing samples were further tested to investigate the effect of the presence of supported noble metal and the kind of treatment conditions on catalyst performance.

Section 4.2 deals with identification of active sites in ZrO_2-based catalysts. To confirm that coordinatively unsaturated zirconium (Zr_{cus}) cations and neighboring O^{2-} are responsible for the high activity of ZrO_2-based catalysts, propane dehydrogenation in the presence and the absence of probe molecules such as O_2, H_2O and CO_2 were investigated. Such molecules react with either Zr_{cus} sites or O^{2-} anions. If a Zr_{cus}-O^{2-} couple is really responsible for activating and breaking the C-H bond in alkane molecules, the presence of O_2, H_2O or CO_2 in the reaction mixture should lead to a decrease in catalyst activity. Such negative effect was actually observed in the experiments. *In situ* UV-vis and O_2-pulse titration experiments were also used to detect formation of Zr_{cus} sites during reductive treatment and to quantify such sites, respectively. The effect of reduction temperature and the presence of supported hydrogenation-active metal on the formation of Zr_{cus} sites is discussed.

In **Section 4.3**, the influence of metal (Li, Mg, Ca, Sm, La or Y) oxide dopant on catalyst activity and selectivity in dehydrogenation of propane, n-butane and isobutane was investigated. To this end, a series of doped ZrO_2-based materials as well as bare ZrO_2 were synthesized,

characterized and tested in the dehydrogenation reactions. Activation energy of olefin formation was determined for each catalyst in order to prove that dopant does affect intrinsic activity of Zr_{cus} sites. O_2-pulse titration experiments were instrumental for determining the number of Zr_{cus} sites created upon catalyst reductive treatment. NH_3-TPD experiments were performed in order to compare acidic properties of the catalysts. Analysis of the dependences of product selectivity on alkane conversion obtained from catalytic tests at different contact times was made to derive reaction pathways leading to selective and non-selective products.

The potential of CrO_x-containing ZrO_2-based catalysts was elucidated in **Section 4.4**. For this purpose, several bulk $CrZrO_x$ and supported $CrO_x/LaZrO_x$ catalysts were synthesized, characterized with XRD, BET, XPS, TPR and NH_3-TPD, and tested in propane dehydrogenation. A synergy effect between two types of active sites (Cr and Zr_{cus}) in the samples is discussed. Selectivity-conversion dependences were used for identifying reaction pathways.

Finally, **Section 4.5** is focused on practical relevance of ZrO_2-based catalysts for propane and isobutane dehydrogenation. Catalyst stability and durability were demonstrated in a series of DH and oxidative regeneration cycles under industrially relevant conditions. The effect of hydrogen presence on catalyst performance is discussed. *In situ* UV-vis spectroscopy was instrumental for monitoring formation of carbon deposits on catalyst surface during DH stage and removal of such deposits during regeneration stage. TPO of deactivated catalysts was used to quantify carbon deposits.

The main results and relationships established in the current work are summarized in the **Conclusions**. A possible direction for the further studies is suggested in **Outlook**.

3. Experimental part

3.1. Catalyst preparation methods

3.1.1. Supported catalysts

Catalysts with supported Pt, Rh or Ru nanoparticles

$H_2PtCl_6 \cdot nH_2O$ (37.5 wt.% Pt, Aldrich), $RuCl_3 \cdot nH_2O$ (37.2 wt.% Ru, Merck), $RhCl_3 \cdot nH_2O$ (37.4 wt.% Rh, Aldrich), ethylene glycol (99.8%, Aldrich), NaOH (99%, Merck), acetone (>99%, Roth), toluene (99.99%, Acros), methanol (99.8%, Acros) and commercial supports (SiO_2, (Alfa Aesar), Al_2O_3 (Saint-Gobain NorPro), Siral 10 (10 wt.% SiO_2 in Al_2O_3, Sasol), Siral 40 (40 wt.% SiO_2 in Al_2O_3, Sasol), $LaZrO_x$ (ZrO_2 with 10 wt.% La_2O_3, MelChemicals) and $YZrO_x$ (ZrO_2 with 8 wt.% Y_2O_3, MelChemicals) were used for catalyst preparation. To synthesize nanoparticles (NP) of the above mentioned metals, the corresponding metal precursors were dissolved in ethylene glycol to obtain a metal concentration of about 0.04 $mol \cdot l^{-1}$. Then, a solution of 0.5M NaOH in ethylene glycol was added to the metal-containing solution under stirring and continuous Ar flow to attain pH of 12. The final solution was heated up to 150°C under stirring in Ar atmosphere, kept under such conditions for 3 hours and then cooled down to room temperature. Before deposition of so formed metal NP on supports, the following procedure was performed to reduce the amount of ethylene glycol. Firstly, 2 ml of acetone were added to the required volume of NP solution and thoroughly mixed for about 10 seconds. Toluene (10 ml) was then quickly added to the solution resulting in two phases. The NP-containing ethylene glycol phase was collected. The procedure was repeated several times until viscous solution of NP was obtained. Then, it was diluted with methanol (25 ml) and added to 10 g of the support suspended in 100 ml of methanol. The suspension was stirred at room temperature for 18 hours then centrifuged and dried at 50°C for 60 hours.

Cu-supported catalyst

$Cu(NO_3)_2 \cdot 3H_2O$ (99%, Acros), HNO_3 (65%, Roth), $CO(NH_2)_2$ (>99%, Roth) and $LaZrO_x$ (ZrO_2 doped with 10 wt.% La_2O_3, MelChemicals) were used for catalyst preparation. The required amount of copper nitrate was dissolved in deionized water to obtain Cu^{2+} concentration of about 0.01 $mol \cdot l^{-1}$. Hereafter, the obtained solution was added to the suspension of 5 g of $LaZrO_x$ in 10 ml of water. The final mixture was heated up to 85°C. An aqueous solution of urea

(urea/Cu^{2+} molar ratio = 4/1) was added to the suspension dropwise under stirring. A little amount (5 – 10 drops) of HNO_3 was added dropwise until pH decreased to 2. The mixture was heated up to 90°C and stirred for 18 hours at this temperature until pH became 5 – 6. The suspension was filtrated, washed with deionized water, dried at 120°C overnight and calcined at 550°C for 4 hours. The nominal concentration of Cu in the sample was 0.05 wt.%. The sample was denoted as Cu/$LaZrO_x$.

Ni-, Co-, Ag-, and Ru-supported catalysts

$Ni(NO_3)_2 \cdot 6H_2O$ (99%, Merck), $Co(NO_3)_2 \cdot 6H_2O$ (99%, Merck), $AgNO_3$ (99%, Fluka), $RuCl_3 \cdot nH_2O$ (37.2 wt.% Ru, Merck), $LaZrO_x$ (ZrO_2 doped with 10 wt.% La_2O_3, MelChemicals), and $YZrO_x$_NorPro (ZrO_2 with ~ 10 wt.% Y_2O_3, NorPro) were used as initial substances. Nickel, cobalt or silver nitrates were dissolved in a certain amount of deionized water which can be fully absorbed by the used amount of $LaZrO_x$ (about 0.9 g of water per 1 g of $LaZrO_x$). The support was then impregnated with the obtained solutions. The samples were dried at 110°C overnight and calcined at 550°C for 4 hours. The samples were denoted as Ni/$LaZrO_x$, Co/$LaZrO_x$ and Ag/$LaZrO_x$. The nominal concentration of supported metal was set to 0.05 wt.% for Ni- and Co-containing catalysts and 0.2 wt.% for Ag-containing catalyst.

The same procedure was used to prepare Ru-supported samples denoted as 0.05Ru(imp.)/$LaZrO_x$, 0.005Ru(imp.)/$YZrO_x$_NorPro, and 0.05Ru(imp.)/$YZrO_x$_NorPro with the numbers standing for the nominal weight concentration (in %) of Ru. Per each gram of $YZrO_x$_NorPro 1 gram of liquid was used for impregnation.

$Cr_2O_3/LaZrO_x$ and Cr_2O_3/Al_2O_3

$Cr(NO_3)_3 \cdot 9H_2O$ (99%, Aldrich), $LaZrO_x$ (ZrO_2 doped with 10 wt.% La_2O_3, MelChemicals), and Al_2O_3 (Chempur basic) were used as starting materials. Supported $Cr_2O_3/LaZrO_x$ and Cr_2O_3/Al_2O_3 were prepared by impregnation of $LaZrO_x$ and Al_2O_3 with a required amount of an aqueous solution of chromium nitrate. Firstly, chromium nitrate was dissolved in a certain amount of deionized water which can be fully absorbed by the used amount of supports (about 0.9 g of water per 1 g of $LaZrO_x$ and 0.8 g of water per 1 g of Al_2O_3). The supports were then impregnated with the obtained solutions. The samples were dried at 110°C overnight and calcined at 550°C for 4 hours. The samples were denoted as $0.05Cr_2O_3/LaZrO_x$, $0.15Cr_2O_3/LaZrO_x$, $0.5Cr_2O_3/LaZrO_x$, $1.5Cr_2O_3/LaZrO_x$, $3.2Cr_2O_3/LaZrO_x$, $0.08Cr_2O_3/Al_2O_3$,

$0.8Cr_2O_3/Al_2O_3$, and $5.1Cr_2O_3/Al_2O_3$ with the numbers standing for the nominal weight concentration (in %) of Cr_2O_3.

Analogues of commercial catalysts

KOH (Merck), CrO_3 (99.9%, Sigma Aldrich), $H_2PtCl_6 \cdot 6H_2O$ (>98%, Merck), $SnCl_2 \cdot 2H_2O$ (>98%, Merck), ethanol (99.99%, Fischer Chemical), Al_2O_3 (Saint-Gobain NorPro) were used as initial substances.

An analogue of industrial K-CrO_x/Al_2O_3 catalyst was prepared according to procedure described in patent of Süd-Chemie.[75] Briefly, two aqueous solutions with the required amounts of CrO_3 and KOH were separately prepared and then mixed together. Hereafter, Al_2O_3 was impregnated with the resulting solution. The catalyst precursor was dried at 120°C overnight and calcined at 760°C for 4 hours. The nominal concentration of Cr_2O_3 and K_2O in the resulting catalyst was 19.7 wt.% and 0.93 wt.%, respectively.

Pt-Sn/Al_2O_3 catalyst was synthesised according to Weckhuysen et al.[44] Briefly, 63.5 mg of $H_2PtCl_6 \cdot 6H_2O$ and 145.5 mg of $SnCl_2 \cdot 2H_2O$ were dissolved in 30 ml of ethanol. Hereafter, 5 g of Al_2O_3 were impregnated with the solution. Rotor evaporation (50°C, 20 mbar) was used to remove ethanol. The solid was then calcined at 560°C for 3 hours. The nominal concentration of Pt and Sn in the resulting catalyst was 0.5 wt.% and 1.5 wt.%, respectively.

3.1.2. Bulk catalysts

Bare ZrO_2

$ZrOCl_2 \cdot 8H_2O$ (>95%, Fluka) and NH_3 (25% aqueous solution, Roth) were used as starting materials. ZrO_2 was prepared by a precipitation method. Briefly, a required amount of $ZrOCl_2 \cdot 8H_2O$ was dissolved in deionized water to obtain a solution with concentration of Zr^{4+} of 1 $mol \cdot l^{-1}$. An aqueous solution of ammonia was then added dropwise under stirring until pH 9. The precipitate formed was aged overnight, filtered and washed several times with deionized water until no more chloride ions were identified in filtrate (reaction with $AgNO_3$). The solid was dried at 110°C overnight and calcined at 550°C for 4 hours.

Binary catalysts

$ZrO(NO_3)_2 \cdot xH_2O$ (99%, Sigma Aldrich), $Sm(NO_3)_3 \cdot 6H_2O$ (99.9%, Sigma Aldrich), $Al(NO_3)_3 \cdot 9H_2O$ (>98%, Fluka), $Bi(NO_3)_3 \cdot 5H_2O$ (99%, Fluka), $Nd(NO_3)_3 \cdot 6H_2O$ (>98%, Riedel), Ga_2O_3 (>98%, Sigma Aldrich), NH_3 (25% aqueous solution, Roth), HCl (37%, Fisher), zirconium(IV) acetate solution in dilute acetic acid (15.8 wt.% Zr, Aldrich), citric acid (>99%, Merck), $Ca(NO_3)_2 \cdot 4H_2O$ (99%, Alfa Aesar), $Mg(NO_3)_2 \cdot 6H_2O$ (99%, Acros), $Ce(NO_3)_3 \cdot 6H_2O$ (99.5%, Alfa Aesar), titanium(IV) isopropoxide (97%, Sigma Aldrich), zirconium(IV) n-propoxide solution in propanol (70%, Chempur), isopropanol (99.5% extra dry, Acros), Li_2CO_3 (Apolda), polyvinyl alcohol (M = 28000 – 40000, Germed), sucrose (Berlin-Chemie), HNO_3 (65%, Fisher), $ZrOCl_2 \cdot 8H_2O$ (>95%, Fluka), $Cr(NO_3)_3 \cdot 9H_2O$ (99%, Aldrich) were used as starting materials.

To prepare binary $SmZrO_x$, $AlZrO_x$, $BiZrO_x$, and $NdZrO_x$ materials, required amounts of $ZrO(NO_3)_2 \cdot xH_2O$ and nitrate of promoting element were dissolved in deionized water to obtain a solution with a total cation concentration of 0.5 $mol \cdot l^{-1}$ (for $SmZrO_x$, $BiZrO_x$, and $NdZrO_x$) or 1 $mol \cdot l^{-1}$ (for $AlZrO_x$) (M^{3+}/Zr^{4+} molar ratio = 1/9, M^{3+} = Sm^{3+}, Al^{3+}, Bi^{3+}, Nd^{3+}). An aqueous solution of ammonia was then added dropwise under stirring until pH 9. The precipitate formed was aged overnight, filtered and washed several times with deionized water. The solid was dried at 110°C overnight and calcined at 550°C for 4 hours. $GaZrO_x$ was synthesized in the same way with using $GaCl_3$ as soluble salt of doping element. $GaCl_3$ was obtained by dissolving Ga_2O_3 in HCl under stirring at 90°C for 3 hours.

For synthesizing $CaZrO_x$, $MgZrO_x$, and $CeZrO_x$, zirconium acetate solution, citric acid, and nitrates of calcium, magnesium or cerium were used as starting chemicals. A required volume of zirconium acetate solution was initially mixed with an aqueous solution of nitrate of promoting element. The resulting solution was further diluted with deionized water under stirring to obtain an overall cation concentration of about 0.35 $mol \cdot l^{-1}$ (M^{2+}/Zr^{4+} or M^{3+}/Zr^{4+} molar ratio = 1/9, M^{2+} = Ca^{2+} or Mg^{2+}, M^{3+} = Ce^{3+}). Hereafter, a required amount of citric acid (citric acid/(Zr^{4+} + M^{2+} (or M^{3+})) molar ratio = 2/1) was dissolved in 100 ml of water and added to the solution dropwise under stirring. A white gel was formed during this procedure. The gel was dried at 100°C for 36 hours. Hereafter, the obtained substances were calcined at 550°C for 4 hours.

To prepare $TiZrO_x$, the required amounts of zirconium propoxide and titanium isopropoxide solutions (Ti^{4+}/Zr^{4+} molar ratio = 1/9) were mixed together and diluted with isopropanol under stirring (isopropanol/(Zr^{4+} + Ti^{4+}) molar ratio = 10/1). Then, the required amount of deionized water (H_2O/(Zr^{4+} + Ti^{4+}) molar ratio = 4/1) was added to the solution dropwise under stirring at room temperature. A white gel was formed during this procedure. After stirring for the first 3 hours, this gel was aged at room temperature overnight to ensure a complete hydrolysis and then dried at 70°C for 24 hours resulting in a white substance, which was calcined at 550°C for 4 hours.

$LiZrO_x$ was prepared according to the following procedure. Firstly, 1.9 g of Li_2CO_3, 3 g of polyvinyl alcohol and 30 g of sucrose were dissolved in 300 ml of water under stirring. Then, 5 ml of HNO_3 was added to the solution. The resulting mixture was heated up to 50 – 60°C. Hereafter, the required amount (about 9 g) of $ZrO(NO_3)_2 \cdot xH_2O$ was added to the solution under stirring to obtain Li^+/Zr^{4+} molar ratio of 1/9. The solution was then evaporated until sticky dark material was obtained. The material was dried at 150°C for 30 min, and then the temperature was increased to 250°C and kept for 1 hour. The solid was cooled down to room temperature, crushed and calcined at 650°C for 4 hours.

To prepare bulk $CrZrO_x$ samples with different Zr^{4+}/Cr^{3+} molar ratio, required amounts of $Cr(NO_3)_3 \cdot 9H_2O$ and $ZrO(NO_3)_2 \cdot xH_2O$ were dissolved in deionized water to obtain solution with a total cation concentration of 1 $mol \cdot l^{-1}$. The further steps were the same as described above for the preparation of ZrO_2. The samples were denoted as $Zr_{99.5}Cr_{0.5}O_x$, $Zr_{98}Cr_2O_x$, $Zr_{95}Cr_5O_x$ and $Zr_{90}Cr_{10}O_x$ with the numbers standing for molar fraction of each metal.

3.2. Characterization methods

Specific surface area (S_{BET}) of the samples was determined by *nitrogen physisorption experiments* at -196°C using a Belsorp mini II setup (Bel Japan). Desorption isotherms were evaluated according to the BET method.

X-ray diffraction (XRD) measurements were made on a Theta/Theta diffractometer X'Pert Pro (Panalytical) with CuKα radiation (λ = 1.5418Å, 40kV, 40mA) and an X'Celerator RTMS detector. Phase composition of the samples was identified using the program suite WinXPOW

(Stoe & Cie) with inclusion of the powder diffraction file PDF2 of the international center for diffraction data.

Transmission electron microscopy (TEM) (JEM-ARM200F, E = 200 kV) was used to determine size distribution of metal nanoparticles (Pt, Rh and Ru) after their deposition from ethylene glycol solution onto copper grid.

EPR measurements were performed in order to detect any paramagnetic species in ZrO_2-based materials after oxidative and reductive treatments. The spectra were recorded at -196°C on a Bruker EMX microspectrometer with an ER 4119HS-WI high-sensitivity optical resonator using the following settings: 7.2 mW microwave power, 9.4368 GHz microwave frequency (X-band), 100 kHz modulation frequency and 5 G modulation amplitude.

UV-vis measurements were performed in an in-house developed set-up enabling UV-vis catalyst characterization with simultaneous analysis of gas-phase components by an on-line mass spectrometer (Pfeiffer Vacuum OmniStar 200). For investigating the kinetics of $LaZrO_x$ reduction with or without supported Ru NP, UV-vis spectra of such materials (300 mg) were collected every 1 min during their treatment in a H_2-containing (57 vol.% H_2 in Ar) flow (10 $ml \cdot min^{-1}$) for 1 hour at a selected temperature (550, 600 or 650°C). An AVASPEC UV-vis spectrometer (Avantes) equipped with DH-2000 deuterium-halogen light source and a CCD array detector was used for recording the spectra. $BaSO_4$ was used as a white reference material. High-temperature reflection UV-vis probes consisting of 6 radiating optical fibres and 1 reading fibre were threaded through the furnace wall to face quartz reactors. For illustrating reduction process, a relative reflectance (R_{rel}) expressed as the reflectance of sample treated in H_2 related to that of its fully oxidized counterpart was defined as given in equation (3.1). From this relative reflectance, the relative Kubelka-Munk function $F(R_{rel})$ was calculated according to equation (3.2).

$$R_{rel} = \frac{R_{in\ H_2\ flow}}{R_{oxidized}} \tag{3.1}$$

$$F(R_{rel}) = \frac{(1-R_{rel})^2}{2R_{rel}} \tag{3.2}$$

To monitor carbon deposition and removal in PDH and reoxidation stages at 550°C, respectively, UV-vis spectra and MS data were collected. The dehydrogenation stage lasted for 45 min using a flow of 40 vol.% C_3H_8 in Ar (10 $ml \cdot min^{-1}$), while the regeneration stage lasted for

15 min in a flow of 20 vol.% O_2 in Ar (10 ml·min^{-1}). These were separated by purging with Ar (10 ml·min^{-1}) for 15 min. For the dehydrogenation stage, a relative reflectance (R_{rel-DH}) was calculated as the reflectance of the sample treated in C_3H_8 related to that of the fully oxidized one as given in equation (3.3). From this relative reflectance, the relative Kubelka-Munk function $F(R_{rel-DH})$ was calculated according to equation (3.4).

$$R_{rel-DH} = \frac{R_{in\ C_3H_8\ flow}}{R_{oxidized}} \tag{3.3}$$

$$F(R_{rel-DH}) = \frac{(1-R_{rel-DH})^2}{2R_{rel-DH}} \tag{3.4}$$

For regeneration stage, a relative reflectance ($R_{rel-Reg.}$) was calculated as the reflectance of the sample treated in O_2 related to that of the sample after PDH as given in equation (3.5). For a proper comparison of the data obtained during dehydrogenation and regeneration stages, the modified relative Kubelka-Munk function $F(R_{rel-Reg.})$ for regeneration stage was calculated according to equations (3.6) and (3.7).

$$R_{rel-Reg.} = \frac{R_{in\ O_2\ flow}}{R_{after\ DH}} \tag{3.5}$$

$$R_{rel-after\ Reg.} = \frac{R_{after\ regeneration}}{R_{after\ DH}} \tag{3.6}$$

$$F(R_{rel-Reg.}) = \frac{(1-R_{rel-after\ Reg.})^2}{2R_{rel-after\ Reg.}} - \frac{(1-R_{rel-Reg.})^2}{2R_{rel-Reg.}} \tag{3.7}$$

Raman microspectroscopic measurements were performed for proper elucidation of the phase composition of selected ZrO_2-based catalysts. The data were collected using a Renishaw inVia Raman microscope. The samples were irradiated by a 633 nm laser with an output power of 1 – 16 mW.

To quantify oxygen vacancies in ZrO_2-based catalysts *O_2-pulse experiments* were carried out at 550°C in the temporal analysis of products (TAP) reactor.[76] Each catalyst (50 or 100 mg, particle size: 315 – 710 or 250 – 710 µm) was placed in a quartz-tube microreactor between two layers of molten quartz (particle size: 250 – 350 µm). Before starting the pulse experiments, the catalyst was treated in the following way. At first it was heated in an O_2 flow (10 ml·min^{-1}) up to 550°C with a heating rate of 10 K·min^{-1}. Hereafter, the catalyst was further heated in a N_2 flow (10 ml·min^{-1}) up to desired temperature (550, 600 or 625°C). Then it was exposed to an H_2 (57 vol.% H_2 in N_2) flow (10 ml·min^{-1}) for 1 hour. After finishing the reductive treatment, the

catalyst was cooled down to 550°C upon evacuation to ca. 70 Pa. Then it was exposed to high vacuum of 10^{-5} Pa. The pulse experiments were performed using an O_2:Ar = 1:1 mixture. Ar (5.0) and O_2 (4.5) were applied without additional purification. The mixture was pulsed until no changes in the intensity of O_2 pulses were observed during last 30 – 40 pulses. Such experiment was repeated at least 3 times, and an average value of consumed oxygen was used. A quadrupole mass spectrometer (HAL RC 301 Hiden Analytical) was used to quantify O_2 and Ar according to standard fragmentation patterns and sensitivity factors determined in a separate O_2-pulse experiment without catalyst.

X-ray Photoelectron Spectroscopy (XPS) measurements were performed with a ESCALAB220iXL (ThermoFisher Scientific) with monochromatic Al Kα radiation (1486.6 eV) in order to elucidate surface composition of bulk $CrZrO_x$ catalysts. For charge compensation, low-energetic electrons of 10 eV were used (flood gun). The electron binding energy was referenced to adventitious carbon at 284.8 eV according to the advice of NIST. The peaks were fitted after subtracting a Shirley background with Gaussian-Lorentzian curves. The elemental composition of the nearsurface region was determined from the peak area dividing by the elemental-specific Scofield factor and the spectrometer-specific transmission function.

Temperature-programmed ammonia desorption (NH_3-TPD) tests were performed to investigate acidic properties of selected samples. The experiments were carried out in an in-house developed setup containing eight individually heated continuous-flow fixed-bed quartz reactors (Figure 3-1). Prior to NH_3-TPD, the samples (50 mg for each sample) were either calcined in an air flow at 600°C for 1 hour and cooled down in air flow (10 ml·min^{-1}) to 120°C or calcined in air and treated in a flow of 57 vol.% H_2 in Ar (10 ml·min^{-1}) at 600°C or 550°C for 1 hour followed by cooling down in Ar flow to 120°C. Hereafter, they were exposed to a flow of ammonia (1 vol.% NH_3 in Ar, 10 ml·min^{-1}) at 120°C for 1 hour, then purged with Ar (10 ml·min^{-1}) for 5 hours to remove weakly bound NH_3, cooled down in Ar to 80°C, and then heated up to 900°C with a heating rate of 10 K·min^{-1} in an Ar flow (10 ml·min^{-1}). Desorbed ammonia was registered by an on-line mass spectrometer (Pfeiffer Vacuum OmniStar GSD 320) using following atomic mass units (AMUs): 15 (NH) and 40 (Ar). For MS calibration, a mixture of 1 vol.% NH_3 in Ar was used. The signals of NH and Ar were recorded and the ratio of NH/Ar was determined. Ar was used as internal standard.

The number of desorbed NH_3 molecules related to 1 nm^2 of catalyst surface was determined as follows. The ratio of NH/Ar calculated from the corresponding MS signals upon NH_3 desorption was initially plotted against temperature. The obtained temperature NH/Ar profile was integrated under consideration of heating rate and purging flow according to equation (3.8). This number can be considered as an overall density of acidic sites when assuming that one molecule of ammonia can be adsorbed on one acidic site.

$$N(NH_3) = \frac{F \times N_A}{r_{heating} \times m_{catalyst} \times V_{mol} \times S_{BET} \times 10^{18}} \times \int_{T_1}^{T_2} \left({}^{NH}/_{Ar} \times \frac{0.01}{\left({}^{NH}/_{Ar}\right)_{cal}} \right) dT \quad (3.8)$$

Here, F is flow of Ar purging (10 ml·min^{-1}), N_A is the Avogadro constant (6.02·10^{23} mol^{-1}), $r_{heating}$ is a heating rate (10 K·min^{-1}), $m_{catalyst}$ is the amount (g) of sample, V_{mol} is the molar volume (22400 ml·mol^{-1}), S_{BET} is catalyst specific surface area (m^2·g^{-1}), T_1 and T_2 are the temperatures of starting and ending of NH_3 desorption, respectively, NH and Ar are the signals obtained from MS data during NH_3-TPD experiment for 15 and 40 atomic mass units, respectively (a.u.), the signals with subscripts "cal" are related to the data obtained from calibration test with 1 vol.% NH_3 in Ar.

Figure 3-1 NH_3-TPD, TPR and TPO setup with eight individually heated continuous-flow fixed-bed quartz reactors.

For investigating reducibility of selected samples, *temperature-programmed reduction (TPR) experiments* were performed in the same set-up used for NH_3-TPD tests (Figure 3-1). Prior to the experiments, all samples (200 mg for each sample) were calcined in an air flow (10 ml·min^{-1}) at 550°C for 1 hour, cooled down in the same flow to room temperature and then purged with Ar (10 ml·min^{-1}) for 15 min. Hereafter, the oxidized samples were heated in a flow

of 5 vol.% H_2 in Ar (10 ml·min^{-1}) up to 900°C with a heating rate of 10 K·min^{-1}. An on-line mass spectrometer (Pfeiffer Vacuum OmniStar GSD 320) was used to determine hydrogen concentration using the ratio of AMU of 2 to AMU of 40 (H_2/Ar).

To quantify the amount of carbon deposits formed on the surface of selected catalysts used for PDH at 550°C with a feed containing 40 vol.% C_3H_8 in Ar for 50 min on stream, *temperature-programmed oxidation (TPO) experiments* were conducted. After PDH, the catalysts were cooled down in N_2 flow to room temperature, removed from reactors and placed in TPO reactors. The TPO experiments were performed by heating the spent samples in a flow of 5 vol.% O_2 in Ar (10 ml·min^{-1}) up to 900°C with a heating rate of 10 K·min^{-1}. The MS signals related to CO_2, CO and Ar were recorded using on-line mass spectrometer (Pfeiffer Vacuum OmniStar GSD 320) at the atomic mass units of 44 (CO_2), 28 (CO, CO_2) and 40 (Ar), respectively. In order to quantify the TPO tests, the mass spectrometer was calibrated using 1 vol.% CO_2 in Ar and 1 vol.% CO in Ar mixtures. The overall amount of carbon deposits per gram of each catalyst was calculated from the temperature CO_2(AMU of 44)/Ar and CO(AMU of 28)/Ar profiles under consideration of heating rate, total oxygen-containing flow and the calibration factors for CO_2 and CO and Ar (equation (3.9)). The contribution of the CO_2 MS signal to the CO signal was also taken into account.

$$m(C) = \frac{F \times M(C)}{r_{heating} \times m_{catalyst} \times V_{mol}} \times \left(\int_{T_1}^{T_2} \left({CO_2}/{Ar} \times \frac{0.01}{\left({CO_2}/{Ar}\right)_{CO_2\_cal}} \right) dT + \int_{T_1}^{T_2} \left(\left({CO}/{Ar} - \frac{{CO_2}/{Ar}}{\left({CO_2}/{CO}\right)_{CO_2\_cal}} \right) \times \frac{0.01}{\left({CO}/{Ar}\right)_{CO\_cal}} \right) dT \right) \quad (3.9)$$

Here, F is a flow of 5 vol.% O_2 in Ar (10 ml·min^{-1}), $M(C)$ is the molar weight of carbon (12 g·mol^{-1}), $r_{heating}$ is a heating rate (10 K·min^{-1}), $m_{catalyst}$ is the amount of catalyst (g), V_{mol} is molar volume (22400 ml·mol^{-1}), T_1 and T_2 are the temperatures of start and end of CO_x release, respectively, CO_2, Ar and CO are the MS signals recorded in TPO experiment at AMUs of 44, 40 and 28, respectively (a.u.), the signals with subscripts "CO_2_cal" and "CO_cal" are related to the data obtained from calibration tests with 1 vol.% CO_2 in Ar and 1 vol.% CO in Ar, respectively.

For discriminating between Brønsted and Lewis acidic sites, *IR measurements* of adsorbed pyridine were performed on a Tensor 27 spectrometer (Bruker). Prior to the

measurements, the sample was heated up in N_2 flow to 600°C, calcined in air flow at this temperature for 1 hour, flushed with N_2 flow for 15 min and reduced in H_2 flow (57 vol.% H_2 in N_2) for 1 hour. Hereafter, the catalyst was cooled down in N_2 flow to room temperature. So treated sample was pressed into self-supporting wafers with a diameter of 20 mm. Prior to pyridine adsorption, it was again treated in the IR cell according to the following protocol: heating in air to 450°C for 1 hour, flushing with N_2 for 15 min, treating in H_2 flow (57 vol.% H_2 in N_2) for 1 hour. Hereafter, the catalyst was cooled down in N_2 flow to room temperature. Pyridine was adsorbed at 25°C until saturation. Then the reaction cell was evacuated for removing physisorbed pyridine. After heating the sample in vacuum to 100°C, the IR spectrum of adsorbed pyridine was recorded.

3.3. Catalytic tests

Alkane dehydrogenation tests were carried out in an in-house developed setup equipped with 15 continuous flow fixed-bed reactors operating at 1 bar (Figure 3-2). The alkane (propane, isobutane or n-butane) feed consisted of 40% C_nH_{2n+2} in N_2 for all types of experiment if not specified especially. Prior to the tests, the catalysts were initially heated up in N_2 flow to desired temperature followed by feeding air for 1 hour and purging with N_2 for 15 min. Hereafter, if the catalysts are denoted as “oxidized” they were directly exposed to a flow of the alkane-containing feed. If the catalysts are denoted as “reduced” they were also initially oxidized and then treated in a H_2 flow (57 vol.%) in N_2 for 1 hour, purged with N_2 for 15 min followed by DH tests. In some experiments (will be specified when it is necessary), catalyst treatment temperature differed from the temperature of dehydrogenation stage. In this case, increase or decrease of the temperature was carried out during purging stage in a N_2 flow.

For determining apparent activation energy of alkene formation, the corresponding rate for different alkanes over selected catalysts was determined in the temperature range of 525°C – 575°C or 500°C – 600°C. Catalytic tests were performed at a degree of alkane conversion below 10%. In this case, the catalytic reactor can be considered as differential. The rate of propene formation was measured after 190 s on stream, while those of n-butenes and isobutylene were measured after 270 s. Three series of catalytic tests were performed as follows. In the first series of experiments, catalytic tests were performed at 525, 550 and 575°C with the catalysts pre-reduced always at 575°C. The catalysts were initially calcined in air for 1 hour, purged with N_2

flow for 15 min and reduced at 575°C in a flow of H_2 (57 vol.% H_2 in N_2) for 1 hour followed by purging with N_2 for 15 min with simultaneous decreasing the temperature to 525°C. Hereafter, the catalysts were exposed to a flow of reaction mixture, and the rate of alkene formation at 525°C was measured. Then the catalysts were purged with N_2 flow for 15 min with simultaneous increasing the temperature to 575°C, reoxidized in air flow for 30 min, purged with N_2 flow for 15 min, treated with H_2 flow (57 vol.% H_2 in N_2) for 1 hour and cooled down in N_2 flow to 550°C for 15 min. Then the catalysts were exposed to a flow of reaction mixture, and the rate of alkene formation at 550°C was measured. In a next step, the catalysts were treated as described above before being tested at 575°C. A second series of experiments was performed similar as described above, but the catalysts were always oxidized and reduced at each reaction temperature, i.e. at 525, 550, and 575°C, at which the reaction rate was also measured. In a third series of experiments, catalytic tests were performed at 500, 525, 550, 575 and 600°C. Oxidative and reductive catalysts treatments were made in a same way as described for the first series of tests with an exception that the temperature of such treatments was 600°C. To achieve alkane conversion below 10% at each temperature, the total flow of the reaction feed was increased with increasing reaction temperature. Thus, for the first and the second series of experiments, the catalyst amount was set to 20 mg and the total C_3H_8-N_2 flow was adjusted to 6, 10 and 20 $ml \cdot min^{-1}$ for 525, 550 and 575°C, respectively. For the third series of tests, the catalyst amount was varied from 25 to 175 mg depending on sample. The total C_3H_8-N_2 flow was adjusted to 5, 5, 10, 20, and 40 $ml \cdot min^{-1}$ for 500, 525, 550, 575, and 600°C, respectively. The corresponding flows of n-C_4H_{10}-N_2 and i-C_4H_{10}-N_2 mixtures were 10, 20, 40, 60, and 80 $ml \cdot min^{-1}$.

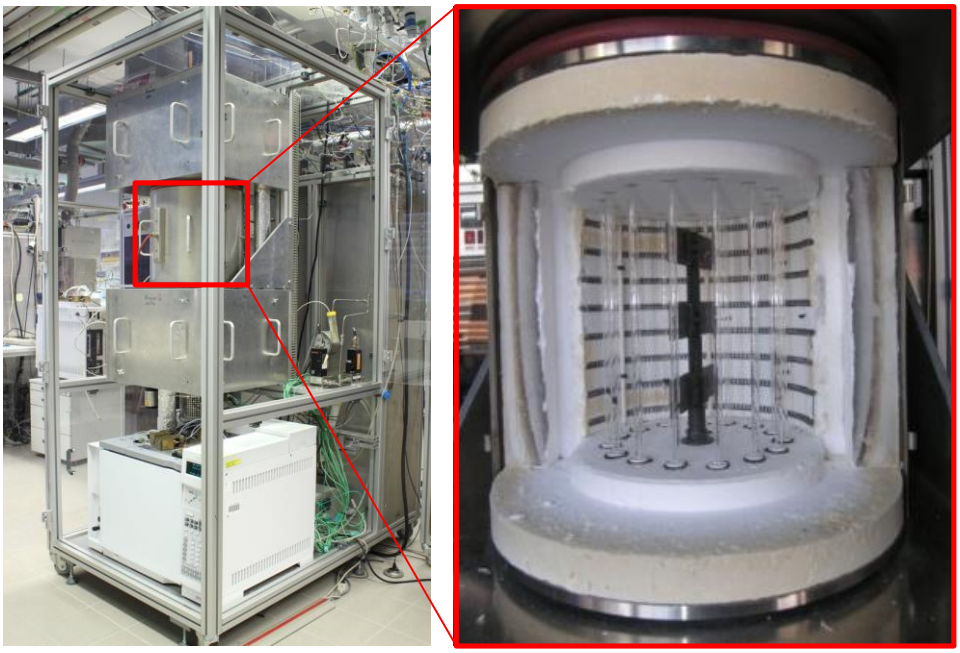

Figure 3-2 Catalytic setup with 15 continuous flow fixed-bed reactors.

For catalytic tests performed at alkane conversion below 10 %, equations (3.10) – (3.12) were used to calculate selectivity to gas-phase products (S_j), alkene formation rate ($r(C_nH_{2n})$) and turn over frequency (TOF) with respect to one surface Ru or Cr atom.

$$S_j = \frac{v_{C_nH_{2n}}}{v_j} \times \frac{x_j}{\sum_i \frac{v_{C_nH_{2n}}}{v_i} \times x_i} \quad (3.10)$$

$$r(C_nH_{2n}) = \frac{F_{feed} \times x(C_nH_{2n})}{V_m \times m_{catalyst}} \quad (3.11)$$

$$TOF = \frac{r(C_3H_6) \times N_A}{60 \times N(Ru_{surf} \text{ or } Cr_{surf})} \quad (3.12)$$

Here, v_i is reciprocal stoichiometric coefficient for product i, x_i is a molar fraction of product i, F_{feed} is a volume flow of feed gas (ml·min^{-1}), V_m is the molar volume (22400 ml·mol^{-1}), $m_{catalyst}$ is the amount of catalyst (g), N_A is the Avogadro constant ($6.02 \cdot 10^{23}$ mol^{-1}), $N(Ru_{surf} \text{ or } Cr_{surf})$ is the number of surface atoms of Ru or Cr per 1 g of catalyst (g^{-1}). In the experiments, where conversion of feed alkane was higher than 10%, coke formation could not be neglected, so that, alkane conversion and selectivity to gas-phase products and selectivity to coke ($S(coke)$) were calculated in a different way, according to the equations (3.13) – (3.15).

$$X(C_nH_{2n+2}) = \frac{\dot{n}^{in}_{C_nH_{2n+2}} - \dot{n}^{out}_{C_nH_{2n+2}} \times \frac{\dot{n}^{in}_{N_2}}{\dot{n}^{out}_{N_2}}}{\dot{n}^{in}_{C_nH_{2n+2}}} \quad (3.13)$$

$$S_j = \frac{v_{C_nH_{2n+2}}}{v_j} \times \frac{\dot{n}^{out}_j \times \frac{\dot{n}^{in}_{N_2}}{\dot{n}^{out}_{N_2}}}{\dot{n}^{in}_{C_nH_{2n+2}} - \dot{n}^{out}_{C_nH_{2n+2}} \times \frac{\dot{n}^{in}_{N_2}}{\dot{n}^{out}_{N_2}}} \quad (3.14)$$

$$S(coke) = 1 - \sum_i S_i \quad (3.15)$$

Yield (Y_j) and space time yield of alkene formed (STY) were calculated according to the equations (3.16) and (3.17).

$$Y_j = S_j \times X(C_nH_{2n+2}) \quad (3.16)$$

$$STY = \frac{F_{feed} \times x^{out}(C_nH_{2n}) \times \frac{x^{in}(N_2)}{x^{out}(N_2)} \times M(C_nH_{2n}) \times \rho_{catalyst} \times 1000 \times 60}{V_m \times m_{catalyst}} \quad (3.17)$$

An overall weight of alkene produced within one catalytic cycle over used amount of the catalyst and that obtained over 1 m^3 or over 1 g of the catalyst were calculated using equations (3.18), (3.19) and (3.20), respectively.

$$m(C_nH_{2n}) = \frac{m_{catalyst}}{1000\rho_{catalyst}} \times \int_0^t STY\, dt \quad (3.18)$$

$$m_{m^3}(C_nH_{2n}) = \int_0^t STY\, dt \quad (3.19)$$

$$m_g(C_nH_{2n}) = \frac{1}{1000\rho_{catalyst}} \times \int_0^t STY\, dt \quad (3.20)$$

Here, $\dot{n}_i$ with superscripts “inlet” and “outlet” is a molar flow of gas-phase components at the reactor inlet and outlet, respectively (mol·min^{-1}), $M(C_nH_{2n})$ is molar weight of alkene (g·mol^{-1}), $\rho_{catalyst}$ is catalyst density (g·ml^{-1}).

The concentration of feed components and reaction products was determined by an on-line gas chromatograph (Agilent 6890) equipped with PoraplotQ (for CO_2), HP-PLOT Al_2O_3 ”KCl” (for hydrocarbons) and Molsieve 5 (for H_2, O_2, N_2, and CO) capillary columns. Flame ionization (FID) and thermal conductivity (TCD) detectors were used for detection of hydrocarbons and other components, respectively.

4. Results and discussion

4.1. Alternative concept of designing alkane dehydrogenation catalysts

4.1.1. Selection of materials

This work demonstrates an alternative concept for designing dehydrogenation catalysts, in which catalytically active sites are defects on the surface of metal oxides but not supported metal or metal oxides as in the conventional dehydrogenation catalysts described in section 1.4. In such alternative concept, supported hydrogenation-active metals or metal oxides can assist in creation of defect sites. Figure 4-1 schematically shows a comparison between the conventional and alternative-type catalysts.

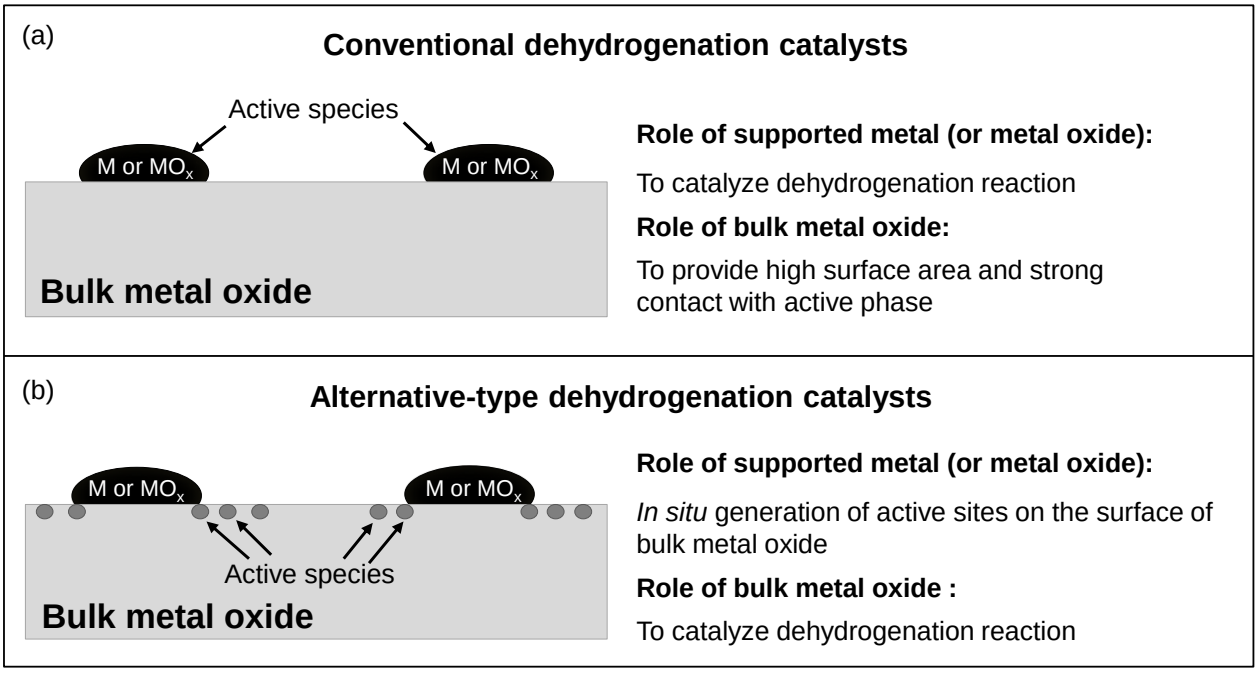

Figure 4-1 General concepts of catalyst functioning for (a) conventional dehydrogenation catalysts and (b) alternative-type dehydrogenation catalysts.

The working hypothesis behind this alternative approach is that metal oxides with high surface oxygen mobility can generate surface defects under reductive conditions, i.e. during hydrogen pre-treatment or *in situ* during alkane dehydrogenation reaction. Such defects were postulated to be coordinatively unsaturated metal cations. ZrO_2 promoted with low valent metal oxides is one of such solid materials with high ionic conductivity [77] and has been actually used

as a support for catalytically active Pt, CrO_x or GaO_x species.[40] However, the loading of supported component was too high to test the intrinsic activity of ZrO_2.

To check if the alternative concept may work, it was initially decided to investigate the effect of oxygen surface mobility (material property affecting its ability to release lattice oxygen and to form coordinatively unsaturated cations) of different bulk oxide materials on their PDH activity. To this end, several commercial supports differing in their oxygen mobility [78] (SiO_2, Al_2O_3, Siral 10 (10 wt.% SiO_2 in Al_2O_3), Siral 40 (40 wt.% SiO_2 in Al_2O_3) and $LaZrO_x$ (ZrO_2 doped with 10 wt.% La_2O_3)) were used. Since noble metals increase reducibility of metal oxides [79-82], the above materials were impregnated with preformed Pt, Rh or Ru nanoparticles (NP) with a narrow size distribution between 1.1 and 1.5 nm as proven by transmission electron microscopy (Figure 4-2). The nominal loading of Rh and Ru on supports was 0.05 wt.%, while that of Pt was 0.1 wt.% in order to ensure similar surface area of each metal (ca. 0.2 $m^2_{metal} \cdot g_{support}^{-1}$ calculated according to [83]).

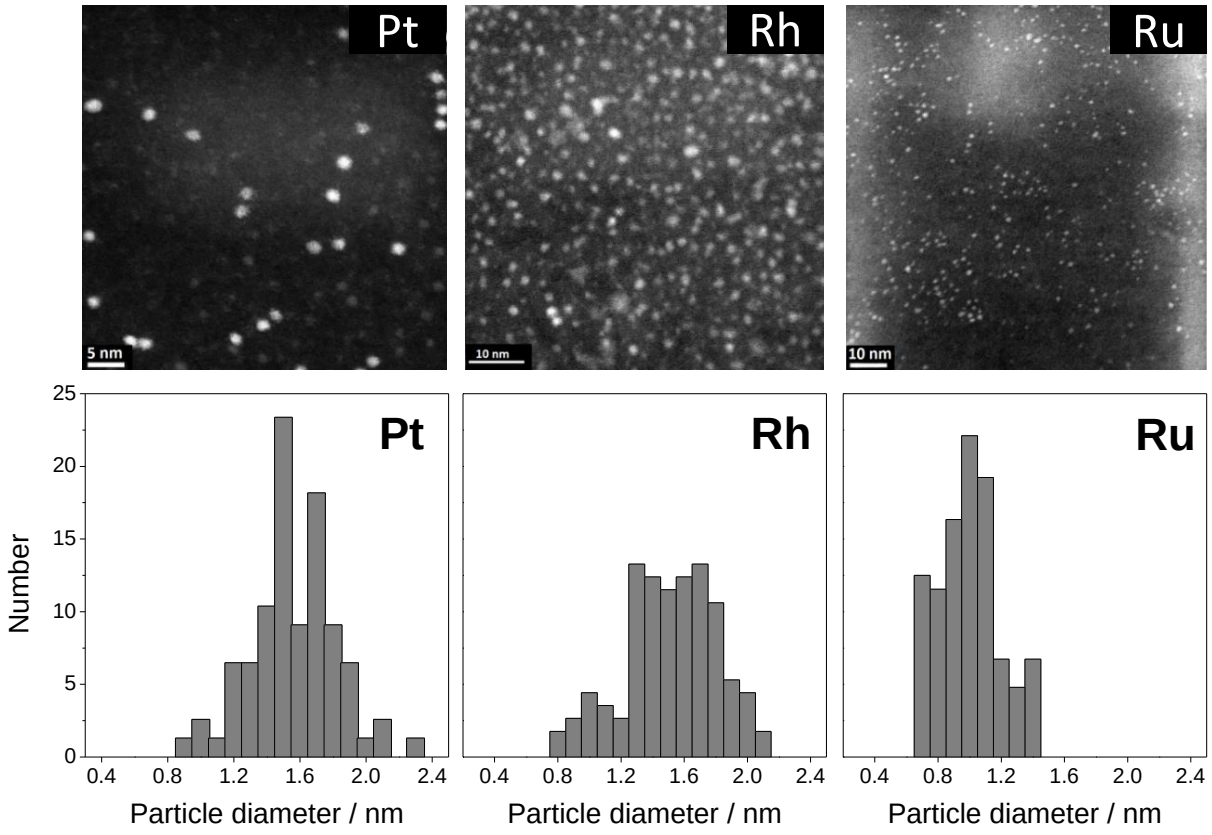

Figure 4-2 TEM images and size distribution of Pt, Rh and Ru NP deposited from ethylene glycol solution on grid.

The above mentioned oxide materials with and without supported metal NP were tested in propane dehydrogenation at 550°C. Prior to the experiments, they were calcined in an air flow at 550°C for 1 hour, purged with N_2 flow for 15 min and pre-treated at the same temperature in a flow of H_2 (57 vol.% H_2 in N_2) for 1 hour. The rate of propene formation obtained on all catalysts tests is shown in Figure 4-3. Generally, the oxides without NP were significantly less active than their counterparts with NP but their activity increased with decreasing the strength of metal-oxygen bond. Noticeably, bare $LaZrO_x$ with the weakest metal-oxygen bond showed the highest rate of propene formation among all supports. Its activity was even higher than the activity of SiO_2-Al_2O_3 (0 – 100 wt.% SiO_2) materials with Ru or Rh NP and only slightly lower than that of their Pt-containing counterparts thus highlighting the dehydrogenation potential of active sites outside noble metal NP. The high activity of Pt-containing samples with Siral 40, Siral 10 and Al_2O_3 as supports can be attributed to the activity of Pt sites since the rate of propene formation does not really depend on the kind of support. Significantly low activity of Pt/SiO_2 may be explained by weak metal-support interaction and therefore loss of platinum during calcination of the catalyst, because volatile PtO_x species can be formed above 450°C in the presence of gaseous oxygen.[84] Remarkably, there was no significant difference in the activity between the metals when they were supported on the surface of $LaZrO_x$. Since the $LaZrO_x$-based materials showed the highest activity among all samples tested, they were further investigated in detail.

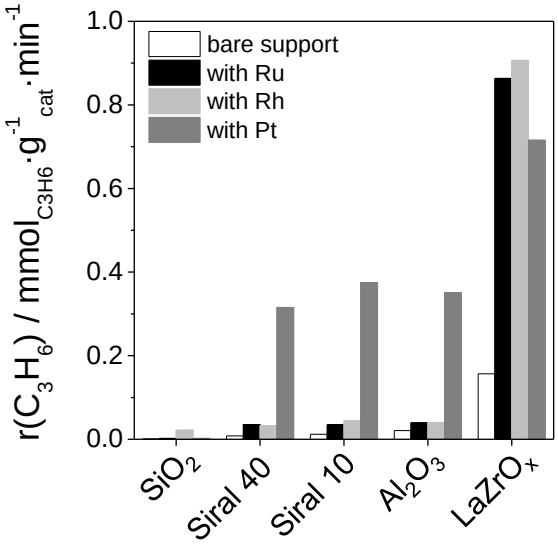

Figure 4-3 Rate of propene formation determined at 550°C over various oxide materials without and with Ru, Rh or Pt NP.

4.1.2. Influence of supported metals on activity of $LaZrO_x$ in propane dehydrogenation

For understanding the origins of the high PDH activity of $LaZrO_x$-based catalysts, additional catalysts from the same batch of Ru NP (1.1 nm) but with Ru content varying between 0.002 wt.% and 0.2 wt.% were prepared and tested in PDH. The rate of propene formation as a function of Ru loading is shown in Figure 4-4 (a). It is clearly seen that there is no linear dependence between the rate of propene formation and Ru loading. Thus, the rate of propene formation raised with Ru loading up to 0.05 wt.% and then decreased with a further increase in the loading. Such dependence can be explained when assuming that Ru is not the species determining catalyst activity in PDH. To check this idea, an apparent turnover frequency (TOF) of propene formation, i.e. the activity related to one surface Ru atom was calculated. Interestingly, TOF strongly decreased with rising Ru loading (Figure 4-4 (b)). Since all samples possessed the same Ru NP on the same support, any effects of the metal-support interaction and/or particle size on TOF are excluded. Therefore, one can conclude that Ru NP indeed do not determine the PDH activity of $Ru/LaZrO_x$ directly. Therefore, it can be suggested that catalytically active sites are located on the surface of $LaZrO_x$.

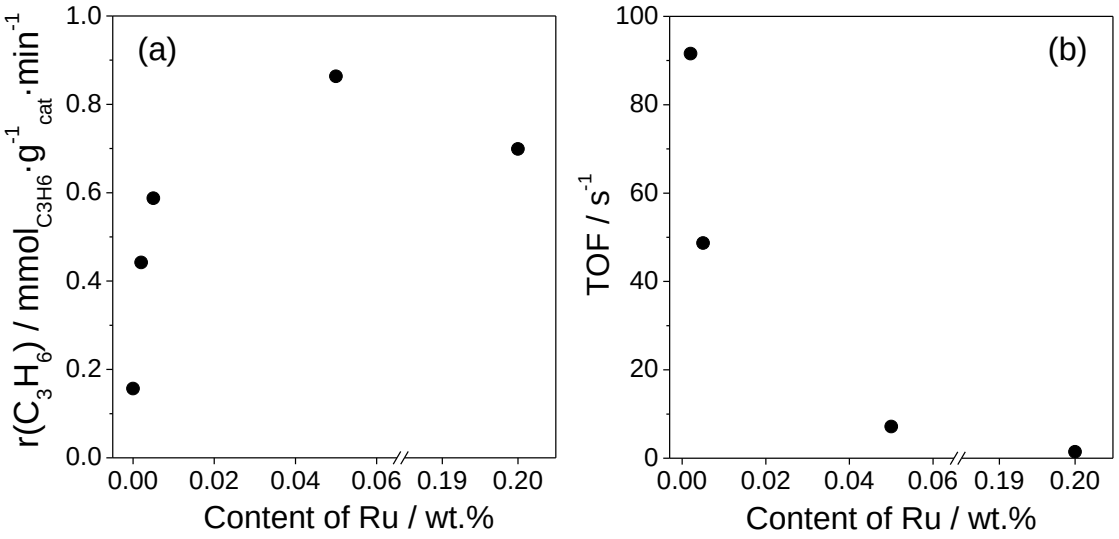

Figure 4-4 (a) Rate of propene formation as a function of Ru content in $Ru/LaZrO_x$; (b) TOF of propene formation as a function of Ru content in $Ru/LaZrO_x$.

To investigate further the effect of supported metal NP on catalyst activity of $LaZrO_x$, additional PDH tests with $LaZrO_x$, $Ru/LaZrO_x$ and $Rh/LaZrO_x$ were performed at different reaction temperatures in the range from 525 to 575°C. The idea behind these tests was to

determine apparent activation energy (E_a) of propene formation and to check if it depends on the presence and/or the kind of noble metal. In the first series of tests, the catalysts were pre-reduced at 575°C every time before testing them in PDH at lower or the same temperatures. This was important to exclude possible temperature effect on the reduction degree of the catalysts. It was found that E_a values determined from the Arrhenius plots (Figure 4-5 (a)) for all catalysts were around 170 kJ·mol^{-1} and were not influenced by the kind of noble metal and its concentration (Figure 4-5 (c)). Such results additionally proved that the tested catalysts possess the same kind of active PDH sites, which are located on surface of $LaZrO_x$ but not Ru or Rh NP.

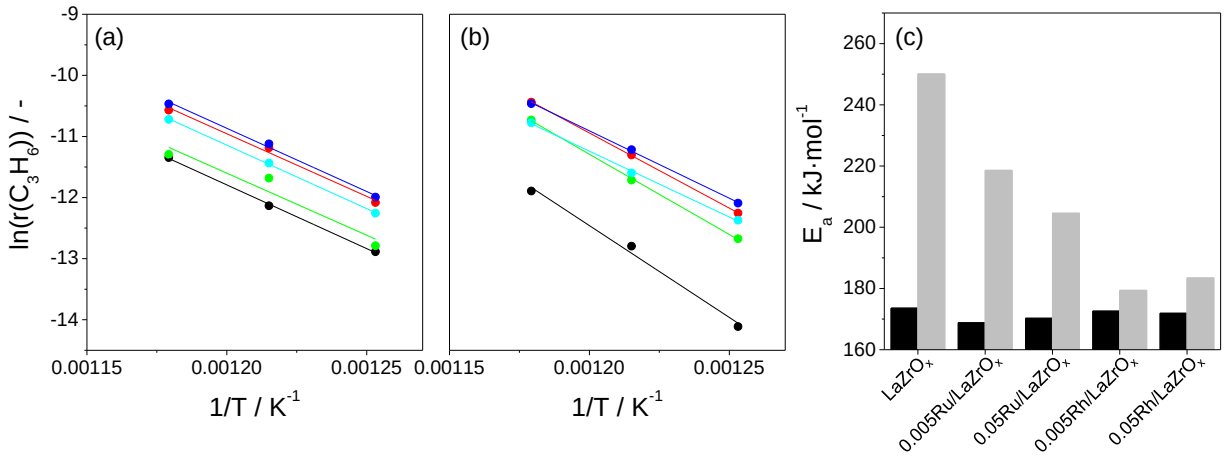

Figure 4-5 Arrhenius plots for ● $LaZrO_x$, ● 0.005Ru/$LaZrO_x$, ● 0.05Ru/$LaZrO_x$, ● 0.005Rh/$LaZrO_x$, and ● 0.05Rh/$LaZrO_x$ pre-reduced (a) at 575°C and (b) at each (525, 550 and 575°C) reaction temperature; (c) apparent activation energy of propene formation in the temperature range from 525 to 575°C determined over $LaZrO_x$-based catalysts pre-reduced at 575°C (■) or at each reaction temperature (■).

A second series of tests was performed with the catalysts reduced at the same temperature, at which the PDH reaction was then carried out. Interestingly, E_a values obtained were higher than those determined at first series of tests and different for all samples tested (Figure 4-5 (b) and (c)). Based on the results obtained one can conclude that it is more likely that active dehydrogenation sites are formed during reductive treatment of the catalysts. The higher values of E_a obtained in the second series of tests must be due to the fact that they additionally include the energy which is required for the formation of active sites upon reductive catalyst treatment. A deeper discussion about the possible nature of the active sites and the importance of reductive treatment for their formation will be provided in section 4.2. For now it is important to

note that the difference in E_a values calculated for the catalysts in different series of tests depends on the sample. Thus, the highest difference of 80 $kJ \cdot mol^{-1}$ was obtained for bare $LaZrO_x$. With the presence of Ru or Rh NP such difference decreases due to the promoting effect of the metals on support reduction.

Taking into account the obtained results, one can conclude that the role of supported noble metal is to induce reduction of $LaZrO_x$. During reductive treatment supported metal adsorbs and dissociates gaseous hydrogen into highly reactive atomic hydrogen species [79, 85, 86] which then leave the metal surface and spillover onto surface of $LaZrO_x$, where they interact with surface lattice oxygen of $LaZrO_x$ resulting in the formation of active sites. If this assumption is correct, not only Ru and Rh can be used to provoke formation of such sites, but any other hydrogenation-active metal. Indeed, $LaZrO_x$ with supported Ni, Co or Cu species (0.05 wt.% of each metal) or $LaZrO_x$ with supported Ag species (0.2 wt.%) showed higher activity than bare $LaZrO_x$ (Figure A-4 in Appendix). The highest activity among these samples was achieved for Cu-containing catalyst. The difference between the catalysts with different supported metals might be due to the different ability of the metals for generating active surface hydrogen species and/or due to the different metal amount (in case of Ag-containing sample).

4.1.3. Effect of treatment conditions on the activity of $LaZrO_x$-based materials in propane dehydrogenation

The effect of the temperature of reductive treatment of $LaZrO_x$-based materials on their activity in propane dehydrogenation was investigated in a series of PDH tests at 550°C with $LaZrO_x$, 0.005Ru/$LaZrO_x$ and 0.05Ru/$LaZrO_x$ pre-reduced at different temperatures before the PDH reaction. Figure 4-6 illustrates how the reduction temperature affects the rate of propene formation determined at 550°C. For bare $LaZrO_x$, the rate rises with increasing reduction temperature. This catalyst showed more than two times higher activity after reduction at 650°C if compare with its activity determined after reduction at 550°C (Figure 4-6). This effect can be explained by an increase in the concentration of active sites formed upon catalyst reduction, i.e. by higher reduction degree of $LaZrO_x$. The catalyst 0.005Ru/$LaZrO_x$ showed only a slight increase in the activity with an increase in reduction temperature up to 625°C. It is worth mentioning that the rate even decreased when the catalyst had been reduced at 650°C. The sample 0.05Ru/$LaZrO_x$ showed lower activity after reduction above 575°C than after reduction at

550 and 575°C. Such behavior of Ru-containing catalysts cannot be due to the irreversible deactivation. The whole experiment was performed without changing initial samples but with their oxidative regeneration at 550°C followed by reductive treatment at desired temperature between the catalytic tests. To check the stability of the catalysts, a control PDH test was performed with the spent catalysts pre-reduced at 550°C. Such catalysts underwent high-temperature (up to 650°C) treatment and any irreversible deactivation would become apparent during control test. However, according to the catalytic data obtained (Figure 4-6, open symbols), the high-temperature treatment did not significantly influence initial catalyst activity of the fresh sample reduced at 550°C.

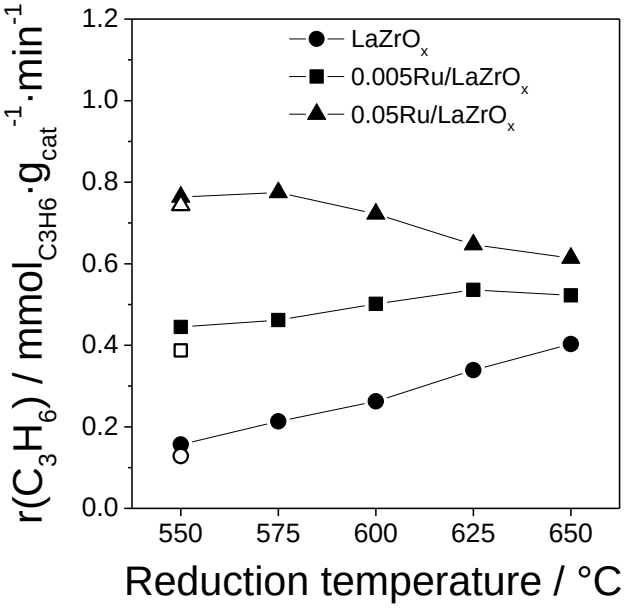

Figure 4-6 Influence of reductive treatment temperature of the samples on the rate of propene formation measured at 550°C over $LaZrO_x$-based catalysts. Open symbols are related to the rate of propene formation measured after completing tests with the catalysts reduced at higher temperatures (up to 650°C) followed by reoxidation and reduction at 550°C.

The unusual behavior of Ru-containing catalysts after high-temperature reductive treatment (Figure 4-6) might be due to their over-reduction. This aspect is further and deeper discussed in section 4.2.4 under consideration of the results of catalyst characterization tests aimed at the identification of the possible nature of active sites.

4.1.4. Summary

An alternative concept for designing the catalysts was developed and verified for propane dehydrogenation over oxide catalysts. In such alternative concept lattice defects of a bulk metal oxide are the catalytically active sites, and supported hydrogenation-active metal promotes formation of such species.

Taking into account the main idea of the concept, highly active ZrO_2-based catalysts with a tiny amount of hydrogenation-active metal (Ru, Rh, Cu, etc.) were developed. The results of kinetic investigations enabled to conclude that dehydrogenation active sites are located on the surface of ZrO_2-based material. The supported metal does not directly participate in propane dehydrogenation but does contribute to the formation of such sites.

It was shown that the pre-treatment of the catalysts under different conditions significantly influences their activity. Thus, reductive treatment of bare $LaZrO_x$ in an H_2 flow at high temperatures has a positive effect on activity due to the increase in reduction degree of ZrO_2-based material that leads to the formation of higher amount of catalytically active defects on the surface. On the contrary, the reductive treatment of Ru-containing catalysts might lead to catalyst over-reduction which negatively affects dehydrogenation activity.

4.2. Possible nature of active sites in ZrO_2-based catalysts

4.2.1. Probing active sites through PDH tests with poison molecules

On the basis of the results of catalytic tests discussed in the preceding section and literature data about propane dehydrogenation on Cr_2O_3 [87, 88], coordinatively unsaturated zirconium (Zr_{cus}) cation and neighboring O^{2-} are suggested to be responsible for C-H bond activation resulting in the formation of Zr_{cus}-C_3H_7 and O-H bonds followed by releasing of C_3H_6 and H_2 molecules. Zr_{cus} sites are created on the surface of $LaZrO_x$ upon removal of lattice oxygen during catalyst reductive pre-treatment or under reaction condition. The latter suggestion is supported by the fact that the initial activity of pre-oxidized catalysts in propane dehydrogenation was lower than that of pre-reduced counterparts but it increased with time on stream (Figure A-5 in Appendix). Such increase is due to *in situ* generation of Zr_{cus} through reduction of $LaZrO_x$ with propane and/or with reaction products, i.e. propene and hydrogen.

To experimentally check if the presence of Zr_{cus} and O^{2-} is important for the high dehydrogenation activity of ZrO_2-based material, bare $LaZrO_x$ was tested for its PDH activity in the absence and the presence of O_2, H_2O or CO_2. The content of propane in reaction mixtures was kept always 40%, while the rest 60% were either pure N_2 (mixture 1) or N_2 with O_2 (mixture 2), H_2O (mixture 3) or CO_2 (mixture 4). These compounds were selected because of the following reasons. O_2 can react with anion vacancies to form lattice oxygen (equation (4.1)). As a consequence, unsaturation degree of neighboring Zr cation will decrease, i.e. the concentration of Zr_{cus} sites will decrease in presence of O_2. A similar effect is achieved in presence of H_2O (equation (4.2)). In addition, catalytic tests with H_2O should provide information about the role of OH groups formed from H_2O for propane dehydrogenation. In comparison with O_2, and H_2O, CO_2 reacts with lattice oxygen according to equation (4.3).[89]

$$2V_O^{\bullet\bullet} + 4e^- + O_2 \rightarrow 2O_o^X \quad (4.1)$$

$$V_O^{\bullet\bullet} + O_o^X + H_2O \rightarrow 2(OH)_o^{\bullet} \quad (4.2)$$

$$O^{2-} + CO_2 \rightarrow [O - CO_2]^{2-} \quad (4.3)$$

Prior to the experiment with the above mentioned reaction feeds, $LaZrO_x$ was pre-reduced in 57 vol.% H_2 in N_2 flow at 600°C for 1 hour. Such treatment condition was chosen to create sufficient number of catalytically active sites as described in section 4.1.3 (Figure 4-6). For each

test, a fresh catalyst sample was used. The PDH reaction was carried out at 550°C and at propane conversion below 10%. The rate of propene formation determined is shown in Figure 4-7. As seen in this figure, the highest rate was obtained when propane was dehydrogenated in the absence of O_2, H_2O or CO_2. The presence of only 0.5 vol.% O_2 in the reaction mixture resulted in more than 15 times lower propene formation rate. Such significant decrease can be explained by refilling oxygen vacancies formed during catalyst reductive pre-treatment with gaseous oxygen according to equation (4.1). As a result, Zr_{cus} sites become coordinatively saturated and, therefore, their concentration decreases thus resulting in a decrease of the rate of propene formation.

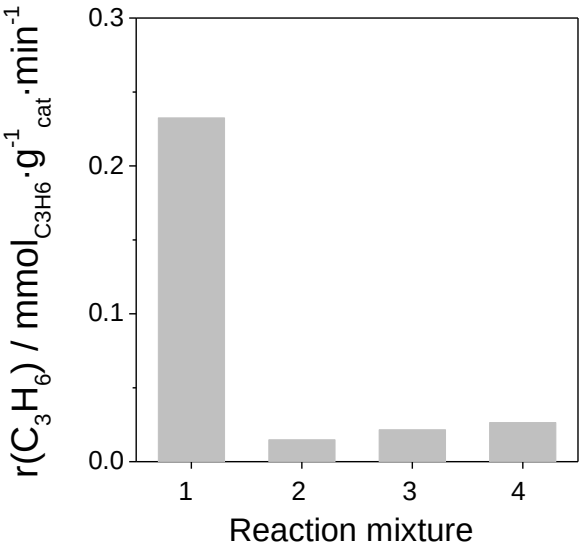

Figure 4-7 Influence of the composition of the reaction mixture (1 – 40 vol.% C_3H_8-60 vol.% N_2, 2 – 40 vol.% C_3H_8-59.5 vol.% N_2-0.5 vol.% O_2, 3 – 40 vol.% C_3H_8-50 vol.% N_2-10 vol.% H_2O, 4 – 40 vol.% C_3H_8-59.5 vol.% N_2-0.5 vol.% CO_2) on the rate of propene formation over reduced $LaZrO_x$ determined at 550°C.

A negative effect on the rate of propene formation was observed in the test where reaction mixture contained water. The activity of $LaZrO_x$ dropped due to a decrease in the concentration of Zr_{cus} sites. Such sites became saturated since oxygen vacancies were filled by water molecules. The water gas reacts with both oxygen vacancy and oxygen of the lattice resulting in the formation of two hydroxyl ions (equation (4.2)).[90] The experiment also proved that Brønsted acidic sites do not contribute to the catalytic activity since the increase of number of acidic hydroxyls did not result in higher activity.

Quite different explanation of activity loss can be proposed for the fourth reaction test where reaction mixture contained small amount of CO_2. The propene formation rate decreased about 9 times if compare with the data obtained in the absence of CO_2 (see the rate determined with reaction mixtures 1 and 4 in Figure 4-7). The reason of the lower catalytic activity can be formation of strongly bound carbonates on the zirconia surface (equation (4.3)). [89] On the one hand, oxygen atom which is supposed to participate in propane activation becomes blocked with CO_2 fragment. On the other hand, the neighboring Zr_{cus} site might be also sterically not available because of interaction with C-O unit (Figure 4-8).

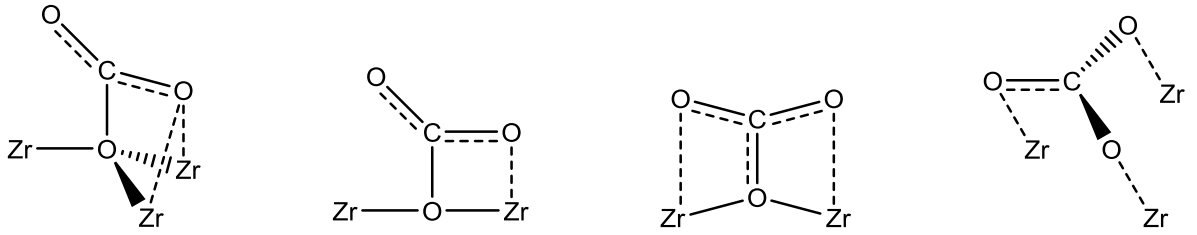

Figure 4-8 Different kinds of surface carbonates formed as a result of CO_2 adsorption on ZrO_2 surface.[89]

Accordingly, it was shown experimentally that the presence of O_2, H_2O or CO_2 in the reaction mixture leads to the drop in activity of ZrO_2-based catalyst due to the decrease in amount of Zr_{cus} active sites or blockage of surface oxygen species participating in propane activation and, probably, of neighboring Zr_{cus} sites.

4.2.2. Identification and quantification of Zr_{cus} active sites

Partial removal of lattice oxygen during hydrogen treatment of zirconia [91] is accompanied with formation of oxygen vacancies according to the equation (4.4):

$$O_o^X + H_2 \rightarrow H_2O + 2e^- + V_O^{\bullet\bullet} \qquad (4.4)$$

Here, O_o^X is an oxygen atom in regular site, e^- – an electron released, $V_O^{\bullet\bullet}$ – the doubly positive ionized oxygen vacancy (F^{2+} color center).

Theoretical calculations [92] showed that the excess electron density is mainly localized in the anion vacancy, however, partial reduction of the neighboring Zr^{4+} cations is also possible. According to Refs. [93, 94], localization of electrons at oxygen vacancies results in formation of differently charged oxygen defects, such as F^+ (a single oxygen vacancy trapping one electron)

and F (a single oxygen vacancy trapping two electrons) color centers. The interaction of electrons with Zr^{4+} cations leads to the formation of Zr^{3+} species. The F^+ and Zr^{3+} species give different EPR signals that makes possible to detect and distinguish them. Thus, F^+ species have symmetric signal with g = 2.0025 and Zr^{3+} species have an axial signal with $g_\perp$ = 1.977 and $g_\parallel$ = 1.960.

To identify if anion vacancies are present in $LaZrO_x$, EPR measurements were performed with oxidized and pre-reduced samples. As it was expected, the EPR spectrum of oxidized $LaZrO_x$ does not have any signals, while EPR spectrum of the pre-reduced sample contains symmetric signal resonating at g = 2.003 (Figure 4-9) which can be assigned to F^+ color centers. No signals related to Zr^{3+} sites could be detected, therefore, one can conclude that pre-reduced $LaZrO_x$ possesses oxygen vacancies but its Zr^{4+} cations remain unreduced. Accordingly, EPR measurements experimentally proved the presence of anion vacancies (a direct indicator for the presence of Zr_{cus}) in the lattice of $LaZrO_x$ after reductive treatment.

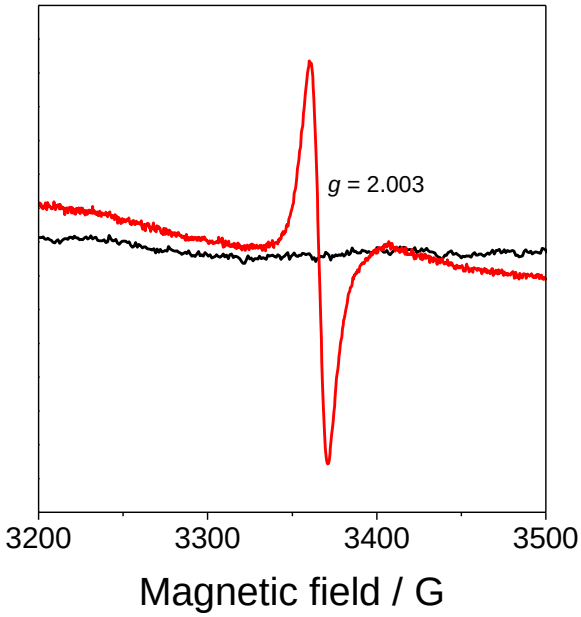

Figure 4-9 Electron paramagnetic resonance spectra of oxidized $LaZrO_x$ (black line) and $LaZrO_x$ pre-reduced in a flow of hydrogen (40 vol.% H_2 in He) at 550°C for 1 hour. The spectra were recorded at -196°C.

Quantification of anion vacancies in $LaZrO_x$-based catalysts was made by O_2-pulse experiments in the temporal analysis of products reactor. This technique is suitable for titrating tiny number of active sites since it enables to perform pulse tests with a minimal pulse size of only 0.1 nmol.[76, 95] The concentration of anion vacancies was calculated from the amount of

O_2 consumed by the samples reduced at 550°C assuming that one O_2 molecule fills two vacancies. The results obtained for bare $LaZrO_x$ and for $LaZrO_x$ containing 0.002, 0.005 and 0.05 wt.% Ru were $2.4 \cdot 10^{16}$, $4.6 \cdot 10^{16}$, $1.2 \cdot 10^{18}$ and $1.0 \cdot 10^{19}$ sites per gram, respectively. It is important to highlight that O_2-pulse experiments performed with Siral 40 (less reducible material) containing the same Ru NPs (0.05 wt. % Ru) showed that only $6.6 \cdot 10^{17}$ oxygen atoms were consumed. This number is significantly lower than $1.0 \cdot 10^{19}$ sites per gram determined for $LaZrO_x$-based catalyst possessing the same amount of Ru NP. Therefore, one can conclude that most of oxygen consumed by $LaZrO_x$-containing samples interacts with surface oxygen vacancies of $LaZrO_x$ and refills them but only minor part of oxygen is spent for oxidation of Ru to RuO_2. Nevertheless, it cannot be completely excluded that bulk oxygen vacancies of $LaZrO_x$ do not participate in these experiments since at high temperature oxygen mobility within zirconia lattice can be significant.[78]

4.2.3. Formation of Zr_{cus} sites: effect of reduction temperature and presence of noble metal

To monitor the formation of oxygen vacancies (and therefore of Zr_{cus} sites) during reductive treatment of $LaZrO_x$ in H_2 flow at different temperatures, *in situ* UV-vis analysis was used. The temporal changes in $F(R_{rel})$ at 550, 600 and 650°C are given in Figure 4-10 (a), (b) and (c), respectively. It is clearly seen that for all conditions, the intensity of the band with a maximum around 450 nm increases with rising time on stream. Such changes in the UV-vis spectra can be explained by the formation of oxygen vacancies [96], which results in the appearance of several transition energy levels of 3.5 – 3.8 eV above the valence band of ZrO_2. Electron transitions from these levels into the conduction band are the reason of optical absorption in the visible light threshold. Based on temporal profiles of $F(R_{rel})$ at 450 nm at 550, 600, and 650°C (Figure 4-10 (d)), one can conclude that the rate of formation of oxygen vacancies increases with rising reduction temperature.

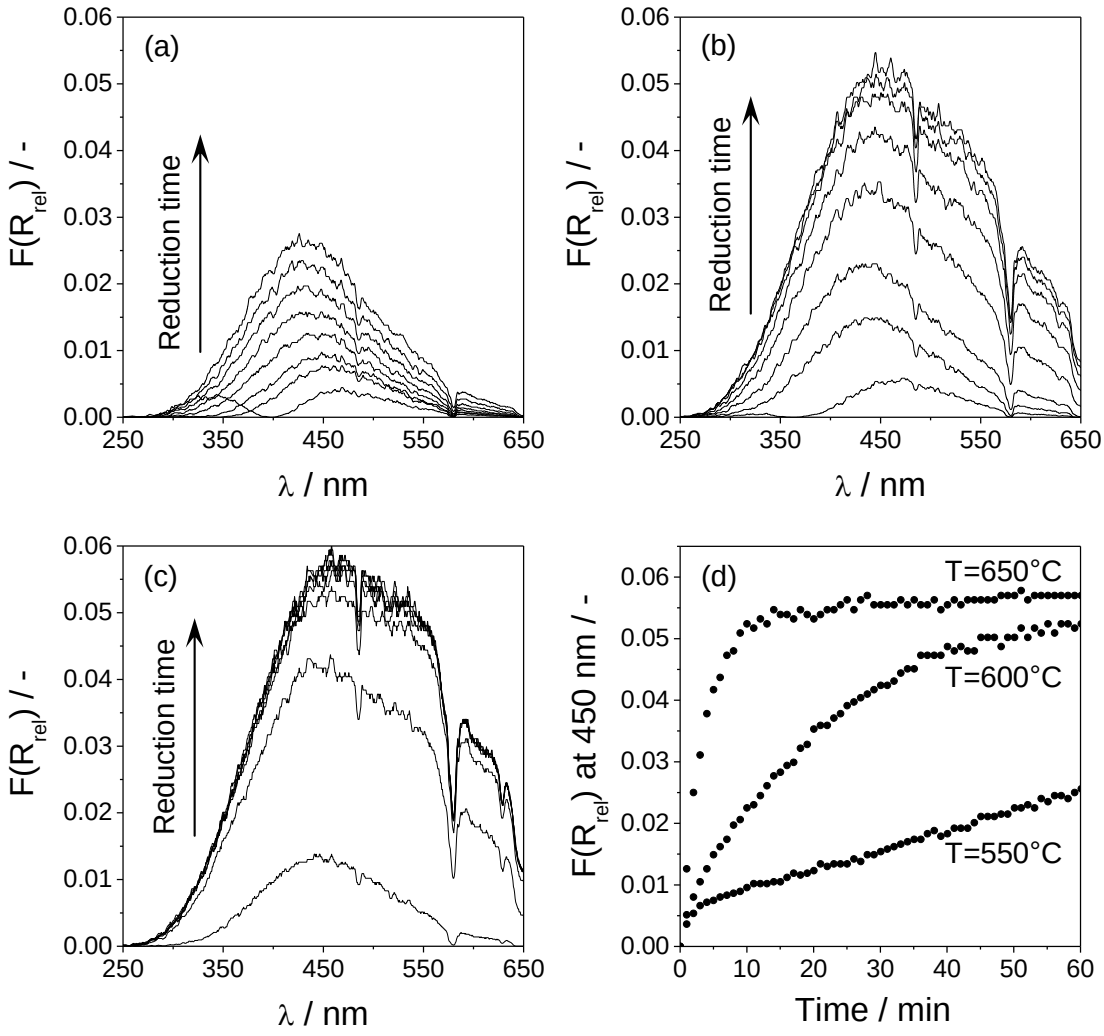

Figure 4-10 UV-vis spectra ($F(R_{rel})$) of $LaZrO_x$ at (a) 550°C, (b) 600°C and (c) 650°C after different times on H_2 stream (57 vol.% in Ar); (d) temporal changes in $F(R_{rel})$ at 450 nm during H_2 treatment of $LaZrO_x$ at 550, 600, and 650°C.

The effect of supported Ru NP on the kinetics of $LaZrO_x$ reduction was also elucidated using on-line UV-vis spectroscopy in diffusion reflection mode. To this end, UV-vis spectra were recorded upon catalyst treatment in an H_2 flow at 550°C and their temporal changes were analyzed. Representative spectra expressed as the relative Kubelka-Munk ($F(R_{rel})$) function after different times on H_2 stream are shown in Figure 4-11 (a) – (c). Again, the increase in intensity of the band at around 450 nm might be caused by the formation of oxygen vacancies.[96] The temporal changes in $F(R_{rel})$ at around 450 nm, which are characteristic for $LaZrO_x$ reduction, were fitted to a simple kinetic model considering removal of lattice oxygen from $LaZrO_x$ by hydrogen (equation (4.5)). For this model, the kinetic equation shown in equation (4.6) is valid.

Since partial pressure of hydrogen does not change significantly during reduction of zirconia, its value can be considered as a constant.

$$xH_2 + ZrO_2 \xrightarrow{k_{red}} ZrO_{2-x} + xH_2O \quad (4.5)$$

$$\frac{dC(ZrO_{2-x})}{dt} = k_{H_2} \cdot p_{H_2} \cdot C(ZrO_2) = k_{red} \cdot C(ZrO_2) \quad (4.6),$$

where k_{red} is a product of the rate constant (k_{H_2}) of ZrO_2 reduction and the partial pressure of H_2 (p_{H_2}), while $C(ZrO_2)$ is concentration of ZrO_2 in UV-vis beam.

Integrating equation (4.6) results in the following expression for the time dependence of the concentration of ZrO_{2-x} (equation (4.7)):

$$C(ZrO_{2-x}) = C^0(ZrO_2) \cdot (1 - exp^{-k_{red} \cdot t}) \quad (4.7),$$

where $C^0(ZrO_2)$ is the maximal concentration of ZrO_2, which can be reduced.

Since the increase in $F(R_{rel})$ at 450 nm is related to the increase in ZrO_{2-x} concentration, the rate constants for the samples containing different Ru loading could be derived from temporal changes of $F(R_{rel})$ at 450 nm. Such changes and the results of their fitting are shown in Figure A-6 in Appendix. The obtained apparent reaction constants are shown in Figure 4-11 (d).

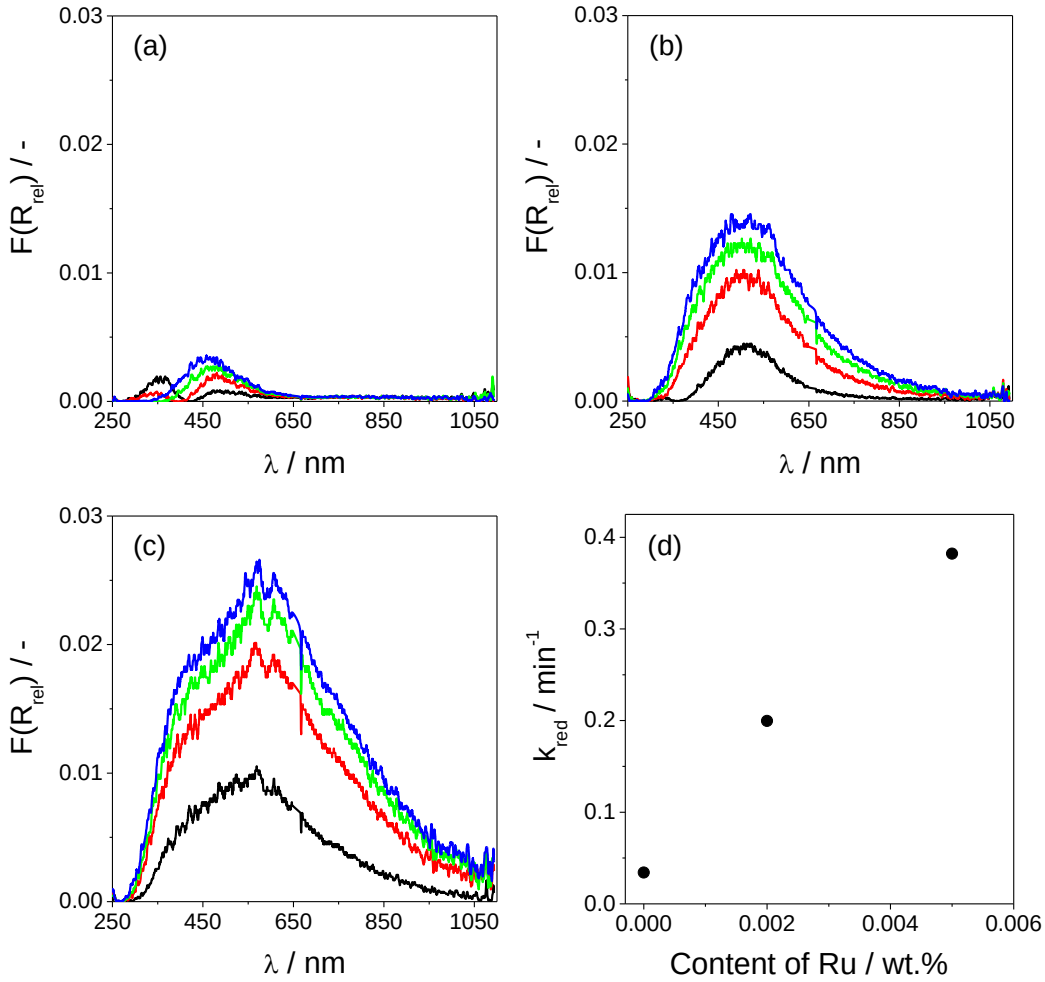

Figure 4-11 $F(R_{rel})$ of (a) $LaZrO_x$, (b) 0.002Ru/$LaZrO_x$, (c) 0.005Ru/$LaZrO_x$ after 1 (–), 5 (–), 10 (–), and 15 (–) minutes on H_2 stream (57 vol.% in Ar) at 550°C. (d) Apparent reaction constant of reduction of Ru/$LaZrO_x$ as a function of Ru content.

Evidently, the rate constant increases with an increase in ruthenium concentration. In other words, Ru NP accelerate reduction of ZrO_2-based oxide. A similar effect of noble metals was reported for other metal oxide supports. For example, noble metals supported on CeO_2-containing materials strongly increase the amount of lattice oxygen removed from this oxide upon catalyst treatment in CO or H_2.[80-82]

4.2.4. Optimizing catalyst composition and treatment for efficient propane dehydrogenation

In order to quantify oxygen vacancies formed at different reduction temperature, O_2-pulse experiments in the TAP reactor were performed with bare $LaZrO_x$ as well as with 0.05Ru/$LaZrO_x$ pre-reduced in H_2 flow at 550, 600 and 650°C for 1 hour. The amount of oxygen vacancies

determined in one gram of the sample as a function of reduction temperature is shown in Figure 4-12. As it was expected, the concentration of oxygen vacancies increases with rising reduction temperature. Such results are in a good agreement with literature data.[97] Interestingly, sample $0.05Ru/LaZrO_x$ contains around 100 times higher amount of anion vacancies compared to bare $LaZrO_x$. Such high amount of oxygen vacancies might be formed due to the well-known phenomenon of support over-reduction in the presence of noble metal in a low loadings (<1 wt.%)).[98-102]

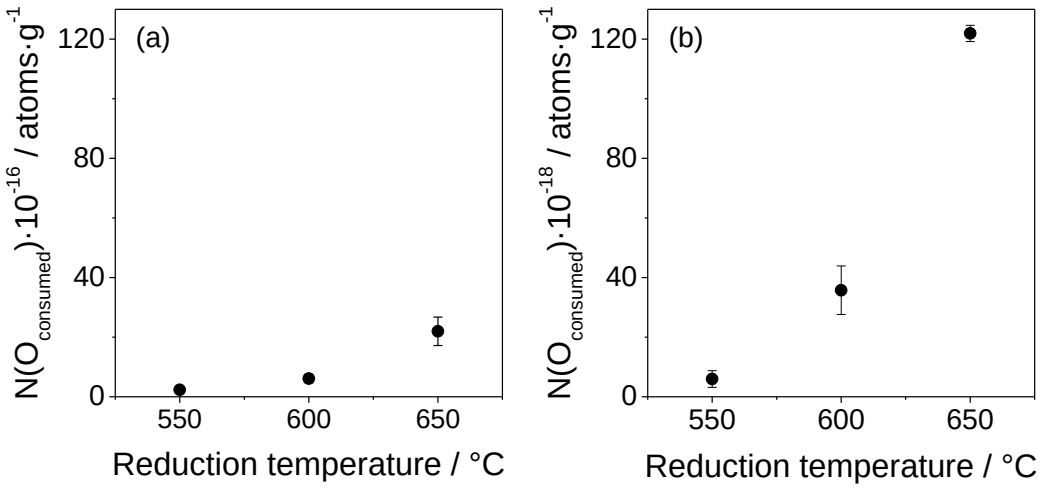

Figure 4-12 Number of oxygen atoms consumed by (a) $LaZrO_x$ and (b) $0.05Ru/LaZrO_x$ upon O_2 pulsing at 550°C as a function of catalyst reduction temperature. Note, the multiplication factor for the Y axis in (a) is 100 times higher than in (b).

Now, the negative effect of over-reduction of $LaZrO_x$ on its catalytic activity observed for Ru-containing samples (see section 4.1.3) will be discussed. A real reason of such effect of over-reduction is not completely clear, however, three possible hypothesizes can exist. Firstly, as it was already proposed (section 4.2.1), both Zr_{cus} and neighboring surface lattice oxygen participate in activation of C-H bond of alkane molecule (Figure 4-13 (a)). The concentration of surface lattice oxygen decreases with increasing degree of catalyst reduction, therefore, activation of C-H bond of propane with the lack of surface oxygen species might become difficult, that prevents C_3H_8 dehydrogenation and results in decreasing activity of the catalysts. Second possible explanation implies that over-reduction of zirconia surface might result in creation of Zr_{cus} sites with higher unsaturation degree which might have lower intrinsic activity in desired reaction. The third hypothesis is related to the high oxygen mobility in zirconia lattice at high temperatures. According to the literature, the higher the temperature, the greater is the oxygen

mobility.[103] Consequently, after certain amount of lattice oxygen is removed from the surface at high temperature, bulk lattice oxygen might diffuse to the surface and refill surface oxygen vacancies, therefore, surface Zr_{cus} sites become saturated and activity of the catalyst drops (Figure 4-13 (b)).

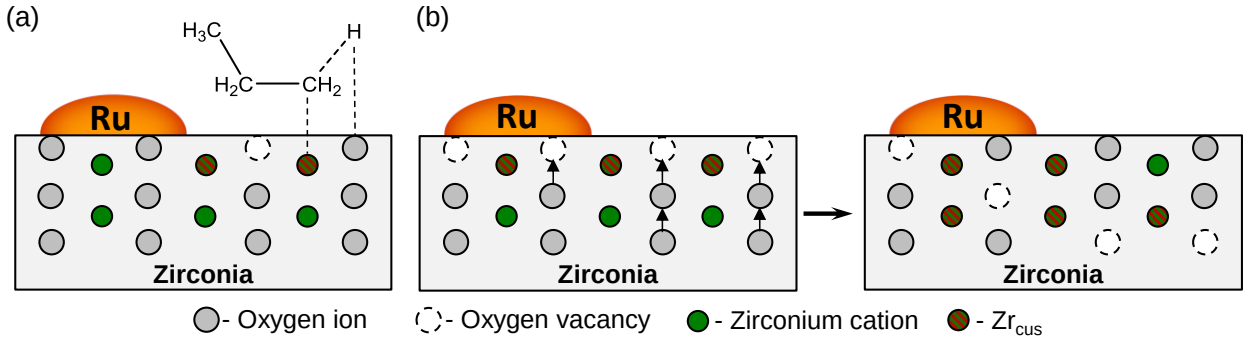

Figure 4-13 Schematic illustration of (a) propane activation over Zr_{cus} and neighboring lattice oxygen and (b) migration of bulk lattice oxygen to the surface.

4.2.5. Summary

The results of catalytic tests performed in an absence and in a presence of probe molecules such as O_2, H_2O and CO_2 as well as some characterization data led to the conclusion that coordinatively unsaturated Zr cations (Zr_{cus} sites) located at oxygen vacancies are active sites in propane dehydrogenation. Their concentration significantly increases during reductive hydrogen treatment in a presence of tiny amounts of hydrogenation-active metals. The role of metal is to contribute to ZrO_2 reduction during hydrogen treatment by creation of highly active hydrogen species which spill over to zirconia surface and remove lattice oxygen. Increasing the temperature of reductive treatment leads to the creation of higher amount of oxygen vacancies and therefore of Zr_{cus} sites. For catalysts containing hydrogenation-active metal, however, reductive treatment at high temperatures might have negative effect on activity due to the over-reduction of ZrO_2-based material. Such effect can be explained by three possible theories. First suggestion implies that over-reduction results in a drop in the concentration of surface lattice oxygen also playing an active role in propane activation. The second idea assumes that intrinsic activity of Zr_{cus} sites might be changed with decreasing their saturation degree. The third hypothesis explains drop in activity by high mobility of zirconia lattice oxygen which causes oxygen diffusion from the bulk to surface resulting in filling surface anion vacancies thus decreasing the concentration of Zr_{cus} sites.

4.3. Doped zirconia for dehydrogenation of propane, n-butane and isobutane

It was shown above that the presence of hydrogenation-active metal on the surface of $LaZrO_x$ provokes formation of oxygen vacancies and respectively of Zr_{cus} during reductive treatment in H_2 flow. The creation of oxygen vacancies, however, is also possible through doping of zirconia with oxides of metals with oxidation state lower than 4+.[104] Here, it will be demonstrated how structural and catalytic properties of zirconia are influenced by the presence and the kind of the dopant.

It is well-known that bare zirconia exists in several structured phases which are stable in different temperature ranges (Figure 4-14).[105] Monoclinic baddelyte structure (m-ZrO_2) is stable below 1175°C, where Zr atoms have distorted sevenfold coordination and O atoms have either fourfold or threefold coordination. Tetragonal distorted fluorite structure (t-ZrO_2) is stable from 1175°C to 2370°C and has eightfold coordinated Zr atoms with two slightly different Zr-O distances and fourfold coordinated O atoms. Cubic fluorite phase (c-ZrO_2) is stable above 2370°C and has perfect eightfold coordination of Zr atoms.[92] Cubic and tetragonal phases can also be stabilized at room temperature after doping of ZrO_2 with Y_2O_3, La_2O_3, CaO, etc. The presence of such additives in the lattice of ZrO_2 leads to the formation of anion vacancies for charge compensation. According to Ref. [106], the formed anion vacancies are responsible for the stabilization of promoted ZrO_2 in the tetragonal or cubic phases. Equations (4.8) and (4.9) illustrate incorporation of di- (M^{2+}) and tri-valent (M^{3+}) metal cations into zirconia lattice in the Kröger–Vink notation.[107]

$$MO \xrightarrow{ZrO_2} M''_{Zr} + O_o^X + V_O^{\bullet\bullet} \qquad (4.8)$$

$$M_2O_3 \xrightarrow{ZrO_2} 2M'_{Zr} + 3O_o^X + V_O^{\bullet\bullet} \qquad (4.9),$$

where M''_{Zr} is a doubly negative ionized substitution site when Zr^{4+} is substituted by M^{2+} and M'_{Zr} is a singly negative ionized substitution site when Zr^{4+} is substituted by M^{3+}.

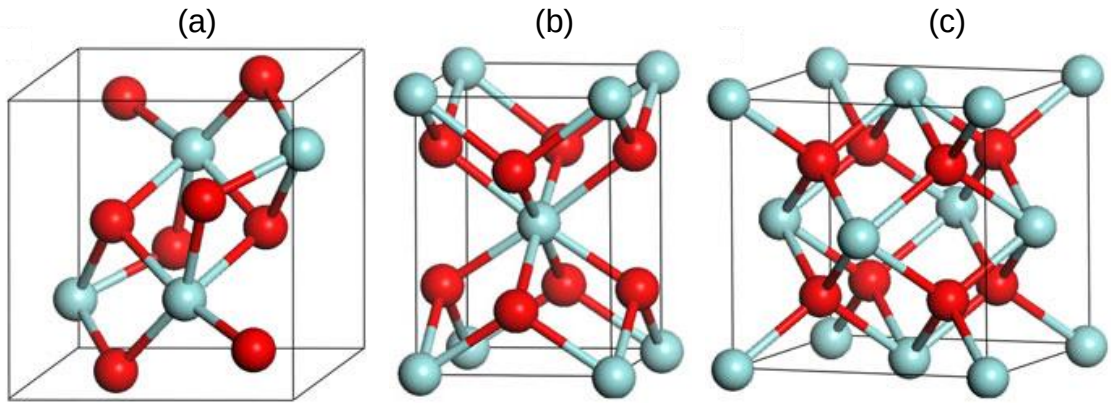

Figure 4-14 Crystal structures of zirconia: a) m-ZrO_2, b) t-ZrO_2 and c) c-ZrO_2. Oxygen and zirconium atoms are illustrated as red and blue spheres, respectively.[105]

Generally, the stabilized t-ZrO_2 and c-ZrO_2 have higher surface area than undoped zirconia even after high-temperature treatment.[108] Moreover, the appearance of oxygen vacancies dramatically influences acid-base, mechanical and electrical properties of resulting stabilized zirconia.[108, 109] For example, Y_2O_3- or CaO-doped zirconia is an excellent ionic conductor which is used in electrochemical oxygen sensors and in solid oxide fuel cells.

In order to study the effect of the presence and the kind of dopant on physicochemical and catalytic properties of zirconia, bare ZrO_2 as well as ZrO_2 promoted with different metal oxides were synthesized, characterized by complementary techniques and tested for their activity and selectivity in dehydrogenation of C_3 – C_4 alkanes. The obtained results are presented and discussed in the next sections.

4.3.1. Selection of materials

As it was mentioned above, the concentration of structural anion vacancies and accordingly Zr_{cus} sites in ZrO_2 can be directly increased through promoting of zirconia with oxides of metals of lower than 4+ oxidation state.[104] Doping with other metals causing distortion in the ZrO_2 lattice can also enhance reducibility of ZrO_2 and thus the concentration of Zr_{cus} sites formed upon reductive treatment. Taking into account this knowledge, several ZrO_2-based oxides possessing different promoting metal cations (Li^+, Mg^{2+}, Ca^{2+}, Ce^{3+}, Al^{3+}, Ti^{4+}, La^{3+}, Bi^{3+}, Nd^{3+}, Sm^{3+}, Ga^{3+}, Y^{3+}) in amount of 10 mol.% (9 mol.% in case of Y^{3+} and 8 mol. % in case of La^{3+}) were either synthesized or used as commercial materials. Their activity for propane dehydrogenation was determined at 550°C after reductive pre-treatment in a flow of 57

vol.% H_2 in N_2 at 550°C for 1 hour. Bare ZrO_2 was also tested. The rate of propene formation determined for the samples is shown in Figure 4-15. It is obvious that not all promoted samples showed higher activity than bare zirconia. Thus, Li_2O-, MgO- and CaO-containing samples demonstrated much lower rates of propene formation than ZrO_2, the activity of Ce_2O_3-, Al_2O_3, and TiO_2-containing samples did not differ significantly from that of ZrO_2; and only other samples possessing La_2O_3, Bi_2O_3, Nd_2O_3, Sm_2O_3, Ga_2O_3, and Y_2O_3 as dopants performed superior to bare ZrO_2.

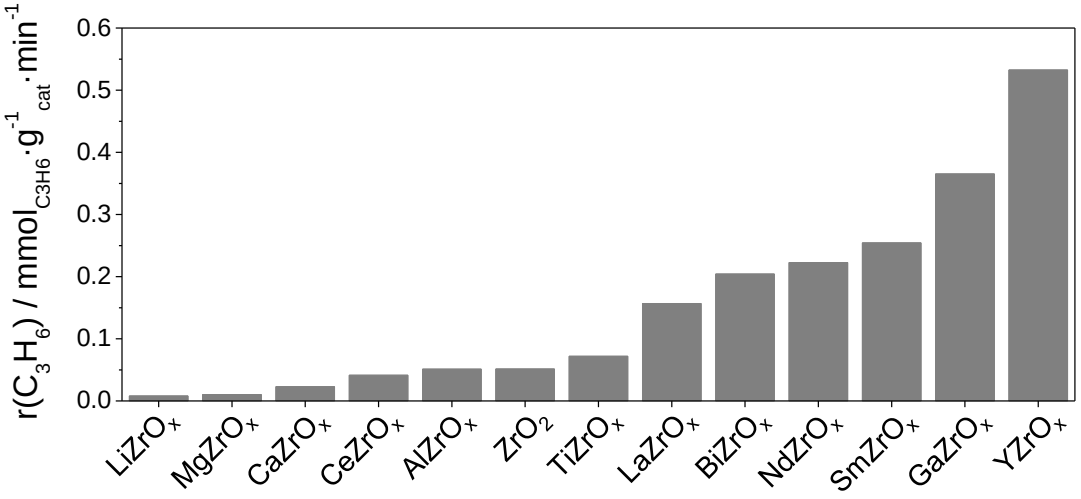

Figure 4-15 Rate of propene formation determined at 550°C for ZrO_2-based mixed oxides.

Based on such primary results, several promoted samples differing in their activity ($LiZrO_x$, $MgZrO_x$, $CaZrO_x$, $LaZrO_x$, $SmZrO_x$, and $YZrO_x$) as well as bare zirconia were chosen for a thorough investigation in order to identify the factors influencing catalytic performance of bulk ZrO_2-catalysts. The samples were characterized by BET, XRD, NH_3-TPD, Raman and O_2-pulse titration methods and tested in dehydrogenation of propane, n-butane and isobutane. Sections 4.3.2 – 4.3.4 deal with catalyst characterisation, while the results of catalytic tests are discussed in sections 4.3.5 – 4.3.6 under consideration of the characterisation data.

4.3.2. Catalysts and their characterization

The composition of ZrO_2-based catalysts and their specific surface areas (S_{BET}) determined according to the BET method are presented in Table 4-1. It is clearly seen that S_{BET} values of the catalysts are significantly influenced by the kind of dopant. Generally, doped catalysts with an exception of $MgZrO_x$ and $LiZrO_x$ have larger specific areas than bare ZrO_2. The

sample $CaZrO_x$ possesses the highest S_{BET} of 95.3 $m^2 \cdot g^{-1}$, while $LiZrO_x$ has the lowest S_{BET} of only 18.4 $m^2 \cdot g^{-1}$.

Table 4-1 Catalyst composition, specific surface area (S_{BET}), amount of oxygen atoms consumed by reduced catalysts during O_2-pulse experiment ($N(O_{consumed})$), and density of acidic sites determined from NH_3-TPD tests with reduced and oxidized samples.

Sample	M^{n+}/Zr^{4+}, mol/mol	S_{BET}, $m^2 \cdot g^{-1}$	$N(O_{consumed}) \cdot 10^{-16}$, atoms$\cdot g^{-1}$	Density of acidic sites, N(sites)$\cdot nm^{-2}$	
				for oxidized samples	for reduced samples
ZrO_2		38.3	0.30 ± 0.04	1.23	1.32
$LaZrO_x$	8/92	84.2	6.1 ± 1.4	0.81	1.06
$YZrO_x$	9/91	73.9	19.0 ± 3.9	0.64	0.87
$SmZrO_x$	10/90	59.5	0.8 ± 0.5	0.53	0.75
$CaZrO_x$	10/90	95.3	BDL*	0.31	0.44
$MgZrO_x$	10/90	37.9	n.m.**	0.42	0.67
$LiZrO_x$	10/90	18.4	BDL*	< 0.01	< 0.01

**BDL – below detection limit*

***n.m. – not measured*

XRD analysis (Figure 4-16) showed that bare ZrO_2 consists of both, m-ZrO_2 and t-ZrO_2 phases with a higher fraction of the former. Sample $LiZrO_x$ mainly consists of a crystallite phase Li_2ZrO_3 with a small admixture of m-ZrO_2. XRD patterns of $LaZrO_x$, $YZrO_x$, $SmZrO_x$, $CaZrO_x$, and $MgZrO_x$ do not have any characteristic peaks of m-ZrO_2 but only contain reflexes related to t-ZrO_2 and/or c-ZrO_2 phases which are however hard to distinguish by XRD due to similar lattice parameters of such phases (a = 0.5094 nm and c = 0.5177 nm for t-ZrO_2 and a = 0.5124 nm for c-ZrO_2).[110] The existence of only metastable tetragonal and/or cubic phases in the doped materials (with an exception of sample $LiZrO_x$) is associated with the stabilizing effect of dopants as it was mentioned elsewhere.[106]

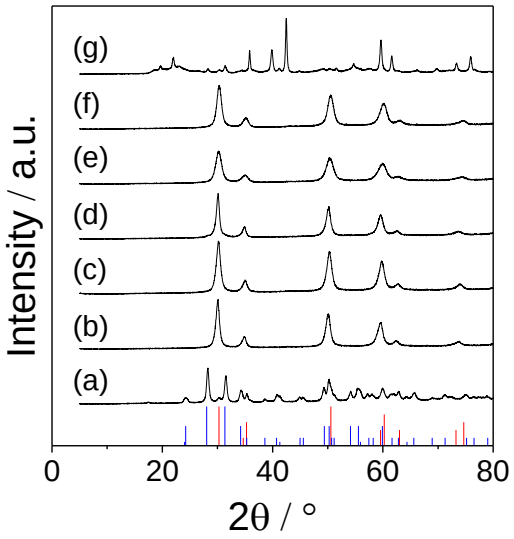

Figure 4-16 XRD patterns of (a) ZrO_2, (b) $LaZrO_x$, (c) $YZrO_x$, (d) $SmZrO_x$, (e) $CaZrO_x$, (f) $MgZrO_x$, and (g) $LiZrO_x$. Blue and red bars are related to m-ZrO_2 (PDF-No. 00-005-0543) and t-ZrO_2 (PDF-No. 01-089-7710) phases, respectively.

ZrO_2, $LaZrO_x$, $YZrO_x$, and $SmZrO_x$ were additionally characterized by Raman spectroscopy in order to determine their phase composition more precisely. This spectroscopy is known to be helpful for distinguishing between cubic and tetragonal ZrO_2 phases.[111] The obtained Raman spectra are shown in Figure 4-17. The spectrum of ZrO_2 contains fourteen Raman bands at 178, 189, 220, 306, 333, 346, 380, 474, 500, 536, 557, 614, 635, and 754 cm^{-1}, which are related to m-ZrO_2.[112] Weak bands at 146 and 265 cm^{-1} might correspond to t-ZrO_2. For the sample $LaZrO_x$ five broad bands specific for t-ZrO_2 at 146, 265, 323, 460, and 633 cm^{-1} were identified. The Raman spectra of $YZrO_x$ and $SmZrO_x$ are similar to that of $LaZrO_x$ but with higher relative intensity of the band located at 633 cm^{-1}, so that, probably the samples contain some admixture of c-ZrO_2 characterized by a broad band in the range 610 – 640 cm^{-1} overlapping with the band of t-ZrO_2.[111] The spectrum of $SmZrO_x$ additionally contains weak bands at 176, 189, and 379 cm^{-1} assigned to m-ZrO_2. The amount of m-ZrO_2 in $SmZrO_x$, however, should not be high since intensity of the characteristic bands of m-ZrO_2 is much lower than that of the bands related to t-ZrO_2.

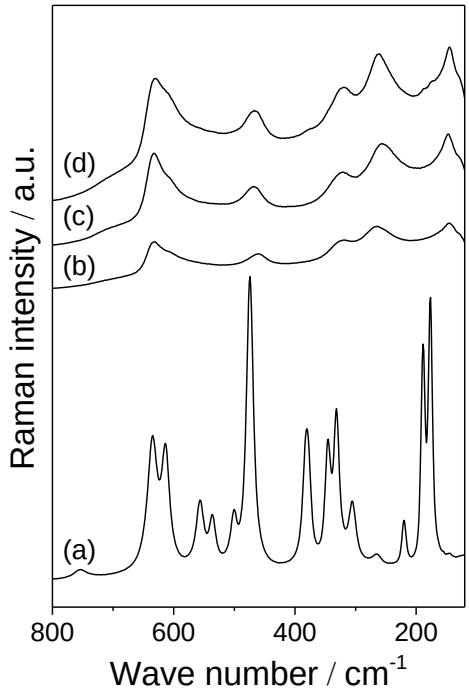

Figure 4-17 Raman spectra of (a) ZrO_2, (b) $LaZrO_x$, (c) $YZrO_x$, and (d) $SmZrO_x$.

4.3.3. Quantification of oxygen vacancies

It was demonstrated in sections 4.2.2 and 4.2.4 that O_2-pulse titration experiments in the TAP reactor are instrumental for determining the concentration of anion vacancies. Therefore, this technique was also applied for characterizing bulk ZrO_2-based catalysts. The concentration of oxygen vacancies in the selected samples pre-reduced at 600°C for 1 hour was determined by O_2-pulse experiment at 550°C. It is worth mentioning that O_2-pulse titration experiments were performed under high-vacuum conditions. Therefore, only highly active anion vacancies, which were created upon reductive catalyst treatment ("generated oxygen vacancies"), can be titrated. Those oxygen vacancies, which appeared in binary ZrO_2-based catalysts for charge compensation ("structural oxygen vacancies"), are stabilized by doped metal cations and unlikely consume gaseous oxygen under such experimental conditions. The number of oxygen atoms consumed by 1 gram of each sample is given in Table 4-1. This number can be considered as the concentration of "generated oxygen vacancies" and is also related to the amount of Zr_{cus} sites located at such defect sites. The highest number of "generated oxygen vacancies" was detected for $YZrO_x$. Since doped zirconia has high mobility of lattice oxygen, the influence of bulk oxygen vacancies on the total amount of oxygen consumed during the O_2-pulse experiments cannot be completely

excluded. The amount of oxygen atoms consumed by $CaZrO_x$ and $LiZrO_x$ was too low to determine it precisely, therefore, according to such results, these samples should contain only negligible amount of surface "generated oxygen vacancies" which is even lower than that of bare ZrO_2. Based on the results obtained, one can conclude that different dopants have different ability to generate/stabilize "generated oxygen vacancies" on the surface of binary ZrO_2-based catalysts. However, the number of "structural oxygen vacancies" is determined by the concentration and valence of doped metal cation. According to Ref. [113], solutions of metal oxides in ZrO_2 are characterized by the stabilization of ZrO_2 into the cubic or tetragonal phases at low temperature. Such stabilization was observed for ZrO_2-based catalysts (Figure 4-16 and Figure 4-17), i.e. binary samples with tetragonal structure should represent solid solutions. Under these considerations and on the basis of equations (4.8) and (4.9), a theoretical number of "structural oxygen vacancies" statistically distributed both in the bulk and on the surface of doped ZrO_2 samples can be estimated. This number changes in the following order: $CaZrO_x$ = $MgZrO_x$ > $SmZrO_x$ > $YZrO_x$ > $LaZrO_x$.

4.3.4. Effect of dopant on acidic properties of ZrO_2-based materials

The surface acidity of the samples calcined in air at 600°C or pre-reduced in 57 vol.% H_2 in Ar at 600°C was investigated by temperature-programmed desorption of ammonia (NH_3-TPD). NH_3-TPD profiles of the samples are shown in Figure 4-18. The corresponding numbers of acidic sites related to one square nanometer of each catalyst calculated according to equation (3.8) are presented in Table 4-1. These numbers were calculated under assumption that one molecule of NH_3 is adsorbed by one acidic site.

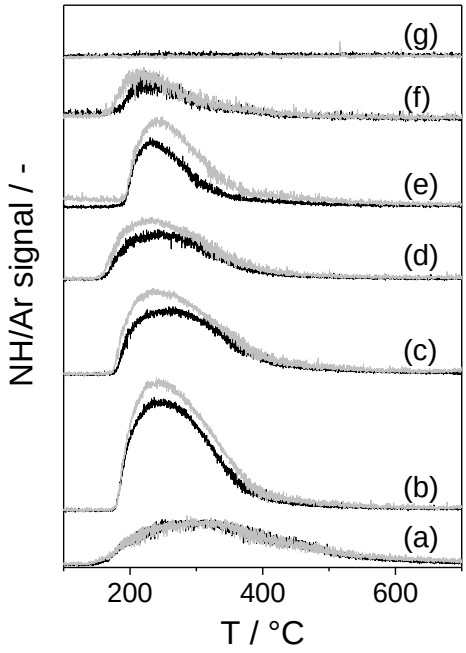

Figure 4-18 The NH_3-TPD profiles for (a) ZrO_2, (b) $LaZrO_x$, (c) $YZrO_x$, (d) $SmZrO_x$, (e) $CaZrO_x$, (f) $MgZrO_x$, (g) $LiZrO_x$. Black and grey lines are related to oxidized and reduced samples respectively.

For $LiZrO_x$, ammonia desorption was detected after neither oxidative nor reductive treatment. Therefore, one can conclude that the surface of this material does not contain any acidic sites able to adsorb ammonia at 120°C. All other samples desorbed ammonia in the temperature range from 150 to 600°C. It is important to mention that the amount of desorbed ammonia was higher for reduced samples than for oxidized ones (Table 4-1). This means that reductive treatment of the samples in hydrogen results in additional creation of acidic sites. Such sites can be only Zr_{cus} sites possessing Lewis acidity.[114] A Lewis character of acidic sites was confirmed by IR data obtained for reduced $YZrO_x$ after pyridine adsorption (Figure A-7 in Appendix). Such sites are located at oxygen vacancies formed through recombination of surface hydroxyl-groups during high-temperature treatment of zirconia as shown in equation (4.10). [91, 115] Creation of oxygen vacancies during reductive treatment might occur through formation of new surface hydroxyls followed by their recombination as shown in equation (4.10) or by direct removal of lattice oxygen with gaseous hydrogen according to equation (4.11). Water release during the heating of $LaZrO_x$ in N_2 flow as well as during reductive treatment of the sample in H_2 in N_2 flow at 600°C was detected by MS technique (Figure A-8 in Appendix). The presence of "generated oxygen vacancies" was proven by the O_2-pulse experiments described in section 4.3.3.

$$-OH + -OH \rightarrow O_{lattice} + vacancy + H_2O \quad (4.10)$$

$$O_{lattice} + H_2 \rightarrow vacancy + H_2O \quad (4.11)$$

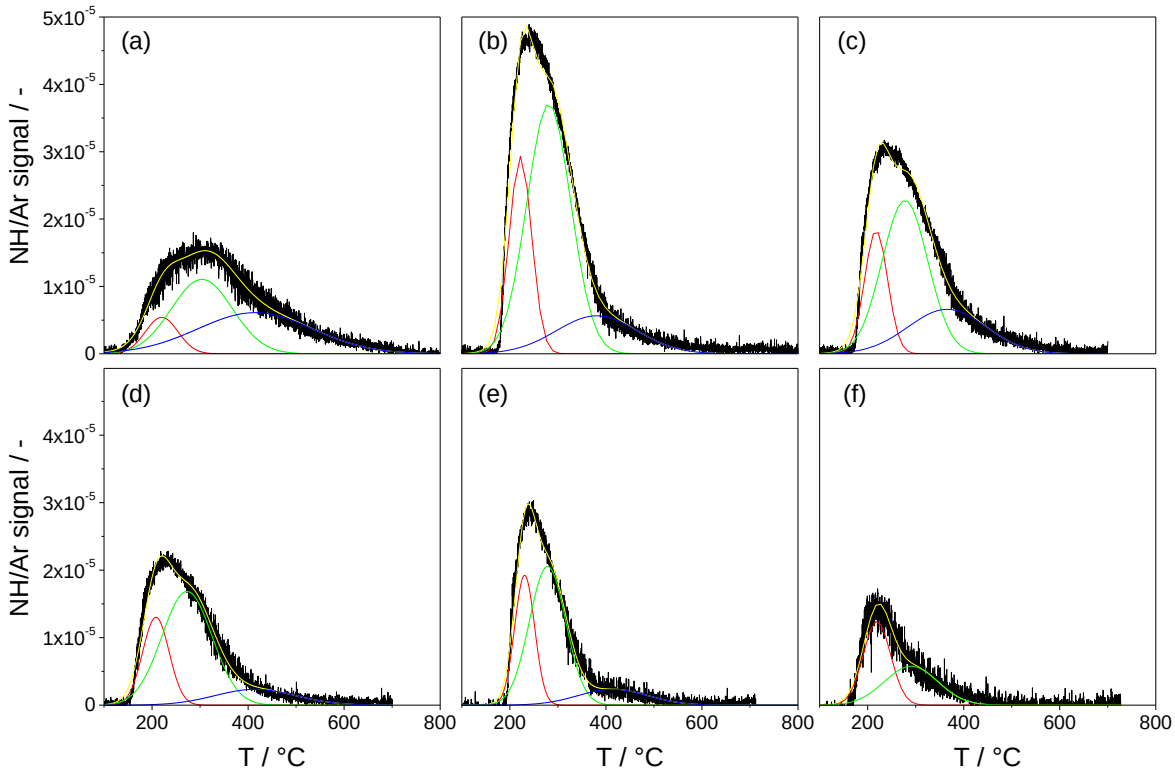

Figure 4-19 Deconvolution of NH_3-TPD profiles for reduced (a) ZrO_2, (b) $LaZrO_x$ (c) $YZrO_x$ (d) $SmZrO_x$, (e) $CaZrO_x$, and (f) $MgZrO_x$.

Noticeably, the presence and the kind of dopant strongly influence the number of acidic sites and their strength. For example, bare ZrO_2 has the highest density of acidic sites, which decreases for promoted samples in the following order: $LaZrO_x$ > $YZrO_x$ > $SmZrO_x$ > $MgZrO_x$ > $CaZrO_x$. Such decrease cannot be only due to the partial substitution of acidic Zr_{cus} by the dopant of a basic nature since it does not correlate with the amount of dopant in zirconia lattice, which was very similar in all these samples. Therefore, it might be possible that the dopant affects the intrinsic acidity of Zr_{cus} sites. Such suggestion is supported by the fact that the temperatures of NH_3 desorption maxima and the fraction of each desorption peak change depending on the sample as was found after deconvolution of NH_3-TPD profiles of reduced catalysts (Figure 4-19 and Table 4-2) using Gaussian function. Three NH_3 desorption maxima at temperatures of 210 – 220°C, 270 – 280°C and at 415°C were identified for each sample (two maxima in case of $MgZrO_x$), which might be related to different types of acidic sites. The position and the fraction

of first two low-temperature maxima are strongly influenced by the kind of promoter, and the fraction of high-temperature maximum at 415°C (related to strong acidic sites) is much smaller for promoted samples compared to bare ZrO_2. Based on the above results, one can conclude that all dopants investigated in the current work cause suppression of strong acidic sites of zirconia.

Table 4-2 Maxima of NH_3-TPD desorption peaks in °C and corresponding amounts of desorbed NH_3 molecules related to nm^2 (numbers in brackets) determined for reduced catalysts.

Sample	1st peak	2nd peak	3rd peak
ZrO_2	220 (0.15)	304 (0.57)	415 (0.60)
$LaZrO_x$	223 (0.25)	283 (0.67)	415 (0.14)
$YZrO_x$	219 (0.16)	281 (0.57)	415 (0.14)
$SmZrO_x$	208 (0.199)	273 (0.46)	415 (0.10)
$CaZrO_x$	231 (0.13)	279 (0.25)	415 (0.06)
$MgZrO_x$	219 (0.35)	291 (0.32)	-
$LiZrO_x$	-	-	-

4.3.5. Influence of the presence and the nature of dopant on dehydrogenation activity of ZrO_2-based materials

Both oxidized (treated with air flow at 600°C for 1 hour) and pre-reduced (treated with 57 vol.% H_2 in N_2 flow at 600°C for 1 hour) samples were tested in propane dehydrogenation at 550°C. The degree of propane conversion was below 10%. This experimental restriction was important to correctly measure the rate of propane dehydrogenation to propene. Figure 4-20 shows the determined rate. For all samples, reductive treatment had a positive effect on the catalytic activity. Such result can be explained by the formation of additional catalytically active sites after the treatment. As discussed in section 4.2, such sites should be Zr_{cus} sites. The formation of additional Zr_{cus} sites during reductive treatment was indirectly confirmed by NH_3-TPD experiment (see section 4.3.4). However, NH_3-TPD tests detected all possible acidic sites on catalyst surface but not all of them are active in PDH since no relationship was found between the difference in a number of acidic sites and the difference in the rate of alkene formation between oxidized and reduced catalysts (Figure A-9 in Appendix). Therefore, certain Zr_{cus} sites with a specified coordination are required for high activity in PDH. A possible structure of active Zr_{cus} sites will be suggested after discussing the results of O_2-titration tests in relation to catalysts activity for dehydrogenation of propane, n-butane and isobutane in this section.

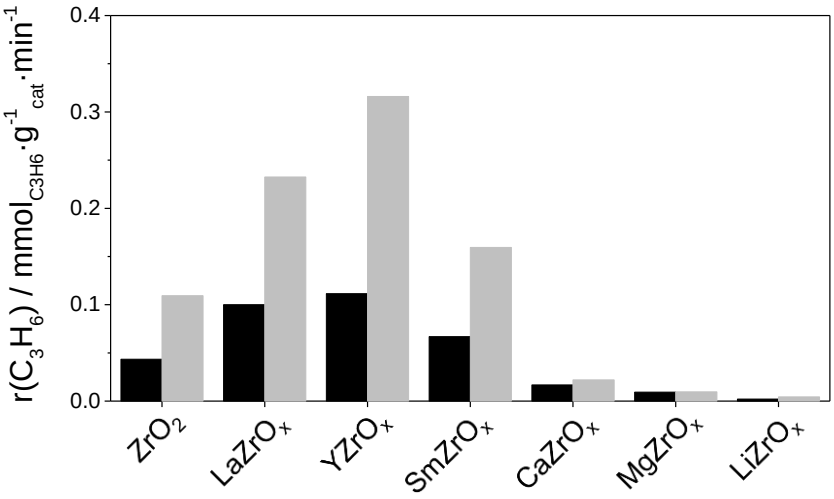

Figure 4-20 Initial rates of propene formation determined at 550°C over oxidized (black bars) and reduced (grey bars) ZrO_2-based catalysts.

From Figure 4-20 it is also seen that the kind of dopant strongly affects catalyst dehydrogenation activity. Regardless the type of catalyst treatment, the presence of La_2O_3, Y_2O_3 and Sm_2O_3 in the lattice of ZrO_2 leads to an increase in the rate of propene formation compared to bare ZrO_2, while the presence of CaO, MgO or Li_2O results in a decrease. The highest rate of propene formation was obtained over reduced $YZrO_x$ which was about three times more active than bare ZrO_2 tested under the same conditions. The results obtained are in a good agreement with the data of O_2-pulse experiments. As seen in Table 4-1, $CaZrO_x$ and $LiZrO_x$ possess lower concentration of "generated oxygen vacancies" (and therefore generated Zr_{cus} sites) than bare ZrO_2. For other samples, the number of "generated oxygen vacancies" increases in the order: $ZrO_2 < SmZrO_x < LaZrO_x < YZrO_x$. The same order was also found for catalyst activity in PDH (Figure 4-20). Therefore, one can conclude that improving dehydrogenation activity of ZrO_2 through doping with La_2O_3, Y_2O_3, and Sm_2O_3 is due to an increase in the number of surface "generated oxygen vacancies". On the other hand, negative effect of the presence of CaO, MgO and Li_2O on the activity of ZrO_2 can be explained by hindering the formation of surface oxygen vacancies (and therefore of Zr_{cus} active sites).

ZrO_2, $SmZrO_x$, $LaZrO_x$, and $YZrO_x$ reduced at 600°C for 1 hour were additionally tested in n-butane and isobutane dehydrogenation. Their activity in these reactions was also found to be in a good correlation with the amount of "generated oxygen vacancies". Figure 4-21 shows the dependence of the rate of propene, n-butenes (1- and 2- (cis- and trans-) isomers) and isobutylene

formation on the amount of oxygen consumed during O_2-pulse experiments. Analyzing these data, one can conclude that the dehydrogenation activity of ZrO_2-based catalysts is strongly influenced by the amount of surface "generated oxygen vacancies". Thus, regardless the fed alkane, the rate of alkene formation increases with rising number of vacancies. The kind of alkane, however, influences the rate of alkene formation which increases in the following order: $r(C_3H_6) < r(n\text{-}C_4H_8) < r(iso\text{-}C_4H_8)$ for all samples. Such difference between propane, n-butane and isobutane dehydrogenation is due to the different strength of the weakest C-H bond in these alkanes.[116]

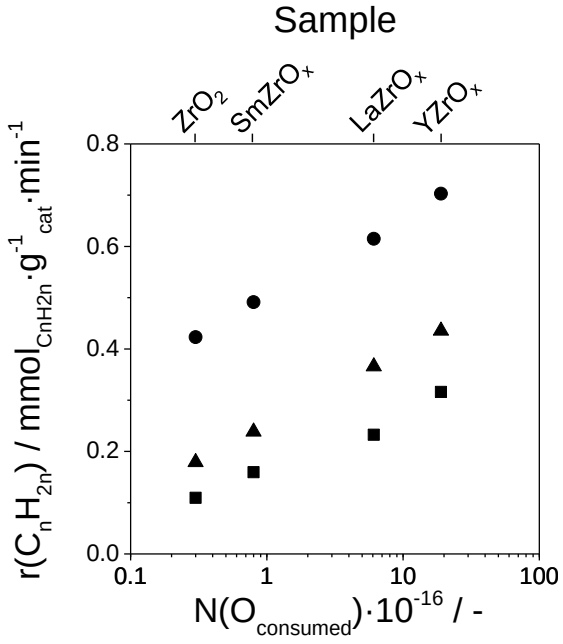

Figure 4-21 Dependence of the rates of (■) propene, (▲) n-butenes, and (●) isobutylene formation on the number of oxygen atoms consumed by ZrO_2, $LaZrO_x$, $YZrO_x$, and $SmZrO_x$ during O_2-pulse experiments.

At this point a possible structure, i.e. coordination, of active Zr_{cus} sites can be proposed after a short discussion. It is obvious that the coordination of zirconium cations located on a flat surface of perfect tetragonal or monoclinic ZrO_2 is 7 or 6. Such sites are coordinatively unsaturated and are more likely able to adsorb ammonia. However, it is unlikely that these sites provide high activity of ZrO_2-based catalysts. As it was shown by O_2-pulse experiments, lattice oxygen is removed from ZrO_2 during reductive treatment. This should result in an additional decrease in the coordination of surface zirconium cations. Since the activity of ZrO_2-based catalysts is in a good correlation with the amount of surface oxygen vacancies created upon

reductive treatment, one can suggest that active Zr_{cus} sites are those with lower than 7 and 6 coordination for t-ZrO_2 and m-ZrO_2, respectively. Such coordination can be achieved if surface zirconium cation is located in steps, kinks, or corners of the lattice of ZrO_2 or neighbors with the oxygen vacancy created due to the presence of dopant.

The effect of the presence and/or the nature of dopant on DH activity was further investigated. To this end, apparent activation energies of propene, n-butenes and isobutylene formation were determined over samples ZrO_2, $LaZrO_x$, $YZrO_x$, $SmZrO_x$, $CaZrO_x$, and $MgZrO_x$ pre-reduced at 600°C. The reaction temperature was varied from 500°C to 600°C. Arrhenius plots obtained are demonstrated in Figure 4-22. The corresponding values of activation energies (E_a) are listed in Table 4-3.

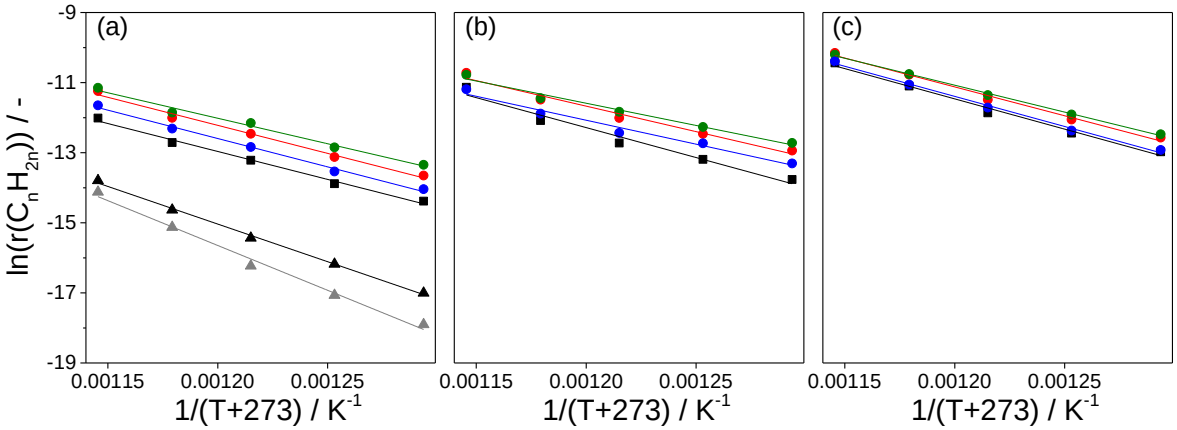

Figure 4-22 Arrhenius plots of (a) propene, (b) n-butenes and (c) isobutylene formation over reduced ■ ZrO_2, ● $LaZrO_x$, ● $YZrO_x$, ● $SmZrO_x$, ▲ $CaZrO_x$, and ▲ $MgZrO_x$ catalysts.

An evident effect of the presence and the kind of dopant on E_a value could be identified. For example, the E_a values for dehydrogenation of different alkanes over $YZrO_x$ were around 10-37 kJ·mol^{-1} lower than over ZrO_2. The E_a values of propane and isobutane dehydrogenation over $LaZrO_x$ and $SmZrO_x$ did not significantly differ from those over ZrO_2. However, the difference became obvious for n-butane dehydrogenation: the E_a values over $LaZrO_x$ and $SmZrO_x$ were about 21 and 28 kJ·mol^{-1} lower than over ZrO_2, respectively. It is also worth mentioning that propane dehydrogenation over $CaZrO_x$ and $MgZrO_x$ is characterized by the highest E_a values among all samples. These values were around 46 and 80 kJ·mol^{-1} higher than that for ZrO_2, respectively (Table 4-3). Therefore, it is more likely that the kind of dopant affects the intrinsic activity of catalytically active sites related to ZrO_2.

O_2-pulse experiments showed that ZrO_2, $LaZrO_x$, $YZrO_x$, and $SmZrO_x$ form "generated oxygen vacancies" after reductive treatment (see section 4.3.3). The number of "structural oxygen vacancies" in bare ZrO_2 should be many orders of magnitude lower than in the binary materials. Therefore, E_a values determined for ZrO_2 can be related only to Zr_{cus} sites located near "generated oxygen vacancies". For other samples, E_a values would be determined by the intrinsic activity of both Zr_{cus} sites located near "generated oxygen vacancies" and near "structural oxygen vacancies". According to the data in Table 4-3, ZrO_2, $LaZrO_x$ and $SmZrO_x$ have similar E_a values for propane and isobutane dehydrogenation. Therefore, for these catalysts, the intrinsic activity of Zr_{cus} sites (structural and generated) in such reactions does not differ strongly. For $YZrO_x$, E_a values lower than for other catalysts tested were obtained. This means that the presence of Y^{3+} in ZrO_2 lattice improves catalytic properties of Zr_{cus} sites. On contrary, Ca^{2+} and Mg^{2+} have a negative effect on Zr_{cus} activity. The E_a values of propane dehydrogenation determined for $CaZrO_x$ and $MgZrO_x$ are much higher than for bare ZrO_2. Since for $CaZrO_x$ no oxygen consumption after reductive treatment could be detected (Table 4-1), this sample might possess only "structural oxygen vacancies" on the surface. The E_a value of propane dehydrogenation over this catalyst is determined by the intrinsic activity of Zr_{cus} sites located near such vacancies. The different effect of the dopants on Zr_{cus} properties might be due to their different electronic properties and radius.[117, 118]

Table 4-3 Apparent activation energies of propene, n-butenes and isobutylene formation determined over catalysts pre-reduced at 600°C.

Sample	$E_a(C_3H_6)$, kJ·mol^{-1}	E_a(n-C_4H_8), kJ·mol^{-1}	E_a(i-C_4H_8), kJ·mol^{-1}
ZrO_2	133 ± 6	142 ± 14	144 ± 8
$LaZrO_x$	133 ± 7	121 ± 10	137 ± 7
$YZrO_x$	121 ± 8	105 ± 8	128 ± 3
$SmZrO_x$	135 ± 6	114 ± 10	143 ± 6
$CaZrO_x$	179 ± 5	n.m.*	n.m.*
$MgZrO_x$	213 ± 12	n.m.*	n.m.*

**n.m. – not measured*

4.3.6. Mechanistic network of alkane dehydrogenation

To check if and how the promoter affects reaction pathways of product formation, mechanistic network of dehydrogenation of propane, n-butane and isobutane over ZrO_2-based catalysts was elucidated. To this end, catalytic tests were performed at 550°C at different degrees

of alkane conversion by varying contact time with the catalysts pre-reduced at 600°C. Analyzing such dependences, parallel and sequential stages of the reaction can be distinguished.[119] On the basis of the obtained results, selectivity-conversion plots were constructed (Figure 4-23).

For propane dehydrogenation, the selectivity to propene decreases with rising conversion for all samples (Figure 4-23 (a)). The strength of the decrease, however, depends on the catalyst studied. Bare ZrO_2 showed the greatest selectivity drop. Thus, propene selectivity of only around 80% was achieved at a degree of propane conversion of 17%. $SmZrO_x$ showed propene selectivity of about 94% at the same conversion degree. The lowest effect of the conversion on propene selectivity was obtained for $LaZrO_x$ and $YZrO_x$. For these samples, the selectivity dropped from about 100% at near to zero conversion to about 96% at 30% propane conversion. The propene selectivity of nearly 100% is achieved for all samples when extrapolating propene selectivity curves to zero conversion. That means that propene is the only product directly formed from propane. Selectivity to coke and cracking products (methane and ethylene) increase from zero (Figure 4-23 (b), (c)) with rising conversion, therefore, coke and cracking products are formed from propene during sequential stages (Figure 4-24 (a)). It should be, however, mentioned that the selectivity towards cracking products did not strongly depend on the catalyst and was about only 2% at the highest propane conversion of 30%. In contrast, coke formation is a major undesired reaction and strongly depends on catalyst composition and conversion degree. The highest coke selectivity of about 18% was achieved over bare ZrO_2 at the conversion of about 17%. All promoted catalysts showed less pronounced tendency to form coke even at higher conversion. Thus, $SmZrO_x$ outperformed ZrO_2 in terms of suppressing coke formation and catalysts $LaZrO_x$ and $YZrO_x$ showed the lowest tendency to coke formation. The difference in catalytic behavior of the samples can be due to their different surface acidity. According to NH_3-TPD results (Figure 4-19 and Table 4-2), the surface of bare ZrO_2 contains high amount of strong acidic sites characterized by a maximum of NH_3 desorption at 415°C. Such sites might strongly adsorb propene and, as a consequence, make favorable condition for the formation of carbon deposits. The presence of dopant decreases surface acidity of zirconia, therefore, formation of coke is suppressed for promoted samples.

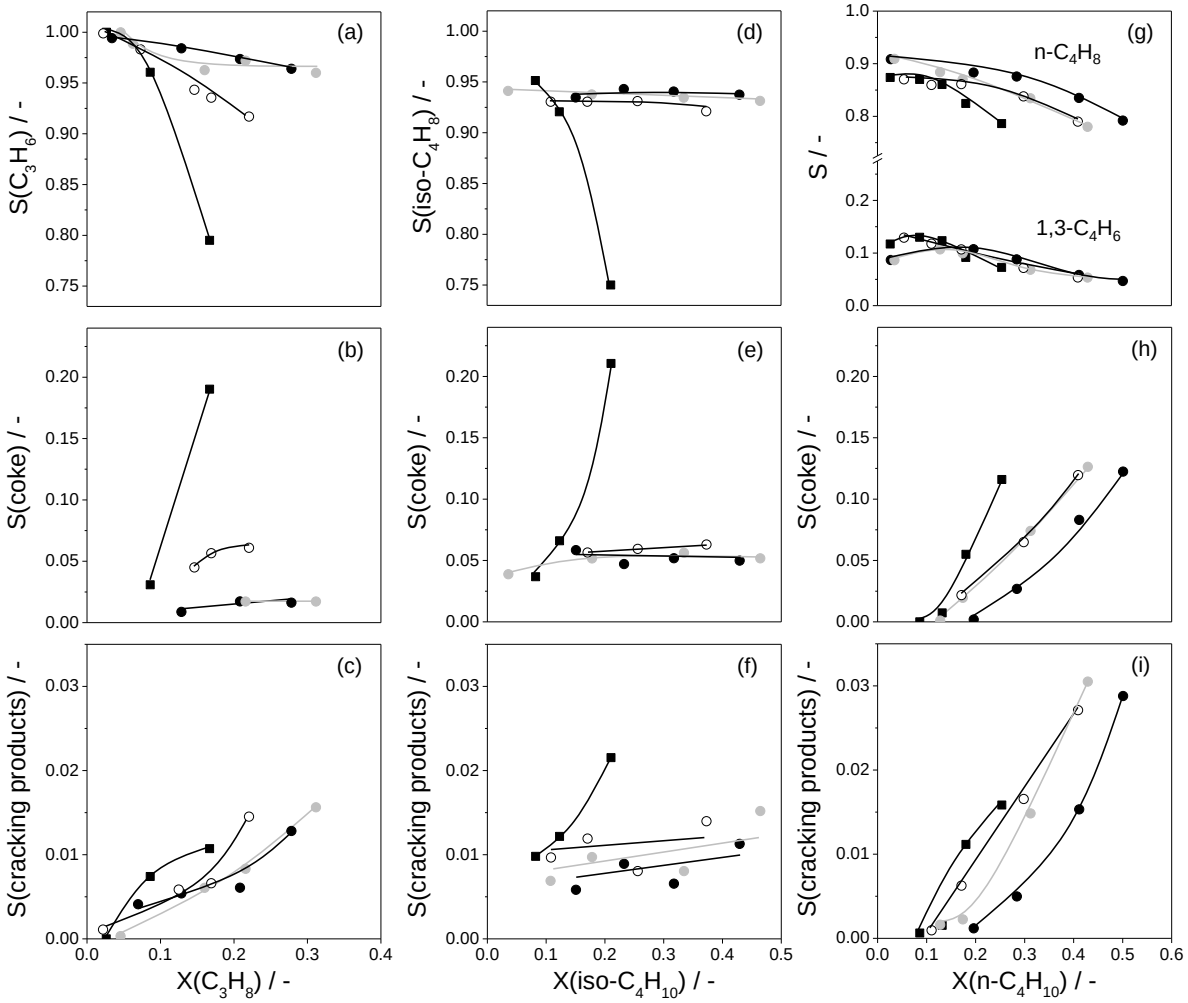

Figure 4-23 Dependence of selectivity to the desired olefins, coke, and cracking products on conversion of propane ((a) – (c)), isobutane ((d) – (f)), and n-butane ((g) – (i)) at 550°C for reduced ■ ZrO_2, ● $LaZrO_x$, ● $YZrO_x$, and ○ $SmZrO_x$ catalysts.

For isobutane dehydrogenation all promoted samples behave similarly in terms of selectivity change. With rising alkane conversion, the selectivity to isobutylene only slightly decreases with the conversion, while the selectivity to coke and cracking products (methane, ethylene, and propene) increases accordingly (Figure 4-23 (d) – (f)). In contrast to propane dehydrogenation, isobutylene selectivity did not achieve 100% at a near to zero isobutane conversion, and extrapolation of selectivity to coke and cracking products to zero conversion did not give 0%. This means that dehydrogenation and side reactions are parallel stages, so that, isobutylene, coke and cracking products are formed from the alkane directly (Figure 4-24 (b), left scheme). Bare ZrO_2 behave differently: isobutylene selectivity dramatically dropped from 95% till 75% with increasing conversion degree from 8% up to 20%. The selectivity to side products

(coke and cracking products) increases accordingly. Based on such results, one can conclude that coke formation and cracking over ZrO_2 occur via parallel and sequential stages with higher contribution of the latter (Figure 4-24 (b), right scheme). Noticeably, formation of coke on ZrO_2 surface was much preferable compared to cracking: the highest coke selectivity of 22% was achieved at a conversion degree of about 20%, while selectivity to cracking products did not exceed 3%. In analogy to propane dehydrogenation, different behavior of bare ZrO_2 in comparison to its promoted counterparts might be related to the presence of strong acidic sites which adsorb isobutylene molecules, thus, provoking their oligomerization.

Dehydrogenation of n-butane over all ZrO_2-based catalysts results in the formation of n-butenes (1- and 2- (cis- and trans-) isomers) and 1,3-butadiene as main gas-phase products (Figure 4-23 (g)). The selectivity to n-butenes decreases with rising conversion and selectivity to 1,3-butadiene slightly increases at the beginning, passed over a maximum at n-butane conversion between 5 and 10%, and decreases at a conversion degree higher than 10%. Extrapolation of selectivity curves to zero conversion gives 88 – 92% and 8 – 12% for n-butenes and 1,3-butadiene, respectively. Thus, n-butenes are directly formed from n-butane, and 1,3-butadiene is formed from n-butane as well as from n-butenes. Moreover, both n-butenes and 1,3-butadiene, participate further in secondary reactions which are formation of coke and cracking products (Figure 4-24 (c)) since the selectivity to these products increases with rising conversion starting from zero (Figure 4-23 (h), (i)). Similar to propane and isobutane dehydrogenation, bare ZrO_2 showed the highest tendency to form undesired side products due to the presence of strong acidic sites.

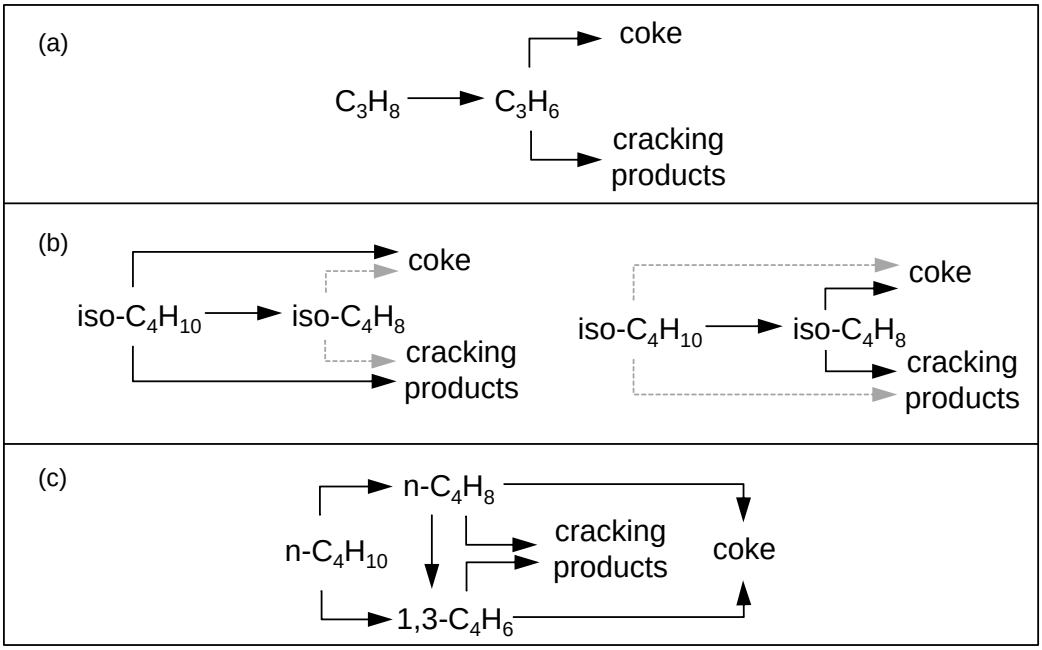

Figure 4-24 Proposed mechanistic schemes for (a) propane, (b) isobutane (left scheme – for $LaZrO_x$, $YZrO_x$ and $SmZrO_x$; right scheme – for bare ZrO_2) and (c) n-butane dehydrogenation. Main reaction paths are marked by solid arrows, while dashed grey arrows represent minor reactions.

4.3.7. Summary

The effect of the presence and the kind of dopant on the activity and selectivity of ZrO_2-based catalysts in dehydrogenation of propane, n-butane and isobutane was investigated. Doping of ZrO_2 with Y_2O_3, La_2O_3 and Sm_2O_3 was found to increase the rate of olefin formation at 550°C compared to bare ZrO_2, while the presence of CaO, MgO and Li_2O has a negative effect on ZrO_2 activity. Different dopants were found to have different ability to generate/stabilize Zr_{cus} sites during reductive catalyst treatment. Moreover, dopant influences intrinsic activity of Zr_{cus} sites. Based on characterization and catalytic data, it was suggested that coordination of Zr_{cus} sites active in dehydrogenation reaction is lower than for the flat surface sites.

Direct and consecutive reaction pathways in the course of dehydrogenation reactions were identified from steady-state tests. The presence of dopant in ZrO_2 lattice was established to inhibit side reactions especially those leading to coke. Better performance of promoted samples compared to bare zirconia in terms of selectivity to desired products is due to the lower concentration of strong acidic sites on their surface.

4.4. CrO_x-containing ZrO_2-based catalysts for propane dehydrogenation

In this chapter, the potential of both bulk $CrZrO_x$ and supported $CrO_x/LaZrO_x$ for propane dehydrogenation is elucidated. The idea behind this is to investigate if there is a synergy effect between two types of dehydrogenation active sites (Cr and Zr_{cus}) in the catalysts in terms of their activity in PDH.

Generally, industrial chromia-based catalysts contain alumina as a support. However, the usage of zirconia instead of alumina is known to result in a higher activity of the catalyst in propane dehydrogenation.[37, 120-123] Some authors suggested that such effect is due to the ability of ZrO_2 to stabilize highly dispersed supported CrO_x species which are easily reduced to the active mononuclear Cr^{3+} species under reaction conditions.[120, 121] Not only supported but also bulk Cr_2O_3–ZrO_2 catalysts were found to be highly efficient catalysts for propane dehydrogenation, nevertheless, these catalysts are not investigated thoroughly. Only recently, Wu et al. introduced such catalysts in their short communication.[124] The authors determined that calcined catalysts possessed high amount of Cr^{6+} species, which can be transformed into highly dispersed catalytically active Cr^{3+} species under reductive conditions positively influencing catalyst activity. It was concluded that the presence of such species in mixed Cr_2O_3–ZrO_2 oxides is the key factor determining their high activity. The role of ZrO_2 was not discussed by the authors. However, as it was shown in the previous chapters of this thesis, zirconia also shows high activity in alkane dehydrogenation reaction. Therefore, the objective was to investigate if there is a synergy effect between two types (Cr and Zr_{cus}) of catalytically active sites in PDH.

4.4.1. Catalysts and their characterization

The samples studied in the current work can be divided into three groups: bulk $CrZrO_x$ catalysts containing Zr_{cus} or both Zr_{cus} and Cr active sites (ZrO_2, $Zr_{99.5}Cr_{0.5}O_x$, $Zr_{98}Cr_2O_x$, $Zr_{95}Cr_5O_x$, and $Zr_{90}Cr_{10}O_x$), supported $CrO_x/LaZrO_x$ catalysts containing both Zr_{cus} and Cr active sites ($0.05Cr_2O_3/LaZrO_x$, $0.15Cr_2O_3/LaZrO_x$, $0.5Cr_2O_3/LaZrO_x$, $1.5Cr_2O_3/LaZrO_x$, and $3.2Cr_2O_3/LaZrO_x$) and supported CrO_x/Al_2O_3 catalysts containing only Cr active sites ($0.08Cr_2O_3/Al_2O_3$, $0.8Cr_2O_3/Al_2O_3$, and $5.1Cr_2O_3/Al_2O_3$). The nominal weight percentage of Cr_2O_3 in the catalysts (Table 4-4) was calculated under the assumption that all chromium in the samples would exist as Cr_2O_3 after reductive treatment.

Table 4-4 Catalysts and their characteristics: total chromium content ($\omega(Cr_2O_3)$), specific surface area (S_{BET}), surface chromium content ($N(Cr_{surf})$) and temperatures of maximal consumption of hydrogen (T_{maxH2}).

Group	Sample	$\omega(Cr_2O_3)$, wt.%	S_{BET}, $m^2 \cdot g^{-1}$	$N(Cr_{surf})$, atoms$\cdot g^{-1}$	T_{maxH2}, °C
	ZrO_2	0	38.3	0	> 620
	$Zr_{99.5}Cr_{0.5}O_x$	0.31	47.4	$2.0 \cdot 10^{18}$	330, 372, 470
I	$Zr_{98}Cr_2O_x$	1.24	63.2	$1.1 \cdot 10^{19}$	321, 367, 468
	$Zr_{95}Cr_5O_x$	3.14	97.5	$4.2 \cdot 10^{19}$	339, 367, 452
	$Zr_{90}Cr_{10}O_x$	6.42	135.5	$1.2 \cdot 10^{20}$	386, 447
	$0.05Cr_2O_3/LaZrO_x$	0.05	119.0	$4.0 \cdot 10^{18}$	
	$0.15Cr_2O_3/LaZrO_x$	0.15	119.9	$1.2 \cdot 10^{19}$	404
II	$0.5Cr_2O_3/LaZrO_x$	0.5	103.2	$4.0 \cdot 10^{19}$	404
	$1.5Cr_2O_3/LaZrO_x$	1.5	135.4	$1.2 \cdot 10^{20}$	390
	$3.2Cr_2O_3/LaZrO_x$	3.2	128.5	$2.5 \cdot 10^{20}$	427
	$0.08Cr_2O_3/Al_2O_3$	0.08	171.2	$6.3 \cdot 10^{18}$	
III	$0.8Cr_2O_3/Al_2O_3$	0.8	172.0	$6.3 \cdot 10^{19}$	423
	$5.1Cr_2O_3/Al_2O_3$	5.1	176.0	$4.0 \cdot 10^{20}$	402

The specific surface area (S_{BET}) of freshly prepared samples is shown in Table 4-4. For the bulk catalysts, an increase in Cr content resulted in an augmentation of the S_{BET} which reached the highest value of 135.5 $m^2 \cdot g^{-1}$ for $Zr_{90}Cr_{10}O_x$. The surface area of the catalysts from the second group was in the range from 103.2 to 135.4 $m^2 \cdot g^{-1}$. Such high surface area of the catalysts was achieved due to the usage of non-calcined $LaZrO_x$ as a support with S_{BET} of 309.6 $m^2 \cdot g^{-1}$. Since the presence of small amount of dopant in zirconia lattice results in stabilization of metastable tetragonal (and/or cubic) ZrO_2 phase, $LaZrO_x$ has higher surface area than undoped ZrO_2. The high surface area can be maintained even after calcination at high temperatures.[108] Therefore, the usage of $LaZrO_x$ as a support might help to stabilize highly dispersed CrO_x species.[125] It is worth mentioning that bare $LaZrO_x$ calcined at the same temperature as supported samples (550°C for 4 hours) had lower S_{BET} (only 84.2 $m^2 \cdot g^{-1}$) than $CrO_x/LaZrO_x$. The higher surface area of Cr-containing samples can be explained by the stabilizing function of chromium which was previously observed.[125, 126] The samples from the third group were prepared by using commercial Al_2O_3 with S_{BET} of 199.7 $m^2 \cdot g^{-1}$. The surface area of the catalysts did not differ significantly with changing chromium content thus proving that pores of bare Al_2O_3 were not blocked.

The surface chromium content ($N(Cr_{surf})$) for bulk $CrZrO_x$ catalysts was calculated under assumption that the (101) face is the most common plane in t-ZrO_2.[127] Therefore, about 8.6 surface atoms of Zr are located in 1 nm^2 of ZrO_2. It will be, however, shown below that the

samples $Zr_{99.5}Cr_{0.5}O_x$, $Zr_{98}Cr_2O_x$, $Zr_{95}Cr_5O_x$ contain both m-ZrO_2 and t-ZrO_2, nevertheless, the most stable (111) and ($\bar{1}11$) surfaces of m-ZrO_2 contain about 8.1 and 9.0 surface atoms of Zr in 1 nm^2, respectively,[115, 128] which are close to the corresponding number for t-ZrO_2. Taking into account that for $CrZrO_x$ some surface Zr atoms are substituted with Cr atoms, the N(Cr_{surf}) values were calculated in accordance with a nominal Zr/Cr ratio (see Table 4-4). For supported $CrO_x/LaZrO_x$ and CrO_x/Al_2O_3 samples, the N(Cr_{surf}) values were calculated from nominal content of chromium under assumption that all chromium species are located on the surface.

The XRD patterns of the bulk $CrZrO_x$ materials are shown in Figure 4-25 (a). For the catalysts with a Cr loading below 10 mol.%, both m-ZrO_2 and t-ZrO_2 phases were identified. It is, however, worth mentioning that the fraction of t-ZrO_2 increased with rising Cr content. Thus, XRD patterns of $Zr_{90}Cr_{10}O_x$ contained only characteristic reflexes of t-ZrO_2. For all bulk catalysts, no reflexes related to phases of chromium oxides were identified. Stabilization of t-ZrO_2 phase and the absence of any separate CrO_x phase indirectly confirmed incorporation of chromium ions into ZrO_2 lattice with the formation of binary solution. Moreover, XPS analysis additionally confirmed the formation of homogeneous binary CrO_x-ZrO_2 solution by determining atomic ratio of Zr/Cr in the near-surface region. For the samples $Zr_{90}Cr_{10}O_x$ and $Zr_{95}Cr_5O_x$, this ratio was found to be 11 and 17 which is close to the theoretical values of 9 and 19 calculated based on sample composition. Therefore, chromium is incorporated into ZrO_2 lattice, and any enrichment of Cr at the surface of the samples can be excluded. For the samples $Zr_{98}Cr_2O_x$ and $Zr_{99.5}Cr_{0.5}O_x$, the content of Cr on the surface was too low to be determined by XPS analysis.

The XRD patterns of supported $CrO_x/LaZrO_x$ (Figure 4-25 (b)) contain only characteristic reflexes of t-ZrO_2 phase related to $LaZrO_x$. No reflexes corresponding to phases of chromium oxides were identified probably due to the low amount of chromium oxide and/or its high dispersion on the support.[129] The XRD patterns of supported CrO_x/Al_2O_3 catalysts (Figure 4-25 (c)) contained only reflexes related to γ-Al_2O_3 support.

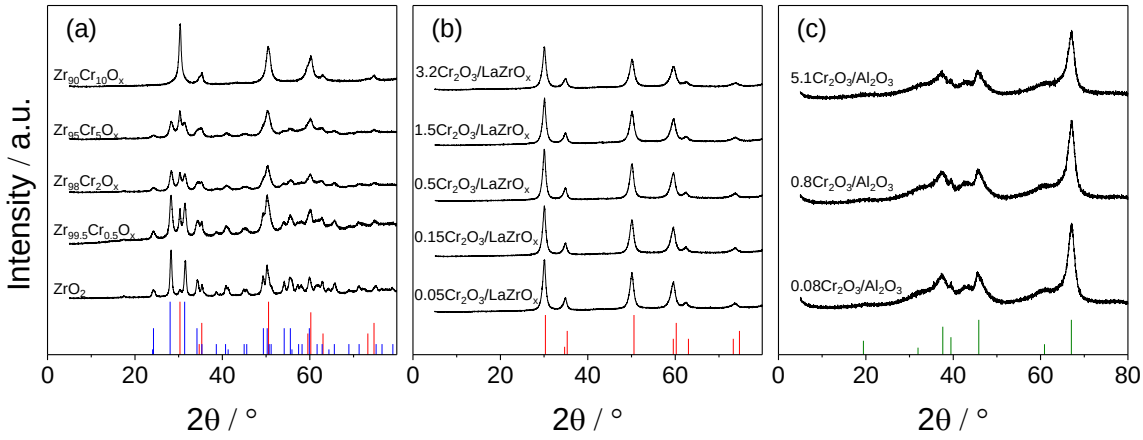

Figure 4-25 XRD patterns of (a) bulk $CrZrO_x$, (b) supported $CrO_x/LaZrO_x$ and (c) supported CrO_x/Al_2O_3. Blue and red bars are related to m-ZrO_2 (PDF-No. 00-005-0543) and t-ZrO_2 (PDF-No. 01-089-7710) phases, respectively, and green bars are related to γ-Al_2O_3 (PDF-No. 00-010-0425) phase.

Redox properties of the samples were investigated by H_2-TPR tests. The H_2-TPR profiles of all samples are shown in Figure 4-26, and the temperatures of maximal consumption of hydrogen (T_{maxH2}) are listed in Table 4-4. Figure 4-26 (a) shows the data for bulk $CrZrO_x$ catalysts. According to the obtained results, ZrO_2 consumed only a small amount of hydrogen at temperatures higher than 620°C due to the reaction of gaseous hydrogen with surface oxygen of zirconia.[79] For the catalysts $Zr_{99.5}Cr_{0.5}O_x$, $Zr_{98}Cr_2O_x$, and $Zr_{95}Cr_5O_x$, three signals of hydrogen uptake between 320 – 340°C, 365 – 375°C and 450 – 470°C can be distinguished. For $Zr_{90}Cr_{10}O_x$, the first two peaks are not well resolved. Since the intensity of the first and second peaks increases with rising chromium content, they might be related to the reduction of surface (low-temperature peak) and bulk (high-temperature peak) Cr^{6+} species. The intensity of the third weak peak of hydrogen uptake between 450 and 470°C only slightly increases with increasing chromium content, however, the position of the peak is shifted to lower temperatures for the samples containing high amount of chromium. Therefore, the third peak might be attributed to the reaction of hydrogen with surface lattice oxygen bonded to zirconium cations. Chromium species are suggested to activate H_2 with the formation of highly reactive hydrogen species. Such species can then react with zirconia removing its lattice oxygen.[130] Therefore, T_{maxH2} became lower with increasing chromium content.

The H_2-TPR profiles of supported $CrO_x/LaZrO_x$ are shown in Figure 4-26 (b). For the sample $0.05CrO_x/LaZrO_x$, the TPR profile is characterized by a strong signal background, no

well-resolved peaks of hydrogen consumption could be identified. For other samples, one peak of hydrogen uptake between 390 and 430°C caused by reduction of Cr^{6+} species to Cr^{3+} was detected. No correlation between position of the peak and chromium amount was found; however, T_{maxH2} values for all samples are shifted to higher temperatures compared to those determined for bulk $CrZrO_x$ catalysts. Therefore, one can conclude that redox properties of CrO_x-species are strongly affected by the type how chromium cations are connected with ZrO_2, i.e. supported CrO_x vs. Cr located in cation positions inside the lattice of ZrO_2. The H_2-TPR profiles of supported CrO_x/Al_2O_3 catalysts (Figure 4-26 (c)) are generally characterized by one consumption peak due to the single stage reduction of Cr^{6+} species to Cr^{3+}.[131] Similarly to $CrO_x/LaZrO_x$, T_{maxH2} of CrO_x/Al_2O_3 catalysts are shifted to higher temperatures compared to those of $CrZrO_x$ catalysts. For $0.08Cr_2O_3/Al_2O_3$ no visible hydrogen uptake was detected due to the low content of chromium in the sample.

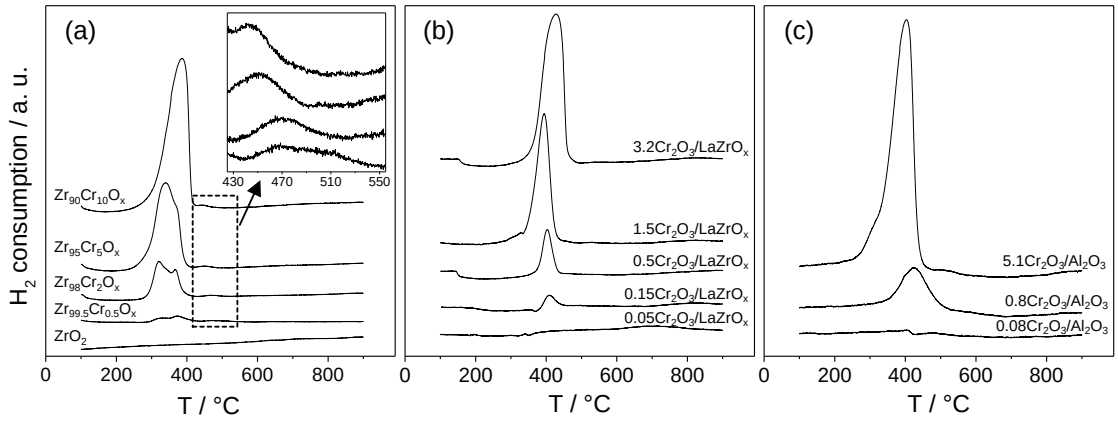

Figure 4-26 The H_2-TPR profiles of (a) bulk $CrZrO_x$, (b) supported $CrO_x/LaZrO_x$ and (c) supported CrO_x/Al_2O_3.

4.4.2. Effect of chromium on acidic properties of ZrO_2-based catalysts

Bulk $CrZrO_x$ as well as selected supported $CrO_x/LaZrO_x$ ($0.5CrO_x/LaZrO_x$ and $3.2CrO_x/LaZrO_x$) catalysts were compared with each other in terms of surface acidity. The NH_3-TPD profiles are shown in Figure 4-27 for the samples pre-reduced in 57 vol.% H_2 in Ar at 550°C for 1 hour. The deconvolution of such profiles resulted in identification of three peaks with maxima in the temperature ranges 202 – 231°C, 235 – 304°C and 317 – 403°C (Figure 4-27 and Table 4-5). Such maxima could be referred to three types of surface acidic sites differing in their strength, i.e. the higher the temperature, the stronger are the acidic sites.

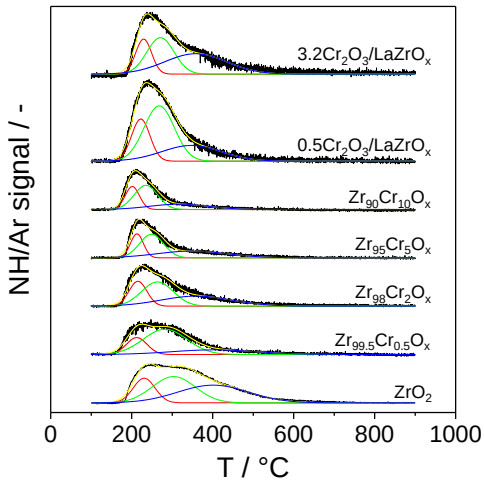

Figure 4-27 The NH_3-TPD profiles and their deconvolution for reduced bulk $CrZrO_x$, $0.5CrO_x/LaZrO_x$ and $3.2CrO_x/LaZrO_x$.

An overall density of acidic sites was calculated under assumption that one molecule of ammonia can be adsorbed on one acidic site according to equation (3.8). The data obtained for the samples tested are listed in Table 4-5. Bare ZrO_2 is characterized by the highest density of acidic sites as well as by the largest contribution of strong acidic sites (the third maximum in NH_3-TPD profile in Figure 4-27) to the overall surface acidity. For both bulk $CrZrO_x$ and supported $CrO_x/LaZrO_x$ samples, the density of acidic sites decreased with increasing chromium content. Moreover, for bulk $CrZrO_x$, the third NH_3-desorption maximum related to strong acidic sites shifted to lower temperature with rising chromium concentration. In most cases the contribution of the third maximum to the total surface acidity also became lower. Based on such results, one can conclude that the increasing chromium amount in the samples results in decreasing overall acidity and suppressing strong acidic sites.

Table 4-5 Total density of acidic sites, maxima of NH_3-TPD desorption peaks in °C and corresponding fraction of each peak (numbers in brackets) determined for reduced samples.

Sample	Density of acidic sites, N(sites)·nm^{-2}	1st peak	2nd peak	3rd peak
ZrO_2	1.59	231 (18.4%)	304 (38.7%)	401 (42.9%)
$Zr_{99.5}Cr_{0.5}O_x$	0.76	212 (18.9%)	282 (59.8%)	403 (21.3%)
$Zr_{98}Cr_2O_x$	0.60	215 (23.1%)	264 (39.9%)	360 (37.0%)
$Zr_{95}Cr_5O_x$	0.28	213 (23.0%)	249 (41.9%)	349 (35.1%)
$Zr_{90}Cr_{10}O_x$	0.20	202 (27.1%)	235 (47.3%)	317 (25.6%)
$0.5Cr_2O_3/LaZrO_x$	0.60	222 (22.8%)	267 (49.6%)	347 (27.6%)
$3.2Cr_2O_3/LaZrO_x$	0.48	229 (19.8%)	271 (35.4%)	357 (44.8%)

4.4.3. Catalyst activity and the kind of active sites

In order to compare the activity of the catalysts from three different groups as defined in section 4.4.1, all samples were tested in propane dehydrogenation at 550°C and at conversion degree lower than 10%. Prior to the experiment, the catalysts were pre-reduced in a flow of 57 vol.% H_2 in N_2 at 550°C for 1 hour. Figure 4-28 shows the rate of propene formation determined for each sample. The rate of propene formation over bare ZrO_2 was similar to that over the sample $0.8Cr_2O_3/Al_2O_3$ and was about three times higher than over $0.08Cr_2O_3/Al_2O_3$. Doping of zirconia with only 0.5 mol.% Cr (sample $Zr_{99.5}Cr_{0.5}O_x$) resulted in an increase in the activity by a factor of higher than 5. With rising chromium content the activity of the catalysts from all three groups increased gradually. Samples $Zr_{98}Cr_2O_x$ and $0.15Cr_2O_3/LaZrO_x$ from the first and second group possessing both Zr_{cus} and Cr active sites showed much higher activity than $5.1Cr_2O_3/Al_2O_3$ from the third group possessing only Cr active sites. It is worth mentioning that the former two catalysts contained about 4 and 34 times lower total amount of chromium than $5.1Cr_2O_3/Al_2O_3$, respectively (see Table 4-4). It should be, however, mentioned that the surface concentration of chromium in the bulk catalyst from the first group is significantly lower than for supported samples from the second and third groups. The highest activity among all catalysts was achieved over $Zr_{90}Cr_{10}O_x$. The rate of propene formation over $3.2Cr_2O_3/LaZrO_x$ was only about 7% lower than that of $Zr_{90}Cr_{10}O_x$ and about 6.5 times higher than that of $5.1Cr_2O_3/Al_2O_3$. However, chromium content for $5.1Cr_2O_3/Al_2O_3$ is about 1.6 times higher than that for $3.2Cr_2O_3/LaZrO_x$.

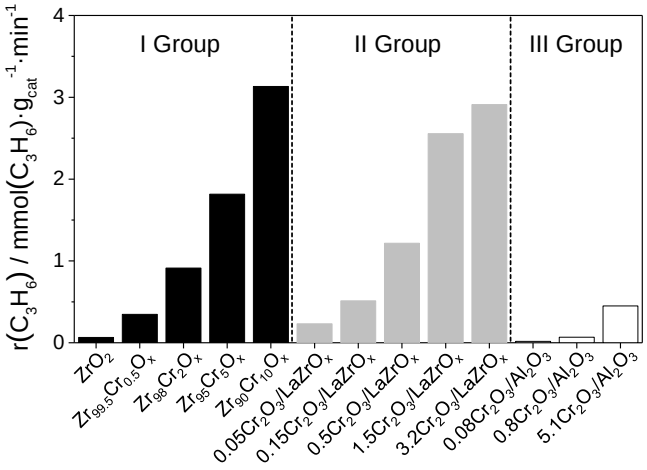

Figure 4-28 Rate of propene formation determined at 550°C over pre-reduced bulk $CrZrO_x$ (I Group), supported $CrO_x/LaZrO_x$ (II Group) and supported CrO_x/Al_2O_3 (III Group) catalysts.

To check if Cr sites are the only active species, TOF values with respect to one surface Cr atom were calculated for each sample. For bulk catalysts, an apparent surface density of chromium was calculated based on the XPS data and nominal concentration of the metal according to Cr/Zr molar ratio, for supported catalysts, an overall amount of chromium was used. Figure 4-29 shows the TOF values as a function of apparent surface density of chromium determined for the catalysts from different groups. It is obvious that the TOF values for bulk $CrZrO_x$ catalysts are higher than for supported $CrO_x/LaZrO_x$ and CrO_x/Al_2O_3 thus implying that for achieving high intrinsic activity of Cr atoms, bulk catalysts are preferable compared to their supported counterparts. Noticeably, for both bulk $CrZrO_x$ and supported $CrO_x/LaZrO_x$, the TOF values decreased with an increase in surface density of chromium. Such observation additionally confirmed that Cr is not the only active species in the catalysts containing ZrO_2. Zr_{cus} sites might also contribute to the total activity of $CrZrO_x$ and $CrO_x/LaZrO_x$ catalysts. In contrast to $CrZrO_x$ and $CrO_x/LaZrO_x$ materials, the TOF values for supported CrO_x/Al_2O_3 catalysts did not depend on chromium surface density thus proving that Cr is the only catalytically active species for the latter samples.

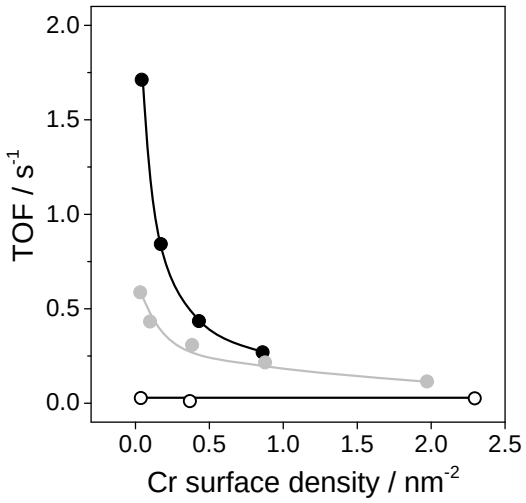

Figure 4-29 Effect of Cr surface density on turn over frequency of propene formation with respect to one surface Cr atom for (●) bulk $CrZrO_x$, (●) supported $CrO_x/LaZrO_x$ and (○) supported CrO_x/Al_2O_3 catalysts.

Under the above considerations, one can conclude that coexisting of Zr_{cus} and Cr sites results in their synergy effect in terms of overall catalyst activity. Indeed, if compare the sum of the rates of propene formation obtained for ZrO_2 (Zr_{cus} sites are the only active sites) and CrO_x/Al_2O_3 (Cr sites are the only active sites) with the rate of propene formation determined for

$CrZrO_x$ (both Zr_{cus} and Cr sites participate in propane dehydrogenation) containing a similar surface density of Cr as CrO_x/Al_2O_3 sample, one can see that the latter value is much higher. For example, the catalysts $Zr_{95}Cr_5O_x$ and $0.8Cr_2O_3/Al_2O_3$ possess similar surface chromium content (see Table 4-4), however, the rate of propene formation for the former catalyst (1.82 mmol(C_3H_6)·g^{-1}·min^{-1}) was much higher than the sum of the rates for $0.8Cr_2O_3/Al_2O_3$ and bare ZrO_2 (0.13 mmol(C_3H_6)·g^{-1}·min^{-1}). The same conclusion is also valid for supported $CrO_x/LaZrO_x$ catalyst: bare $LaZrO_x$ with only Zr_{cus} active sites showed the rate of propene formation of about 0.16 mmol(C_3H_6)·g^{-1}·min^{-1} (see section 4.1), together with $0.8Cr_2O_3/Al_2O_3$ (Cr sites are the only active sites) it would give the total rate of propene formation of about 0.23 mmol(C_3H_6)·g^{-1}·min^{-1}, however, this value is much lower than that obtained for $0.5Cr_2O_3/LaZrO_x$ (1.22 mmol(C_3H_6)·g^{-1}·min^{-1}), which possesses both Zr_{cus} and Cr active sites and has similar surface chromium content as $0.8Cr_2O_3/Al_2O_3$ (see Table 4-4). Therefore, for both bulk $CrZrO_x$ and supported $CrO_x/LaZrO_x$ containing two types of active sites (Zr_{cus} and Cr), the activity is much higher compared to the catalysts possessing only one type of active sites. This might be due to the mutual influence of Zr_{cus} and Cr sites on their intrinsic activity or because of enhancing reducibility of ZrO_2 in a presence of chromium species and creation of higher amount of Zr_{cus} sites as it was indirectly shown by H_2-TPR experiments (see Figure 4-26 (a)).

4.4.4. Reaction scheme of product formation

In order to check if reaction scheme of PDH is affected by the kind of Cr species in the ZrO_2-based catalysts, i.e. supported CrO_x vs. Cr incorporated into the lattice of ZrO_2, additional catalytic tests at different degrees of propane conversion were performed with reduced bulk $CrZrO_x$ and supported $CrO_x/LaZrO_x$ ($0.5Cr_2O_3/LaZrO_x$ and $3.2Cr_2O_3/LaZrO_x$) catalysts. The tests were instrumental to identify primary and secondary reaction pathways in the course of propane dehydrogenation. Both total flow (10, 20, 40 and 60 ml·min^{-1}) of the reaction feed and catalyst amount (0.01 – 1.2 g) were varied to achieve different contact times and accordingly different degrees of propane conversion. Figure 4-30 shows the obtained dependence of selectivity to C_3H_6, cracking products (CH_4, C_2H_6 and C_2H_4), and coke on propane conversion.

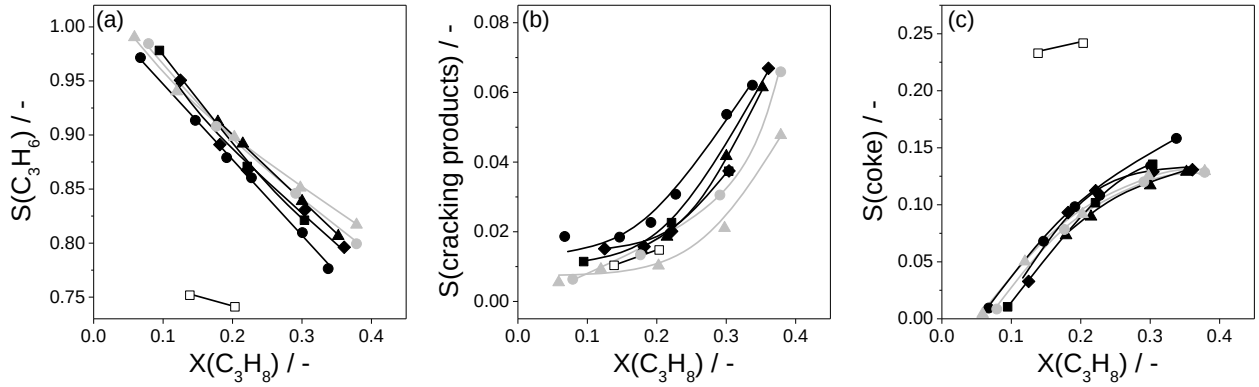

Figure 4-30 Dependence of selectivity to (a) propene, (b) cracking products, and (c) coke on propane conversion for □ ZrO_2, ■ $Zr_{99.5}Cr_{0.5}O_x$, ♦ $Zr_{98}Cr_2O_x$, ▲ $Zr_{95}Cr_5O_x$, ● $Zr_{90}Cr_{10}O_x$, ▲ $0.5Cr_2O_3/LaZrO_x$, and ● $3.2Cr_2O_3/LaZrO_x$.

For all catalysts, the selectivity to propene (Figure 4-30 (a)) decreases with increasing propane conversion thus indicating the presence of a sequential stage(-s) involving propene. Extrapolation of all propene selectivity curves for all Cr-containing materials to zero degree of conversion gives near to 100% selectivity. This means that propene is the only product formed directly from propane. For ZrO_2, the extrapolated selectivity is only about 80% implying that not only propene but also other side products are formed directly from propane. For all samples, the selectivity to cracking products starts at about 0% at near zero propane conversion and increases with increasing conversion. Such dependence indicates that cracking products are formed during a sequential stage involving propene primarily formed from propane. In general, supported catalysts showed slightly lower selectivity to cracking products compared to bulk ones. All samples except ZrO_2 behave similar in terms of conversion-induced changes of coke selectivity: the selectivity starts from zero at zero propane conversion and rises with increasing conversion. No significant difference between curves related to different catalysts can be found. Therefore, similar to cracking, coke formation is mainly formed from propene. Bare ZrO_2 behave differently: coke selectivity over this sample starts from about 20% and increases with propane conversion. This implies that coke is formed during the parallel stage (directly from propane) as well as during the sequential stage (from propene). Based on the above results, the reaction networks of propane dehydrogenation over Cr-containing catalysts (Figure 4-31 (a)) and over ZrO_2 (Figure 4-31 (b)) are proposed.

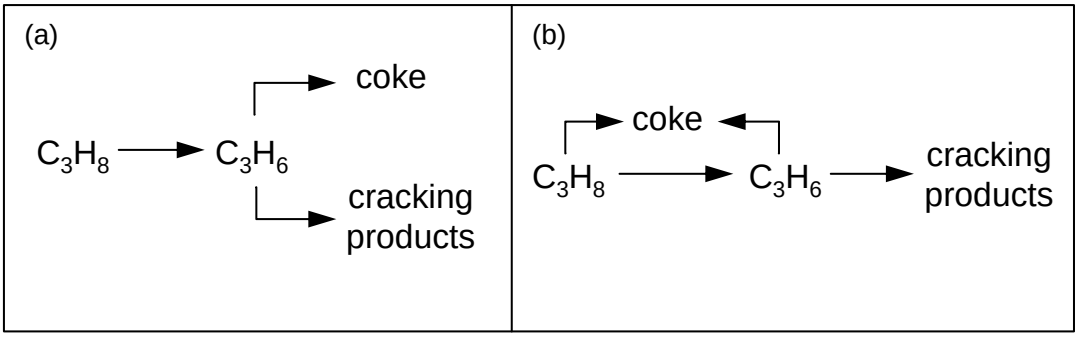

Figure 4-31 Proposed mechanistic schemes for propane dehydrogenation (a) over Cr-containing samples ($Zr_{99.5}Cr_{0.5}O_x$, $Zr_{98}Cr_2O_x$, $Zr_{95}Cr_5O_x$, $Zr_{90}Cr_{10}O_x$, $0.5Cr_2O_3/LaZrO_x$, and $3.2Cr_2O_3/LaZrO_x$) and (b) over ZrO_2.

The difference between Cr-containing catalysts and bare ZrO_2 could be due to the different surface acidity of the samples. As it was shown by NH_3-TPD experiments (section 4.4.2.), bare ZrO_2 possesses much higher surface density of acidic sites (see Table 4-5). Moreover, the concentration of strong acidic sites characterized by high temperature of ammonia desorption in most cases is higher for ZrO_2 than for Cr-containing samples. Due to the high surface acidity of ZrO_2, the intermediates formed from propane might have longer lifetime on the surface of the sample. Therefore, such intermediates can react with each other forming precursors for carbon deposits.

4.4.5. Summary

Bulk $CrZrO_x$ and supported $CrO_x/LaZrO_x$ catalysts possess both Zr_{cus} and Cr active sites, and demonstrate extremely high activity in propane dehydrogenation despite of quite low chromium content. The catalysts perform superior to supported CrO_x/Al_2O_3 counterparts which possess only Cr active sites. Moreover, the activity of $CrZrO_x$ and $CrO_x/LaZrO_x$ catalysts is even higher than a sum of activities of CrO_x/Al_2O_3 (with only Cr active sites) possessing similar chromium content and of bare ZrO_2 or $LaZrO_x$ (with only Zr_{cus} active sites). The high activity of $CrZrO_x$ and $CrO_x/LaZrO_x$ catalysts is related to the synergy effect between Zr_{cus} and Cr active sites which appears due to the mutual influence of Zr_{cus} and Cr sites on their intrinsic activity or because of creation of high amount of Zr_{cus} sites under reductive treatment in a presence of chromium species.

The presence of Cr was shown to decrease the total surface acidity of ZrO_2. Moreover, the contribution of strong acidic sites becomes smaller. This leads to the suppressing side reactions (coke formation and cracking) which can happen under reaction condition. Mechanistic investigation of PDH showed that the formation of coke over Cr-containing samples occurs as secondary reaction involving propene, while over bare ZrO_2 coke forms not only during sequential stage but also directly from propane.

4.5. Practical relevance of ZrO_2-based catalysts. Comparison with industrial analogues

4.5.1. Long-term stability of Cr-free catalysts in propane dehydrogenation

A practical relevance of selected Cr-free ZrO_2-based catalysts (bare $LaZrO_x$ and $YZrO_x$, Cu-containing $Cu/LaZrO_x$ with 0.05 wt.% Cu, Ru-containing $Ru/LaZrO_x$ and $Ru/YZrO_x$ with 0.05 wt.% Ru) was investigated in a series of 60 PDH/oxidative regeneration cycles at 550, 600, and 625°C. Contact time for all catalysts was chosen based on the performance of an analogue of industrial $K\text{-}CrO_x/Al_2O_3$ to achieve propane conversion between 30 and 45% for this catalyst. In order to operate in this conversion range at different temperatures, a total flow of C_3H_8-N_2 mixture was increased with the reaction temperature (10, 40, and 60 $ml \cdot min^{-1}$ for 550, 600, and 625°C, respectively). The first 20 cycles were performed at 550°C, then the temperature was increased up to 600°C and next 20 cycles were made at this temperature. Hereafter, the temperature was again decreased to 550°C and 10 cycles were carried out at this temperature. Finally, the catalysts were tested at 625°C (10 cycles). The regeneration stage consisted of oxidation in air for 15 min followed by flushing with N_2. No reductive pre-treatment was performed since the catalysts can be reduced *in situ* under reaction condition. An analogue of industrial $K\text{-}CrO_x/Al_2O_3$ was also tested under the same conditions as a reference material. The amount of all catalysts was set to 300 mg.

The time of oxidative regeneration treatment of only 15 min was chosen based on the results of separate experiments performed with selected catalysts. Such experiments performed at 550°C involved *in situ* catalyst characterization by UV-vis spectroscopy with a simultaneous analysis of gas-phase products during PDH and regeneration stages by an on-line mass spectrometer. The formation of carbon-containing deposits during PDH was monitored by UV-vis spectroscopy. The UV-vis spectra (Kubelka-Munk function $F(R_{rel})$) after different times on PDH stream are shown in Figure 4-32 (a). It is obvious that the UV-vis spectrum of $LaZrO_x$ significantly changes with rising time on stream. Particularly, a maximum of $F(R_{rel})$ appears at 365 nm. The changes differ from those observed during H_2 treatment (section 4.2.3), therefore, such changes might be related to the formation of carbon-containing deposits and can be used for investigating the kinetics of coke formation. Figure 4-32 (b) exemplifies temporal changes in $F(R_{rel})$ at 365 nm recorded in PDH and regeneration stages over the same catalyst. A gradual

increase in $F(R_{rel})$ at 365 nm during PDH stage is referred to the formation of carbon-containing deposits on catalyst surface, while quite fast drop of this value during regeneration stage implies removal of coke. It can be concluded from the $F(R_{rel})$ profiles that the formation of carbon-containing deposits in the course of PDH is significantly slower than the oxidation of such species in the presence of O_2. Such deposits were completely removed within only first 5 – 7 min on air stream (Figure 4-32 (b)), while about 40 min on PDH stream was necessary for their formation. Thus, 15 min oxidative regeneration stage should be enough to completely oxidize carbon-containing species formed during 40 min PDH stage. Such conclusion is additionally supported by MS data collected upon oxidative regeneration of spent $LaZrO_x$, $YZrO_x$ and $Ru/LaZrO_x$. CO_2 signal was observed only during the first 7 min on air stream (Figure A-10 in Appendix).

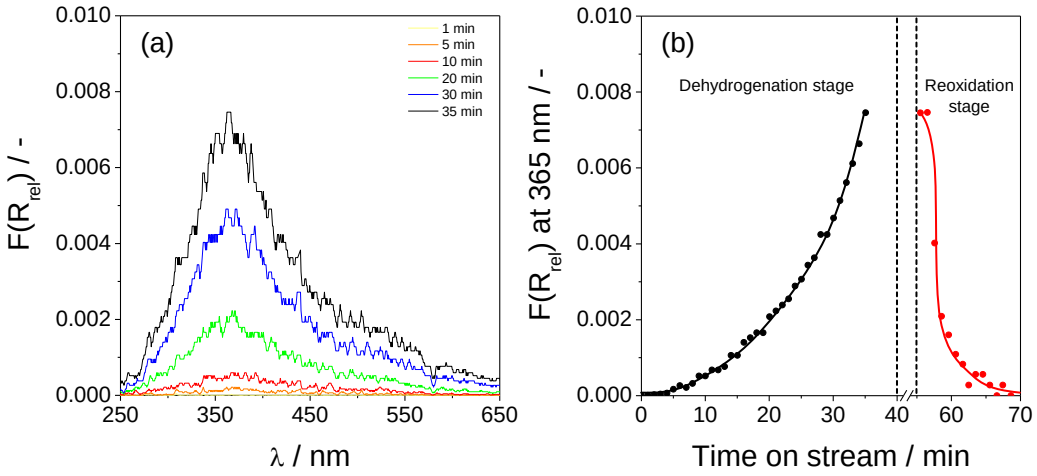

Figure 4-32 (a) $F(R_{rel})$ of $LaZrO_x$ during PDH stage recorded after different time on PDH stream, (b) temporal changes in $F(R_{rel})$ of $LaZrO_x$ at 365 nm during PDH and during regeneration stages.

Now, catalytic data obtained during a series of dehydrogenation/oxidative regeneration cycles are discussed. Time-on-stream profiles of propene yield in the first dehydrogenation stage at each reaction temperature (550, 600 and 625°C) are shown in Figure 4-33. Figure A-11 in Appendix shows changes in propene yield with time on stream for all dehydrogenation stages at each temperature. During the whole experiment the selectivity to propene was higher than 85% for all catalysts.

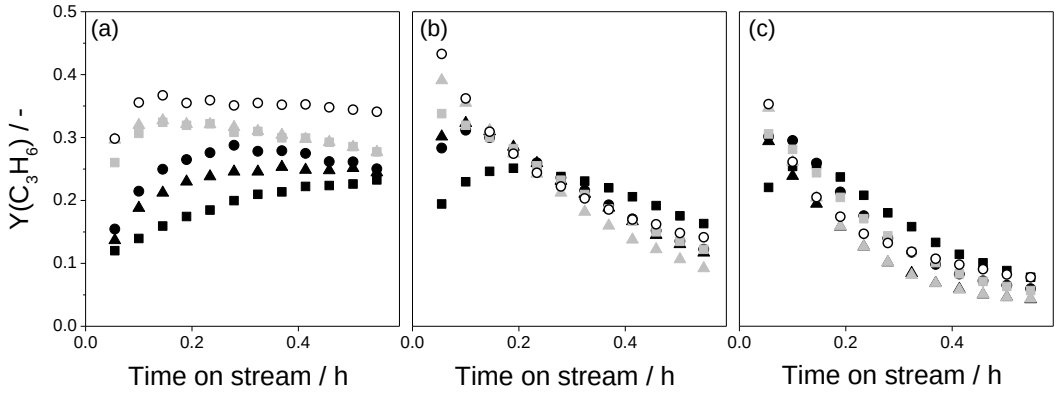

Figure 4-33 Time-on-stream change of propene yield obtained for ■ $LaZrO_x$, ● $Cu/LaZrO_x$ ▲ $Ru/LaZrO_x$, ■ $YZrO_x$, ▲ $Ru/YZrO_x$, and ○ $K\text{-}CrO_x/Al_2O_3$ during first cycle at 550, 600 and 625°C ((a), (b) and (c), respectively).

At 550°C, bare $LaZrO_x$ showed continuous increase of propene yield with time on stream (Figure 4-33 (a)), while for all other samples, propene yield passed over a maximum after first 10 – 20 min. The increase in the yield of propene for all samples supports the idea of *in situ* reduction of the catalysts under reaction conditions resulting in the formation of active Zr_{cus} sites. Interestingly, the presence of the metal on the surface of $LaZrO_x$ influences the strength of propene yield increase during the first minutes of PDH stream. The positive effect of the metal can be explained by its ability to provoke reduction of ZrO_2-based material. Therefore, the formation of Zr_{cus} sites occurs faster resulting in higher extent of propene yield increase. The most pronounced increase in propene yield was found for $Cu/LaZrO_x$. It is, however, worth mentioning that for $YZrO_x$-containing catalysts the change of propene yield with time on stream does not depend on the presence of metal: the behavior of bare $YZrO_x$ seems to be similar to that of $Ru/YZrO_x$. In general, $YZrO_x$-containing catalysts demonstrated higher initial propene yield than their $LaZrO_x$-based counterparts. Such results prove that, in comparison with La_2O_3, Y_2O_3 is a more efficient promoter for ZrO_2 in terms of generation of Zr_{cus} sites. The initial yield of propene obtained over $K\text{-}CrO_x/Al_2O_3$ was found to be the highest among all samples tested. The slight decrease in propene yield for the most of the samples in the end of PDH stage might be due to the formation of coke on the catalyst surface which might block catalytically active sites. No irreversible deactivation of the catalysts was identified since the catalysts completely restored their performance after oxidative regeneration at reaction temperature (Figure A-11 in Appendix).

At 600 and 625°C, the yield of propene continuously decreased or passed through a maximum with time on stream for all samples (Figure 4-33 (b), (c)). For $LaZrO_x$- as well as for $YZrO_x$-containing catalysts, the presence of metal resulted in a higher initial propene yield. However, deactivation of metal-containing samples was more pronounced than in case of bare $LaZrO_x$ and $YZrO_x$. The deactivation rate increased with rising reaction temperature. Similar tendency was also found for K-CrO_x/Al_2O_3.

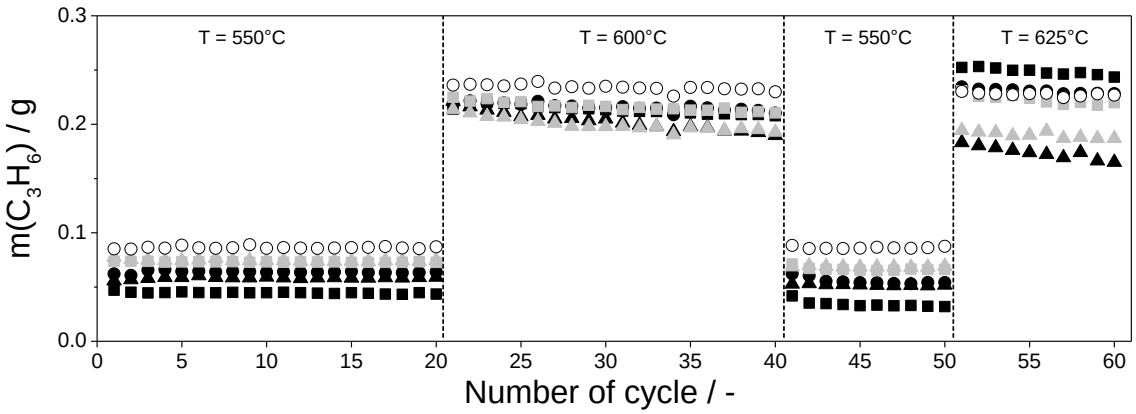

Figure 4-34 Amount of propene ($m(C_3H_6)$) formed in each cycle over ■ $LaZrO_x$, ● Cu/$LaZrO_x$ ▲ Ru/$LaZrO_x$, ■ $YZrO_x$, ▲ Ru/$YZrO_x$, and ○ K-CrO_x/Al_2O_3 in a series of 60 PDH/regeneration cycles at different temperatures.

Catalyst durability is now to be discussed. For each catalyst, an overall amount of propene formed during each catalytic cycle was calculated using the molar fraction of propene obtained every 190 s upon PDH stage from the chromatographic data according to equations (3.17) and (3.18) (Figure 4-34). At 550°C all catalysts showed good durability with no changes in performance from cycle to cycle. The lowest amount of propene was formed over bare $LaZrO_x$. Propene production increased in the presence of Ru or Cu. Bare $YZrO_x$ and Ru/$YZrO_x$ did not differ from each other and formed only slightly lower amount of propene than K-CrO_x/Al_2O_3.

The $m(C_3H_6)$ values determined at 600°C were significantly higher than those determined at 550°C (Figure 4-34). This is due to the positive effect of reaction temperature on the rate of propene formation. The highest amount of propene was again detected over K-CrO_x/Al_2O_3, while the lowest $m(C_3H_6)$ values were found for Ru-containing catalysts (Ru/$LaZrO_x$ and Ru/$YZrO_x$). Such behavior might be due to the fast catalyst deactivation caused by coke formation (see Figure 4-33 (b)). The catalysts showed a slight decrease in the $m(C_3H_6)$ from cycle to cycle. When comparing the amount of propene formed over bare $LaZrO_x$ and $YZrO_x$, no significant difference

were detected despite of the fact that $YZrO_x$ had much higher initial activity (see Figure 4-33 (b)). The catalysts did not practically change their performance from cycle to cycle.

During the following 10 cycles performed at 550°C all catalysts showed $m(C_3H_6)$ values similar to that determined for the first 20 cycles at the same temperature. All catalysts did not practically change their performance from cycle to cycle (Figure 4-34).

An increase in the reaction temperature up to 625°C resulted in an increase in the amount of propene formed over $LaZrO_x$, $Cu/LaZrO_x$ and $YZrO_x$ with the former showing the highest $m(C_3H_6)$ values among all catalysts. Performance of $K\text{-}CrO_x/Al_2O_3$ did not practically change compared to that at 600°C, and Ru-containing catalysts produced the lowest propene amount which slightly decreased from cycle to cycle (Figure 4-34). This is probably due to the fact that some irreversible changes in the structure/morphology of the catalysts might happen under alternating dehydrogenation/reoxidation cycles.

4.5.2. Effect of hydrogen on catalyst performance

It is well-known that propane dehydrogenation in the Oleflex industrial process is performed in the presence of hydrogen.[43] Hydrogen increases on-stream stability as well as durability of Pt-based catalysts. Higher on-stream stability is reached by the competitive adsorption of hydrogen on catalyst surface which results in decrease in amount of coke precursors adsorbed on catalyst surface. This leads to less coke being deposited on active sites and, therefore, to higher catalyst stability. The positive effect of H_2 on catalyst durability is typically explained as follows. Sintering of catalytically active Pt species mostly occurs during oxidative regeneration stage. The heat released upon combustion of carbon-containing deposits results in hot spots in the catalyst bed and thus facilitates sintering. Thus, when the amount of the deposits in alkane DH stage is suppressed in H_2 presence, less heat is released upon its combustion and sintering of Pt species is also hindered.[132]

In order to investigate if and how the presence of gaseous hydrogen influences catalytic performance of Cr-free ZrO_2-based catalysts in propane dehydrogenation, a series of catalytic tests was performed with selected catalysts. The reaction feed contained 40 vol.% of C_3H_8 and different amounts of H_2 (0, 10, and 30 vol.%). N_2 was balance. The experiments were performed at 550 and 600°C with the catalysts pre-reduced at the reaction temperature. The tested catalysts were $Cu/LaZrO_x$ (with 0.05 wt.% Cu) and Ru-containing samples prepared by simple

impregnation: 0.05Ru(imp.)/$LaZrO_x$, 0.005Ru(imp.)/$YZrO_x$_NorPro, and 0.05Ru(imp.)/$YZrO_x$_NorPro. The duration of one PDH stage was 95 min. Since the presence of hydrogen in the reaction mixture provokes proceeding dehydrogenation reaction in the reverse direction, the total flow of reaction mixture was decreased with increasing hydrogen content in order to achieve similar initial conversion (about 20 – 30%). Thus, the PDH tests at 550°C with the reaction mixtures containing 0, 10, or 30 vol.% H_2 were performed at total flows of 10, 7, and 5 ml·min^{-1}, respectively. The corresponding flows for the tests at 600°C were 40, 20, and 20 ml·min^{-1}. Temporal changes of propane conversion and selectivity to propene obtained during 95 min on stream at 550°C for each catalyst with different reaction feeds are shown in Figure 4-35. The corresponding data obtained at 600°C are presented in Figure A-12 in Appendix.

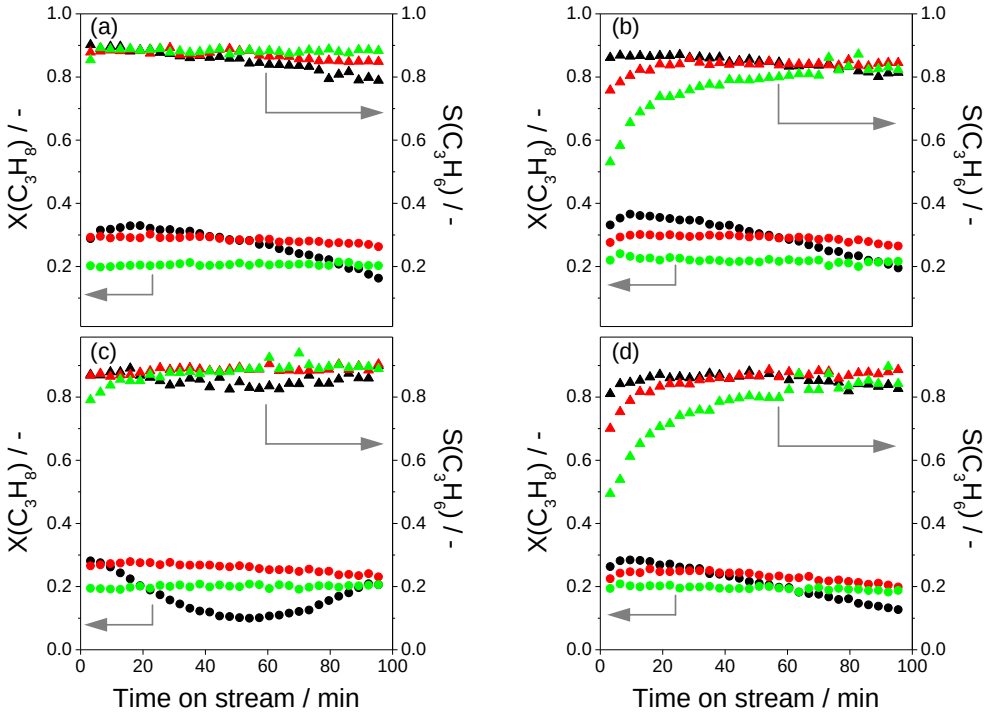

Figure 4-35 Temporal change of propane conversion (circles) and propene selectivity (triangles) for (a) Cu/$LaZrO_x$, (b) 0.05Ru(imp.)/$LaZrO_x$, (c) 0.005Ru(imp.)/$YZrO_x$_NorPro, and (d) 0.05Ru(imp.)/$YZrO_x$_NorPro obtained at 550°C by using different composition of reaction mixture: ●, ▲ – 40 vol.% C_3H_8 , ●, ▲ – 40 vol.% C_3H_8 and 10 vol.% H_2, ●, ▲ – 40 vol.% C_3H_8 and 30 vol.% H_2, N_2 was balance in all cases.

The data clearly demonstrate that co-feeding of hydrogen improves on-stream stability of all catalysts. For a proper comparison of catalyst deactivation behavior with different reaction feeds, a deactivation parameter (D) for each condition was calculated according to equation

(4.12). The obtained D values are given in Table 4-6. One can clearly see that the higher the hydrogen content, the lower is the deactivation parameter. This can be associated with the fact that hydrogen suppresses formation of carbon-containing deposits. Indeed, the ratio of the amount of such deposits formed during one PDH stage to the amount of propane converted decreases with increasing content of hydrogen in the reaction feeds (Figure 4-36). This means that an average selectivity to coke decreases in the presence of hydrogen.

$$D(\%) = \frac{X_{initial} - X_{final}}{X_{initial}} \times 100\% \qquad (4.12),$$

where $X_{initial}$ is initial propane conversion (after 190 s on stream), X_{final} is propane conversion registered after 95 min on stream.

Table 4-6 Deactivation parameter (D) determined for each catalyst tested at 550°C and 600°C using reaction mixture with 0, 10, and 30 vol.% H_2.

Sample	0% H_2	10% H_2	30% H_2	0% H_2	10% H_2	30% H_2
	D at T = 550°C			D at T = 600°C		
Cu/$LaZrO_x$	44%	10%	0%	90%	78%	47%
0.05Ru(imp.)/$LaZrO_x$	41%	4%	2%	95%	87%	67%
0.005Ru(imp.)/$YZrO_x$_NorPro	27%	13%	0%	94%	82%	57%
0.05Ru(imp.)/$YZrO_x$_NorPro	52%	12%	3%	91%	83%	65%

It is worth mentioning that co-feeding of H_2 also affects selectivity to gas-phase products. The effect, however, depends on the type and concentration of supported metal and reaction temperature. Thus, the selectivity to propene obtained over Cu/$LaZrO_x$ did not strongly depend on the presence of H_2 and did not practically change within 95 min PDH stage (Figure 4-35 (a) for 550°C and Figure A-12 (a) in Appendix for 600°C). For all Ru-containing samples used for PDH at 550°C, the higher the H_2 content, the lower was the initial (after 190 s on stream) selectivity to propene. Moreover, the samples with high Ru content (0.05Ru(imp.)/$LaZrO_x$ and 0.05Ru(imp.)/$YZrO_x$_NorPro) demonstrated much lower initial propene selectivity in H_2 presence compared to the sample with low Ru content (0.005Ru(imp.)/$YZrO_x$_NorPro). The reason of such low initial propene selectivity is the formation of side gas-phase products such as methane and ethane. They are probably formed through propane hydrogenolysis catalyzed by Ru species.[133, 134] The selectivity slowly increased with time on stream (Figure 4-35 (b), (c), (d)). Such increase may be due to the blocking sites for this undesired reaction by carbon deposits. For the experiments performed at higher temperature (600°C), the negative effect of H_2 on the initial propene selectivity is less pronounced (Figure A-12 (b), (c), (d) in Appendix).

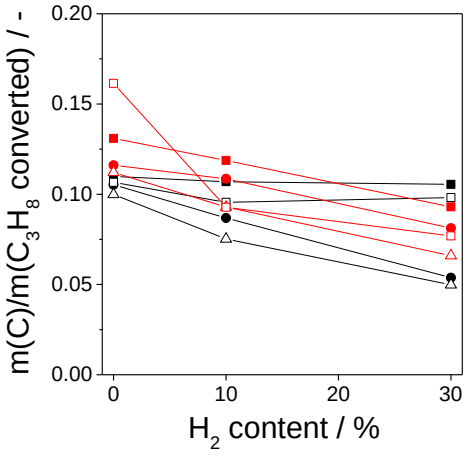

Figure 4-36 Total amount of carbon deposits formed during PDH stage related to the total amount of propane converted at 550°C (black symbols) and at 600°C (red symbols) over ●, ● – Cu/LaZrO$_x$, ■, ■ – 0.05Ru(imp.)/LaZrO$_x$, Δ, Δ – 0.005Ru(imp.)/YZrO$_x$_NorPro, and □, □ – 0.05Ru(imp.)/YZrO$_x$_NorPro.

Accordingly, it was shown that the presence of hydrogen in reaction mixture suppresses formation of coke on the surface of ZrO_2-based catalysts. This leads to increasing catalyst on-stream stability. However, for Ru-containing samples, the presence of hydrogen provokes undesired hydrogenolysis reaction. Cu-containing sample demonstrated less pronounced tendency to catalyze such side reaction.

4.5.3. Performance of Cr-containing catalysts in propane dehydrogenation

Long-term stability of bulk $CrZrO_x$ and selected supported $CrO_x/LaZrO_x$ ($0.5Cr_2O_3/LaZrO_x$ and $3.2Cr_2O_3/LaZrO_x$) catalysts as well as of an analogue of industrial K-CrO_x/Al_2O_3 was investigated in a series of tests consisting of 10 PDH/regeneration cycles performed at 550°C. The degree of initial conversion was about 30% and 20% for all Cr-containing catalysts and for bare ZrO_2, respectively. To achieve such conversion degrees, the amount of catalysts was varied depending on their activity. Due to experimental reasons and the low activity of ZrO_2, it was impossible to achieve conversion higher than 20% for this sample. Prior to PDH, the catalysts were pre-reduced in a flow of 57 vol.% H_2 in N_2. Each dehydrogenation stage lasted about 50 min using 10 ml·min^{-1} flow of 40 vol.% C_3H_8 in N_2. One regeneration stage involved 30 min of oxidative catalyst treatment in an air flow followed by 1 hour of reductive catalyst treatment in a flow of 57 vol.% H_2 in N_2. All steps were separated by 15 min flushing with N_2 flow.

Time-on-stream profiles of propane conversion as well as corresponding data for propene selectivity obtained for all catalysts during the first catalytic cycle are shown in Figure 4-37. The corresponding data for all catalytic cycles are shown in Figure A-13 in Appendix. Analogue of industrial K-CrO_x/Al_2O_3 was found to be the most stable against deactivation among all Cr-containing catalysts tested. It lost 25% of its initial conversion after 48 min on PDH stream. Noticeably, the rate of deactivation of both bulk $CrZrO_x$ and supported $CrO_x/LaZrO_x$ catalysts increased with rising chromium content (Figure 4-37 (a)). Thus, $Zr_{90}Cr_{10}O_x$ and $3.2Cr_2O_3/LaZrO_x$ lost about 75% and 60% of the corresponding initial conversion after 48 min on propane stream. Although bare ZrO_2 is less active than Cr-containing catalysts, it demonstrated quite good on-stream stability. It lost only 13% of initial activity after 48 min on PDH stream. Based on the above results, one can conclude that the presence of chromium in the ZrO_2-based catalysts results in faster catalyst deactivation.

For the most of the catalysts tested, the selectivity to propene did not change significantly with time-on-stream during one PDH stage. However, bulk $CrZrO_x$ catalysts were less selective than their supported counterparts (Figure 4-37 (b)). The selectivity obtained over the former catalysts varied from about 75 to 85%, while $0.5Cr_2O_3/LaZrO_x$ and $3.2Cr_2O_3/LaZrO_x$ showed the selectivity in a narrow range from 82 to 87%. K-CrO_x/Al_2O_3 showed the highest propene selectivity of about 85 – 89%.

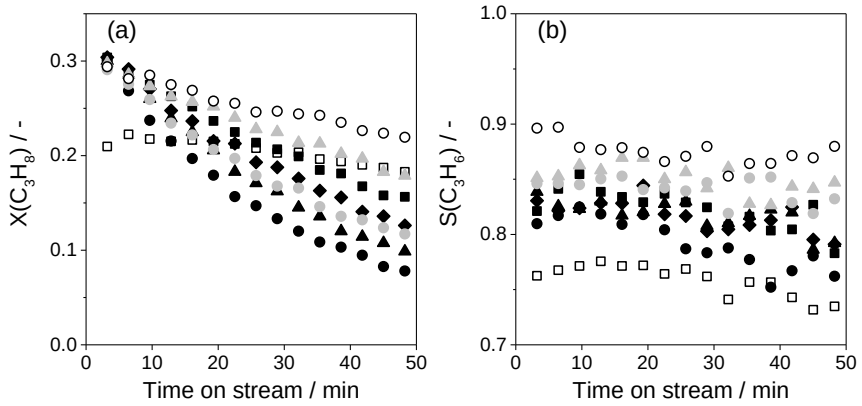

Figure 4-37 Time-on-stream change of (a) C_3H_8 conversion and (b) C_3H_6 selectivity obtained for reduced □ ZrO_2, ■ $Zr_{99.5}Cr_{0.5}O_x$, ♦ $Zr_{98}Cr_2O_x$, ▲ $Zr_{95}Cr_5O_x$, ● $Zr_{90}Cr_{10}O_x$, ▲ $0.5Cr_2O_3/LaZrO_x$, ● $3.2Cr_2O_3/LaZrO_x$, and ○ K-CrO_x/Al_2O_3 during the first catalytic cycle performed at 550°C.

For a proper comparison of productivity and durability of the catalysts, the space time yield (STY) of propene and the total amount of propene produced during each PDH stage were

calculated according to equations (3.17) and (3.19). The corresponding data are shown in Figure 4-38 and Figure 4-39, respectively. The highest initial (after 190 s on stream) productivity was obtained over $Zr_{90}Cr_{10}O_x$: the STY value for this catalyst was about 3.7 times higher than that of analogue of industrial K-CrO_x/Al_2O_3. The initial productivity of $Zr_{95}Cr_5O_x$, $Zr_{98}Cr_2O_x$, $3.2Cr_2O_3/LaZrO_x$, and $0.5Cr_2O_3/LaZrO_x$ was also found to be higher than that of K-CrO_x/Al_2O_3. For all catalysts, the STY values gradually decreased with rising time on PDH stream within all catalytic cycles, however, the deactivation rate is different for different samples. Despite of demonstrating the high deactivation rate, $Zr_{90}Cr_{10}O_x$ still showed higher productivity in the end of each catalytic cycle (after 48 min on stream) than K-CrO_x/Al_2O_3. After regeneration stage all catalysts restored their initial activity. Therefore, one can conclude that catalyst deactivation is caused by blocking catalytically active sites with carbon-containing species formed from propene as discussed in section 4.4.4. Such deposits are removed during oxidative regeneration stage (Figure 4-40 (a)).

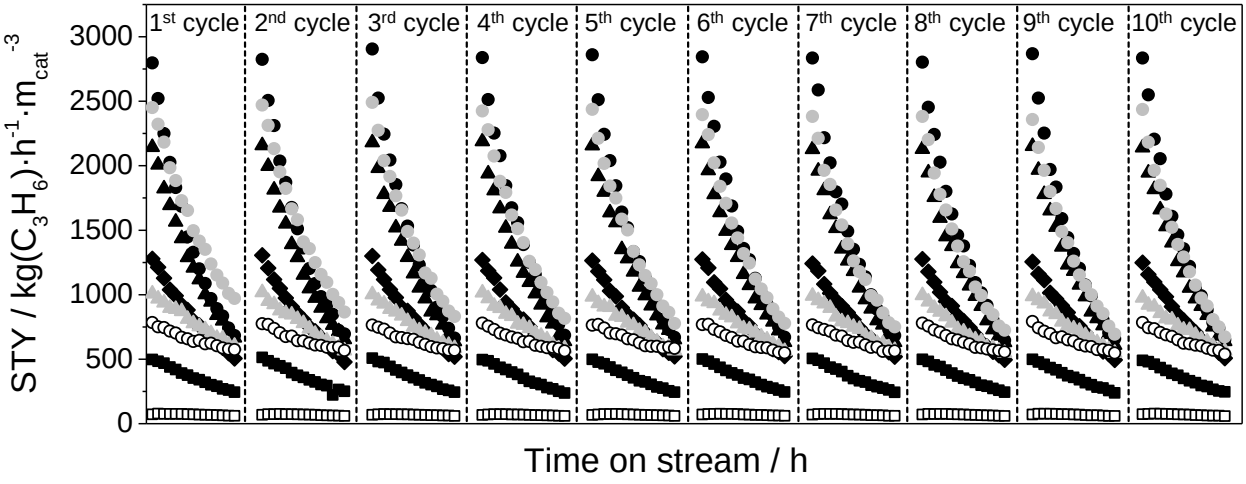

Figure 4-38 Time-on-stream change of STY for □ ZrO_2, ■ $Zr_{99.5}Cr_{0.5}O_x$, ♦ $Zr_{98}Cr_2O_x$, ▲ $Zr_{95}Cr_5O_x$, ● $Zr_{90}Cr_{10}O_x$, ▲ $0.5Cr_2O_3/LaZrO_x$, ● $3.2Cr_2O_3/LaZrO_x$, and ○ K-CrO_x/Al_2O_3 obtained in each catalytic cycle from a series of 10 PDH/regeneration cycles.

Now, durability of the catalysts is discussed. Interestingly, despite of having the same initial activity in each PDH stage (Figure 4-38), the sample $3.2Cr_2O_3/LaZrO_x$ showed slight decrease in the total amount of propene produced during catalytic cycle with rising number of cycle (Figure 4-39). Thus, sample $3.2Cr_2O_3/LaZrO_x$ showed the highest amount of propene produced in the first catalytic cycle among all samples tested, however, in the last cycle this

catalyst produced about 16% less propene. The lower durability of the sample $3.2Cr_2O_3/LaZrO_x$ is due to the fact that its time-on-stream deactivation rate slightly increased with rising number of cycle (Figure 4-38). $0.5Cr_2O_3/LaZrO_x$ also demonstrated slight decrease in amount of propene produced within one catalytic cycle with rising number of cycle. Such behavior of supported catalysts might be due to the irreversible deactivation caused by some structural changes of active phase under alternating dehydrogenation/reoxidation cycles, e.g. agglomeration of CrO_x species. All bulk samples showed good durability; they produced similar amount of propene during each catalytic cycle. Interestingly, the samples $Zr_{98}Cr_2O_x$ and $0.5Cr_2O_3/LaZrO_x$ produced higher amount of propene within one cycle than $K\text{-}CrO_x/Al_2O_3$ despite of the fact that they possessed about 16 and 39 times less total chromium content, respectively.

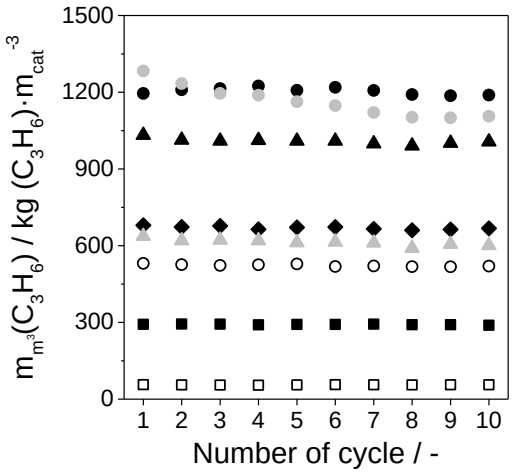

Figure 4-39 Overall amount of propene produced during each catalytic cycle over 1 m^3 of each catalyst: □ ZrO_2, ■ $Zr_{99.5}Cr_{0.5}O_x$, ♦ $Zr_{98}Cr_2O_x$, ▲ $Zr_{95}Cr_5O_x$, ● $Zr_{90}Cr_{10}O_x$, ▲ $0.5Cr_2O_3/LaZrO_x$, ● $3.2Cr_2O_3/LaZrO_x$, and ○ $K\text{-}CrO_x/Al_2O_3$.

Additionally, after the last catalytic cycle was completed, the spent catalysts were used for TPO experiments in order to determine the amount of carbon deposits formed during 50 min of PDH reaction. CO_2 was the main reaction product, while CO was formed in traces. Figure 4-40 (a) shows the TPO profiles for each sample in form of a change of CO_2/Ar signal with the temperature. The corresponding data for CO/Ar signal are shown in Figure A-14 in Appendix. The temperature of maximum of CO_2 release (T_{maxCO2}) and the amount of carbon deposits per gram of each catalyst calculated from the sum of CO_2 and CO released during TPO experiment (CO contribution was much lower than that of CO_2) according to equation (3.9) for all samples are listed in Table 4-7. The maximal T_{maxCO2} value of 395°C was determined for ZrO_2. Such

value decreased with rising chromium amount in both bulk $CrZrO_x$ and supported $CrO_x/LaZrO_x$ catalysts. Noticeably, coke removal from the former catalysts appeared at lower temperatures when considering apparent surface density of Cr sites. The effect of Cr content on T_{maxCO2} might be due the participation of CrO_x species in coke combustion. The higher the concentration of these species, the higher is the combustion rate; therefore, the T_{maxCO2} values are shifted to lower temperatures.

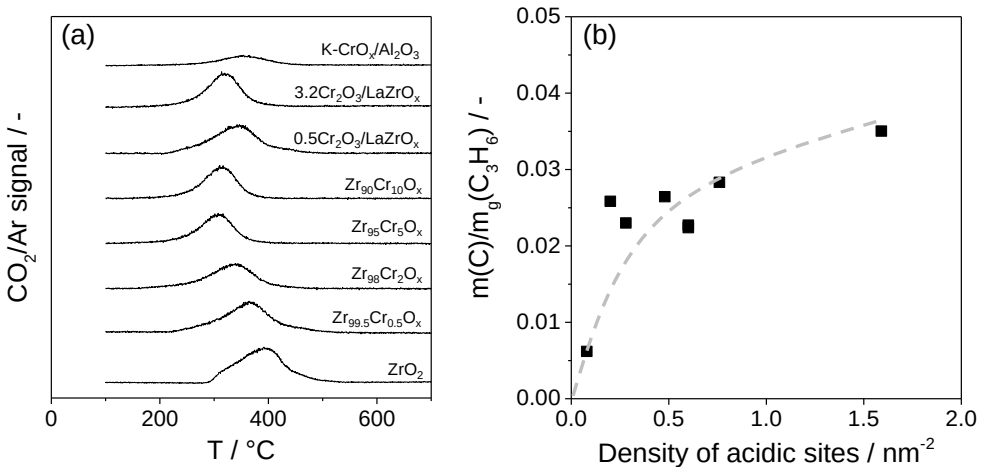

Figure 4-40 (a) TPO profiles of spent catalysts: dependence of CO_2/Ar signal on temperature; (b) effect of the concentration of surface acidic sites on the ratio of $m(C)/m_g(C_3H_6)$.

Now, the effect of catalyst composition on the amount of coke formed during the last PDH stage of a series of 10 PDH/regeneration stages is discussed. The lowest amount formed per catalyst gram was determined for ZrO_2 followed by $K\text{-}CrO_x/Al_2O_3$ (Table 4-7). Bulk $CrZrO_x$ and supported $CrO_x/LaZrO_x$ catalysts deposited higher amounts. For these both types of the catalysts, coke amount increased with chromium content. Such tendency does not appear to correlate with the concentration of acidic sites determined from NH_3-TPD experiments. According to the data (Table 4-5), the concentration of acidic sites decreases with increasing Cr loading. However, one should also take into account the amount of propene formed and relate it to the amount of coke since propene is the main gas-phase precursor for carbon-containing deposits (Figure 4-30). To this end, the amount of propene formed during the 10^{th} PDH stage per gram of each catalyst ($m_g(C_3H_6)$) was calculated according to equation (3.20). Using this amount, the ratio of $m(C)/m_g(C_3H_6)$ was determined in order to take into account the fact that carbon-containing deposits are formed from propene. Figure 4-40 (b) shows this ratio as a function of the density of

acidic sites. The relationship obtained demonstrates that the $m(C)/m_g(C_3H_6)$ ratio increases with the density thus supporting the positive role of acidic sites for coke formation from propene.

Despite of the fact that $Zr_{90}Cr_{10}O_x$ possesses the lowest concentration of acidic sites (Table 4-5), it demonstrated the highest deactivation rate (Figure 4-37 (a)). Such behavior can be explained when taking into account an apparent surface density of Cr sites. From a mechanistic viewpoint, coke is formed from higher-molecular weight compounds originated upon oligomerization of adsorbed olefin molecules. Such coupling reactions can proceed when adsorbed olefin molecules are located close to each other. Under these considerations, the higher the density of DH active sites, where propene molecules are formed and also adsorbed, the higher is the probability for their reaction to coke precursors. Due to higher rate of coke formation, active sites of catalysts containing high amount of Cr are covered by coke resulting in their deactivation.

Table 4-7 The data obtained from evaluation of TPO results: the temperature of maximum of CO_2 release (T_{maxCO2}), the amount of carbon deposits formed per gram of each catalyst (m(C)).

Sample	T_{maxCO2}, °C	m(C), $g \cdot g_{catalyst}^{-1}$
ZrO_2	395	$1.7 \cdot 10^{-3}$
$Zr_{99.5}Cr_{0.5}O_x$	365	$6.1 \cdot 10^{-3}$
$Zr_{98}Cr_2O_x$	341	$13 \cdot 10^{-3}$
$Zr_{95}Cr_5O_x$	311	$21 \cdot 10^{-3}$
$Zr_{90}Cr_{10}O_x$	314	$23 \cdot 10^{-3}$
$0.5Cr_2O_3/LaZrO_x$	347	$15 \cdot 10^{-3}$
$3.2Cr_2O_3/LaZrO_x$	321	$31 \cdot 10^{-3}$
$K\text{-}CrO_x/Al_2O_3$	357	$4.9 \cdot 10^{-3}$

4.5.4. Performance of bulk catalysts in isobutane dehydrogenation

Based on the previous data obtained for propane dehydrogenation, $YZrO_x$ and $Zr_{90}Cr_{10}O_x$ were selected for additional tests in isobutane dehydrogenation to check their practical relevance. Firstly, to identify appropriate conditions for catalyst treatment and regeneration, catalytic tests lasted for 45 min were performed at 550 and 600°C after oxidative (1 hour in air flow) and reductive (1 hour in a flow of 57 vol.% H_2 in N_2) treatment at the same temperature. Temporal changes in isobutane conversion obtained in these tests are shown in Figure 4-41. Generally, the conversion of isobutane over the oxidized catalysts did not significantly differ from that over their reduced counterparts. Moreover, the selectivity towards isobutylene did not strongly depend

on treatment condition. The initial (determined after 9 min on DH stream) selectivity obtained at 550°C over reduced and oxidized $YZrO_x$ was 93 and 91%, respectively, while the corresponding data for $Zr_{90}Cr_{10}O_x$ were 83 and 84%. The selectivity at 600°C was 83% and about 72%, respectively. Since there was no big difference in performance of oxidized and reduced catalysts, one can conclude that reductive pre-treatment is not required for $YZrO_x$ and $Zr_{90}Cr_{10}O_x$ to perform isobutane dehydrogenation, and active Zr_{cus} sites can be created *in situ* under DH conditions. Therefore, catalyst durability tests were carried out with oxidized catalysts in a series of 30 DH/regeneration cycles at 550 and 600°C.

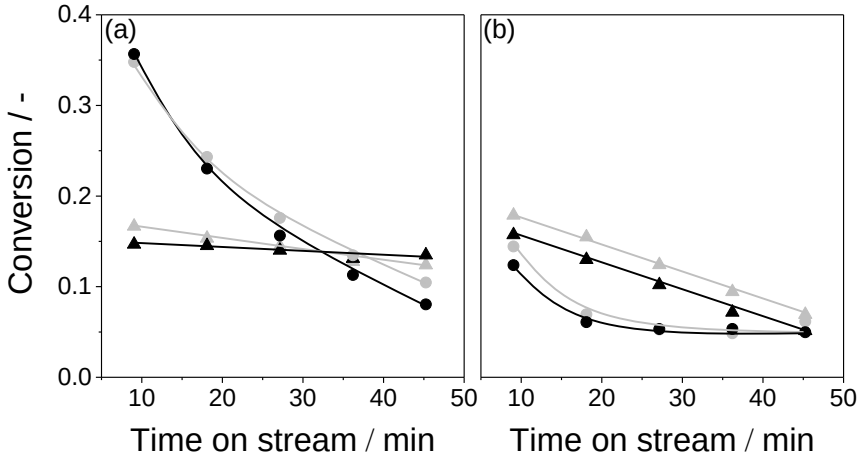

Figure 4-41 Time-on-stream change of isobutane conversion obtained for reduced (▲, ●) and oxidized (▲, ●) $YZrO_x$ (triangles) and $Zr_{90}Cr_{10}O_x$ (circles) during 45 min on DH stream at (a) 550°C and (b) 600°C. Reaction mixture: 40 vol.% iso-C_4H_{10} in N_2, total flow = 10 ml·min^{-1} at 550°C and 30 ml·min^{-1} at 600°C; the catalyst amount was 40 mg.

The first 10 cycles were performed at 550°C, then the temperature was increased to 600°C and the next 10 cycles were carried at this temperature. Hereafter, the temperature was again decreased to 550°C to perform further 10 cycles at this temperature. Each dehydrogenation stage lasted about 27 min using a flow of 40 vol.% iso-C_4H_{10} in N_2 (10 ml·min^{-1} for 550°C and 20 ml·min^{-1} for 600°C), while the regeneration stage involved only 15 min of catalyst reoxidation in an air flow at the same temperature as the DH stage was performed. DH and regeneration stages were always separated by 15 min flushing with N_2 flow. Analogues of industrial K-CrO_x/Al_2O_3 and Pt-Sn/Al_2O_3 catalysts were also investigated in the same experiment. The catalyst amount used in the experiment was chosen in accordance with individual activity of the samples to get about 35 – 45% of isobutane initial conversion at 550°C.

Temporal changes of STY of isobutylene produced over each catalyst during each DH stage are shown in Figure A-15 in Appendix, while the total amount of isobutylene formed during each catalytic cycle is presented in Figure 4-42. The highest isobutylene amount produced at 550°C during one DH stage was obtained over $Zr_{90}Cr_{10}O_x$. The catalyst could produce about 30% more isobutylene than analogue of industrial K-CrO_x/Al_2O_3. Both $Zr_{90}Cr_{10}O_x$ and K-CrO_x/Al_2O_3 showed good durability without any lost in amount of formed isobutylene from cycle to cycle. However, the catalysts differed in their on-stream stability within one catalytic cycle (Figure A-15 (a) in Appendix). Thus, in the end of the first DH stage, the catalyst $Zr_{90}Cr_{10}O_x$ lost about 52% of its initial activity (determined after 9 min on DH stream). On the contrary, catalyst K-CrO_x/Al_2O_3 did not show any significant change in activity with time on stream (Figure A-15 (a) in Appendix). The reason of the fast deactivation of $Zr_{90}Cr_{10}O_x$ is blockage of active sites by carbon-containing deposits. They could be completely oxidized during oxidative treatment thus resulting in restoring the initial catalyst activity. The high on-stream stability of K-CrO_x/Al_2O_3 can be explain by the presence of alkali promoter (potassium) which decreases surface acidity of the catalyst and thus suppresses formation of coke.[40] $YZrO_x$ showed much lower amount of produced isobutylene than Cr-containing samples but did not lose significantly its activity within one cycle and demonstrated good durability (Figure A-15 (a) in Appendix and Figure 4-42). Pt-Sn/Al_2O_3 showed quite high amount of isobutylene formed in the first cycle but in the 10^{th} cycle it produced less than a half of isobutylene generated in the 1^{st} cycle (Figure 4-42). Such low long-term stability of the catalyst is probably because of restructuring Pt species upon oxidative catalyst regeneration.[44, 64]

The highest amount of isobutylene produced at 600°C was achieved over K-CrO_x/Al_2O_3 (Figure 4-42). As expected, this amount was higher than at 550°C. The same effect was also obtained for $YZrO_x$. Nevertheless, one can see a slight decrease in initial activity of the sample with rising number of cycle (Figure A-15 (b) in Appendix), which resulted in a slight decrease of $m_{m^3}(iso - C_4H_8)$ value from cycle to cycle (Figure 4-42). Such decrease is probably due to some structural changes of surface species since regeneration stage could not completely restore the activity of the catalyst. In comparison with these two catalysts, $Cr_{10}Zr_{90}Ox$ produced at 600°C lower amount of isobutylene than at 550°C. This is due to the fast catalyst deactivation at 600°C (Figure A-15 (b) in Appendix). Catalyst Pt-Sn/Al_2O_3 produced the lowest amount of isobutylene

among all samples tested which decreased with rising number of cycles probably due to irreversible sintering of Pt species.

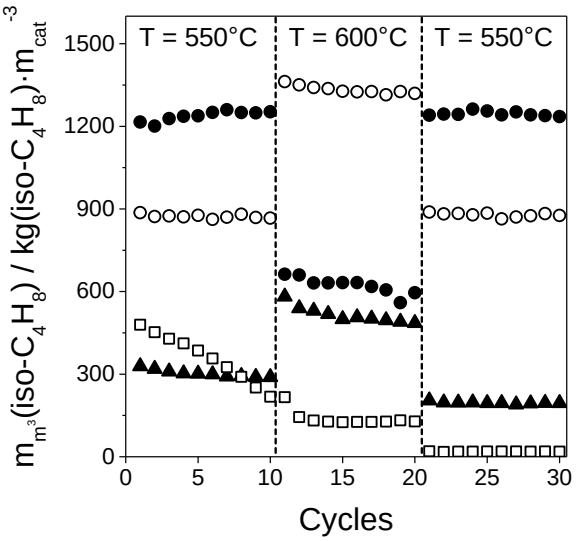

Figure 4-42 Overall amount of isobutylene produced during each catalytic cycle over 1 m^3 of each catalyst: ▲ $YZrO_x$, ● $Zr_{90}Cr_{10}O_x$, ○ K-CrO_x/Al_2O_3, and □ Pt-Sn/Al_2O_3.

The catalyst $Cr_{10}Zr_{90}O_x$ completely restored its high isobutylene productivity when the DH reaction was performed again at 550°C after completing 10 DH/regeneration cycles at 600°C (Figure A-15 (a) in Appendix). The catalyst did not change its performance from cycle to cycle confirming the absence of any severe structural changes which could be possible at high temperatures. Sample K-CrO_x/Al_2O_3 also demonstrated the same performance as it was observed during the first ten cycles. However, the catalyst $YZrO_x$ showed a slight decrease in the productivity and in $m_{m^3}(iso - C_4H_8)$ compared to those for the first ten cycles (Figure A-15 (a) in Appendix and Figure 4-42) probably due to the structural changes happened in the sample at 600°C. The catalyst Pt-Sn/Al_2O_3 was almost inactive; such behaviour additionally proved that Pt-based catalysts cannot be used in alternate DH/regeneration cycles without special regeneration stages.

4.5.5. Summary

ZrO_2-based catalysts are promising alternatives to commercial CrO_x- or Pt-based catalysts in terms of their performance in dehydrogenation of propane and isobutane. Such catalysts show not only high activity and selectivity towards desired products but also good productivity and

durability in a series of DH/regeneration cycles. The productivity of some of the catalysts was even higher than those of analogues of industrial K-CrO_x/Al_2O_3 and Pt-Sn/Al_2O_3. It was demonstrated that decrease in activity of the catalysts with time on stream during dehydrogenation stage is caused by the formation of carbon deposits on the catalyst surface, which block active sites. Such deposits can be completely removed during regeneration stage. The formation of coke on the catalyst surface during dehydrogenation stage is relatively slow process compared to coke removal during regeneration stage in air, so that, regeneration stage can be performed in a short time.

The presence of hydrogen in the reaction mixture was demonstrated to improve catalyst on-stream stability due to the suppressing coke formation. For Ru-containing catalysts, however, the presence of hydrogen induces undesired hydrogenolysis reaction.

The performance of Cr-containing ZrO_2-based catalysts in propane dehydrogenation depends on the chromium content and on the type how chromium species are connected with ZrO_2: either they are supported on the surface of ZrO_2-based material (supported $CrO_x/LaZrO_x$ catalysts) or they are incorporated into ZrO_2 lattice (bulk $CrZrO_x$ catalysts). Supported catalysts demonstrated slight higher propene selectivity at a conversion degree of about 30% than bulk catalysts, while bulk catalyst were more resistant to irreversible deactivation which can happen upon alternate DH/regeneration stages. Compared to analogue of industrial K-CrO_x/Al_2O_3, ZrO_2-based catalyst have some advantages: the same propene productivity can be reached over such catalysts which possess up to 16 (for $CrZrO_x$ catalysts) and 39 (for $CrO_x/LaZrO_x$ catalysts) times less chromium amount. Such results confirm the possibility of strongly minimizing chromium amount in the catalysts with reproduction of industrially relevant high activity at the same time.

5. Conclusions

A novel concept for designing alternative-type catalysts for non-oxidative dehydrogenation of light alkanes has been suggested and experimentally verified. This concept explores the idea of using lattice defects on the surface of bulk metal oxides as active sites. Its feasibility was demonstrated for propane, isobutane and n-butane dehydrogenation over ZrO_2-based catalysts. They revealed high activity, selectivity and durability, which are close or even superior to such performance of industrial CrO_x- or Pt-based catalysts. In comparison with the latter materials, the developed alternative catalysts have several advantages. On the one hand, they do not contain or possess only low amounts of chromium and, therefore, their utilization would be safer in terms of health and environmental issues. On the other hand, the developed catalysts do not contain expensive platinum and do not require complicated regeneration stages with the usage of chlorine as required for commercial Pt-based catalysts. Additionally, as DH active sites are related to lattice defects of bulk ZrO_2-based catalysts, they are free of issues, which are detrimental for supported catalysts, such as incorporation of supported active species into the bulk of support, loss or restructure of such species upon alternating dehydrogenation and oxidative catalyst regeneration stages.

On the basis of the results of thorough *in situ* and *ex situ* catalyst characterization together with comprehensive catalytic tests, surface coordinatively unsaturated zirconium cation (Zr_{cus}) and neighboring oxygen atom were concluded to be responsible for the C-H bond activation in alkanes. Zr_{cus} sites are formed upon removal of oxygen from the lattice of ZrO_2, e.g. during high-temperature reductive catalyst treatment. To reveal high catalytic activity, Zr^{4+} cations should have coordination lower than that of cations located on a flat surface of perfect ZrO_2 phase, i.e. this number should be less than 7 and 6 for tetragonal and monoclinic ZrO_2, respectively. The presence of hydrogenation-active metal on the surface of ZrO_2-based material results in acceleration of lattice oxygen removal thus promoting formation of Zr_{cus} sites. However, over-reduction of zirconia was found to negatively influence catalyst activity.

The presence of low-valent dopant in ZrO_2 lattice significantly influences catalyst activity and selectivity. Thus, promoting of ZrO_2 with La_2O_3, Y_2O_3 or Sm_2O_3 results in an increase in catalyst activity for alkane DH, while promoters CaO, MgO or Li_2O have a negative effect on the activity. The distinctive behavior of the dopants was explained by their different ability to

generate/stabilize surface Zr_{cus} sites during reductive treatment and their different effect on intrinsic activity of Zr_{cus} sites. It was also shown that the dopants significantly influence acidic properties of zirconia surface. Owing to a decrease in the concentration of strong acidic sites after ZrO_2 promoting with the above dopants, coke formation in alkane DH can be suppressed.

Promoting of ZrO_2 with CrO_x was shown to be a promising method for preparation of binary $CrZrO_x$ catalysts possessing only 1/16 of chromium content of an industrial analogue of $K\text{-}CrO_x/Al_2O_3$ but showing high activity and selectivity in propane and isobutane dehydrogenation. In comparison with ZrO_2-based catalysts with supported CrO_x, the binary counterparts demonstrated higher activity related to a surface chromium atom and superior durability. The results of catalyst characterization suggest that the high activity of both catalyst types is related to a synergy effect between two types of active sites (Zr_{cus} and CrO_x). The presence of chromium was also established to reduce the concentration of acidic sites related to ZrO_2 thus resulting in suppressing coke formation.

Finally, practical relevance of ZrO_2-based catalysts was shown in a series of propane and isobutane dehydrogenation and oxidative catalyst regeneration cycles. The catalysts demonstrated high productivity compared to that of analogues of industrial CrO_x- and Pt-based catalysts and good durability. Time-on-stream deactivation of the catalysts is caused by formation of coke, which can be totally removed during oxidative treatment. After regeneration stage, the catalysts restore their activity, no significant change of productivity from cycle to cycle was observed.

6. Outlook

ZrO_2-based catalysts were shown to be promising alternatives to CrO_x- and Pt-based catalysts commonly used in industry for the non-oxidative dehydrogenation of light alkanes. In addition to the relationships derived in the frame of this thesis, further studies are required for elucidating factors affecting activity, selectivity and, particularly, on-stream stability of ZrO_2-based catalysts with the purpose to provide fundamentals for their tailored design. For example, in order to exclude any effects of metal oxide dopants or supported metal on intrinsic activity of catalytically active Zr_{cus} sites, it is suggested to systematically investigate bare zirconia. The focus should be put on the synthesis of ZrO_2 with a certain phase composition (monoclinic, tetragonal or cubic), size of crystallites or/and morphology (e.g. rods, spheres, nanosheets) with the purpose to vary reducibility of ZrO_2 and concentration of Zr_{cus}. Such comparative analysis may help to establish fundamental relationships between the structural properties (phase composition and morphology) and catalytic performance of ZrO_2. In order to identify proper conditions for performing dehydrogenation reaction over ZrO_2-based catalysts with high selectivity and stability, it is suggested to deeper elucidate the effect of reaction parameters such as reaction temperature, composition of reaction mixture, duration time of DH and regeneration stages on catalyst performance.

In addition, the reaction pathways leading to carbon deposits should be studied in detail. To this end, long-term catalytic tests should be combined with *operando* catalyst characterization by UV-Vis and/or Raman spectroscopy and with *in situ* temperature-programmed oxidation of deactivated catalysts. Such studies can help to understand origins and nature of coke species formed during alkane dehydrogenation and to investigate catalysts durability (stability over several dehydrogenation/regeneration cycles).

From a fundamental point of view, Density Functional Theory (DFT) calculations can be useful for the characterization of the interaction between alkane molecule and Zr_{cus} sites located at different surfaces (planar and stepped). The calculations will also help to identify the main intermediates formed during dehydrogenation reaction and to determine the most favorable pathways of the reaction.

References

[1] A. Akah, M. Al-Ghrami, *Appl. Petrochem. Res.*, **2015**, 1-16.
[2] S.M. Sadrameli, *Fuel*, 173, **2016**, 285-297.
[3] H.M. Torres Galvis, K.P. de Jong, *ACS Catal.*, 3, **2013**, 2130-2149.
[4] Z. Nawaz, *Rev. Chem. Eng.*, 31, **2015**, 413-436.
[5] H. Danner, M. Ürmös, M. Gartner, R. Braun, *Appl. Biochem. Biotechnol.*, 70, **1998**, 887-894.
[6] J.G. Speight, Naphtha and Solvents, in: *Handbook of Petroleum Product Analysis*, John Wiley & Sons, Inc., **2014**, pp. 88-103.
[7] S.M. Sadrameli, *Fuel*, 140, **2015**, 102-115.
[8] E. Joo, S. Park, M. Lee, *Ind. Eng. Chem. Res.*, 40, **2001**, 2409-2415.
[9] M.R. Gray, W.C. McCaffrey, *Energy Fuels*, 16, **2002**, 756-766.
[10] M. Sedighi, K. Keyvanloo, J. Towfighi Darian, *IJCCE*, 29, **2010**, 135-147.
[11] S.M. Alipour, *Chin. J. Catal.*, 37, **2016**, 671-680.
[12] W.-C. Cheng, G. Kim, A. Peters, X. Zhao, K. Rajagopalan, M. Ziebarth, C. Pereira, *Catal. Rev.*, 40, **1998**, 39-79.
[13] Y.V. Kissin, *J. Catal.*, 163, **1996**, 50-62.
[14] F.C. Jentoft, B.C. Gates, *Topics Catal.*, 4, **1997**, 1-13.
[15] Y. Yoshimura, N. Kijima, T. Hayakawa, K. Murata, K. Suzuki, F. Mizukami, K. Matano, T. Konishi, T. Oikawa, M. Saito, T. Shiojima, K. Shiozawa, K. Wakui, G. Sawada, K. Sato, S. Matsuo, N. Yamaoka, *Catal. Surv. Jpn.*, 4, **2001**, 157-167.
[16] A. Corma, F. Melo, L. Sauvanaud, F.J. Ortega, *Appl. Catal. A*, 265, **2004**, 195-206.
[17] N. Rahimi, R. Karimzadeh, *Appl. Catal. A*, 398, **2011**, 1-17.
[18] K.C. Hunter, A.L.L. East, *J. Phys. Chem. A*, 106, **2002**, 1346-1356.
[19] J.Q. Chen, A. Bozzano, B. Glover, T. Fuglerud, S. Kvisle, *Catal. Today*, 106, **2005**, 103-107.
[20] U. Olsbye, S. Svelle, M. Bjørgen, P. Beato, T.V.W. Janssens, F. Joensen, S. Bordiga, K.P. Lillerud, *Angew. Chem., Int. Ed.*, 51, **2012**, 5810-5831.
[21] M. Khanmohammadi, S. Amani, A.B. Garmarudi, A. Niaei, *Chin. J. Catal.*, 37, **2016**, 325-339.
[22] G. Seo, J.-H. Kim, H.-G. Jang, *Catal. Surv. Asia*, 17, **2013**, 103-118.
[23] S. Maksasithorn, D.P. Debecker, P. Praserthdam, J. Panpranot, K. Suriye, S.K.N. Ayudhya, *Chin. J. Catal.*, 35, **2014**, 232-241.
[24] H.A. Wittcoff, B.G. Reuben, J.S. Plotkin, Chemicals from Natural Gas and Petroleum, in: *Industrial Organic Chemicals*, John Wiley & Sons, Inc., **2005**, pp. 57-99.
[25] W. Jiang, R. Huang, P. Li, S. Feng, G. Zhou, C. Yu, H. Zhou, C. Xu, Q. Xu, *Appl. Catal. A*, 517, **2016**, 227-235.
[26] N. Popoff, E. Mazoyer, J. Pelletier, R.M. Gauvin, M. Taoufik, *Chem. Soc. Rev.*, 42, **2013**, 9035-9054.
[27] Y. Chauvin, *Angew. Chem., Int. Ed.*, 45, **2006**, 3740-3747.
[28] H.H. Kung, *Adv. Catal.*, Volume 40, **1994**, 1-38.
[29] K. Chen, A.T. Bell, E. Iglesia, *J. Phys. Chem. B*, 104, **2000**, 1292-1299.
[30] F. Cavani, F. Trifiro, *Catal. Today*, 24, **1995**, 307-313.
[31] S.F. Håkonsen, A. Holmen, Oxidative Dehydrogenation of Alkanes, in: *Handbook of Heterogeneous Catalysis*, Wiley-VCH Verlag GmbH & Co. KGaA, **2008**.

[32] R. Grabowski, *Catal. Rev.*, 48, **2006**, 199-268.
[33] J.C. Védrine, *Catalysts*, 6, **2016**, 22.
[34] C.A. Carrero, R. Schloegl, I.E. Wachs, R. Schomaecker, *ACS Catal.*, 4, **2014**, 3357-3380.
[35] M.M. Bhasin, J.H. McCain, B.V. Vora, T. Imai, P.R. Pujadó, *Appl. Catal. A*, 221, **2001**, 397-419.
[36] B.V. Vora, *Topics Catal.*, 55, **2012**, 1297-1308.
[37] B.M. Weckhuysen, R.A. Schoonheydt, *Catal. Today*, 51, **1999**, 223-232.
[38] D.E. Resasco, G.L. Haller, Catalytic dehydrogenation of lower alkanes, in: *Catalysis*, The Royal Society of Chemistry, **1994**, pp. 379-411.
[39] S.D. Barnicki, Synthetic Organic Chemicals, in: *Handbook of Industrial Chemistry and Biotechnology*, Springer US, **2012**, pp. 307-389.
[40] J.J.H.B. Sattler, J. Ruiz-Martinez, E. Santillan-Jimenez, B.M. Weckhuysen, *Chem. Rev.*, 114, **2014**, 10613-10653.
[41] R.A. Buyanov, N.A. Pakhomov, *Kinet. Catal.*, 42, **2001**, 64-75.
[42] J.C. Bricker, *Topics Catal.*, 55, **2012**, 1309-1314.
[43] K.J. Caspary, H. Gehrke, M. Heinritz-Adrian, M. Schwefer, Dehydrogenation of Alkanes, in: *Handbook of Heterogeneous Catalysis*, Wiley-VCH Verlag GmbH & Co. KGaA, **2008**.
[44] A. Iglesias-Juez, A.M. Beale, K. Maaijen, T.C. Weng, P. Glatzel, B.M. Weckhuysen, *J. Catal.*, 276, **2010**, 268-279.
[45] J. Zhu, M.-L. Yang, Y. Yu, Y.-A. Zhu, Z.-J. Sui, X.-G. Zhou, A. Holmen, D. Chen, *ACS Catal.*, 5, **2015**, 6310-6319.
[46] H. Zhu, D.H. Anjum, Q. Wang, E. Abou-Hamad, L. Emsley, H. Dong, P. Laveille, L. Li, A.K. Samal, J.-M. Basset, *J. Catal.*, 320, **2014**, 52-62.
[47] I. Kley, Y. Traa, *Microporous Mesoporous Mat.*, 164, **2012**, 145-147.
[48] P. Sun, G. Siddiqi, W.C. Vining, M. Chi, A.T. Bell, *J. Catal.*, 282, **2011**, 165-174.
[49] P. Sun, G. Siddiqi, M. Chi, A.T. Bell, *J. Catal.*, 274, **2010**, 192-199.
[50] S.M. Stagg, C.A. Querini, W.E. Alvarez, D.E. Resasco, *J. Catal.*, 168, **1997**, 75-94.
[51] C. Xu, B.E. Koel, M.T. Paffett, *Langmuir*, 10, **1994**, 166-171.
[52] O.A. Bariås, A. Holmen, E.A. Blekkan, *J. Catal.*, 158, **1996**, 1-12.
[53] V.Z. Fridman, R. Xing, M. Severance, *Appl. Catal. A*, 523, **2016**, 39-53.
[54] C.P. Poole Jr, D.S. MacIver, *Adv. Catal.*, 17, **1967**, 223-314.
[55] M. Santhosh Kumar, N. Hammer, M. Rønning, A. Holmen, D. Chen, J.C. Walmsley, G. Øye, *J. Catal.*, 261, **2009**, 116-128.
[56] B.M. Weckhuysen, R.A. Schoonheydt, F.E. Mabbs, D. Collison, *J. Chem. Soc., Faraday Trans.*, 92, **1996**, 2431-2436.
[57] A. Hakuli, A. Kytökivi, A.O.I. Krause, T. Suntola, *J. Catal.*, 161, **1996**, 393-400.
[58] W. Grünert, R. Feldhaus, K. Anders, E.S. Shpiro, G.V. Antoshin, K.M. Minachev, *J. Catal.*, 100, **1986**, 138-148.
[59] H. Zhao, H. Song, L. Xu, L. Chou, *Appl. Catal. A*, 456, **2013**, 188-196.
[60] S.D. Rossi, G. Ferraris, S. Fremiotti, A. Cimino, V. Indovina, *Appl. Catal. A*, 81, **1992**, 113-132.
[61] N.M. Schweitzer, B. Hu, U. Das, H. Kim, J. Greeley, L.A. Curtiss, P.C. Stair, J.T. Miller, A.S. Hock, *ACS Catal.*, 4, **2014**, 1091-1098.
[62] B. Hu, N.M. Schweitzer, G. Zhang, S.J. Kraft, D.J. Childers, M.P. Lanci, J.T. Miller, A.S. Hock, *ACS Catal.*, 5, **2015**, 3494-3503.
[63] B. Hu, A.B. Getsoian, N.M. Schweitzer, U. Das, H. Kim, J. Nildas, O. Poluektov, L.A. Curtiss, P.C. Stair, J.T. Miller, A.S. Hock, *J. Catal.*, 322, **2015**, 24-37.

[64] S. Sokolov, M. Stoyanova, U. Rodemerck, D. Linke, E.V. Kondratenko, *J. Catal.*, 293, **2012**, 67-75.
[65] M.E. Harlin, V.M. Niemi, A.O.I. Krause, B.M. Weckhuysen, *J. Catal.*, 203, **2001**, 242-252.
[66] G. Liu, Z.-J. Zhao, T. Wu, L. Zeng, J. Gong, *ACS Catal.*, 6, **2016**, 5207-5214.
[67] I. Takahara, M. Saito, M. Inaba, K. Murata, *Catal. Lett.*, 96, **2004**, 29-32.
[68] B. Zheng, W.M. Hua, Y.H. Yue, Z. Gao, *J. Catal.*, 232, **2005**, 143-151.
[69] Y. Liu, Z.H. Li, J. Lu, K.-N. Fan, *J. Phys. Chem. C*, 112, **2008**, 20382-20392.
[70] J.J.H.B. Sattler, I.D. Gonzalez-Jimenez, L. Luo, B.A. Stears, A. Malek, D.G. Barton, B.A. Kilos, M.P. Kaminsky, T.W.G.M. Verhoeven, E.J. Koers, M. Baldus, B.M. Weckhuysen, *Angew. Chem., Int. Ed.*, 53, **2014**, 9251-9256.
[71] P.C.H. Mitchell, S.A. Wass, *Appl. Catal. A*, 225, **2002**, 153-165.
[72] P. Bai, Z. Ma, T. Li, Y. Tian, Z. Zhang, Z. Zhong, W. Xing, P. Wu, X.-m. Liu, Z. Yan, *ACS Appl. Mat. Interf.*, **2016**.
[73] Y.-P. Tian, P. Bai, S.-M. Liu, X.-M. Liu, Z.-F. Yan, *Fuel Proc. Techn.*, 151, **2016**, 31-39.
[74] Y. Xie, W. Hua, Y. Yue, Z. Gao, *Chinese Journal of Chemistry*, 28, **2010**, 1559-1564.
[75] V. Fridman, US Patent 8101541 B2, Sud-Chemie Inc., **2012**.
[76] J. Pérez-Ramírez, E.V. Kondratenko, *Catal. Today*, 121, **2007**, 160-169.
[77] T. Liu, X. Zhang, X. Wang, J. Yu, L. Li, *Ionics*, 22, **2016**, 2249-2262.
[78] D. Martin, D. Duprez, *J. Phys. Chem.*, 100, **1996**, 9429-9438.
[79] D. Hoang, H. Lieske, *Catal. Lett.*, 27, **1994**, 33-42.
[80] H. He, H. Dai, L. Ng, K.W. Wong, C. Au, *J. Catal.*, 206, **2002**, 1-13.
[81] A. Suda, K. Yamamura, Y. Ukyo, T. Tanabe, Y. Nagai, M. Sugiura, *J. Jpn. Soc. Powder Powder Metall.*, 51, **2004**, 815-820.
[82] E.V. Kondratenko, Y. Sakamoto, K. Okumura, H. Shinjoh, *Catal. Today*, 164, **2011**, 46-51.
[83] T. Abe, M. Tanizawa, K. Watanabe, A. Taguchi, *Energy Environ. Sci.*, 2, **2009**, 315-321.
[84] S. Porsgaard, L.R. Merte, L.K. Ono, F. Behafarid, J. Matos, S. Helveg, M. Salmeron, B. Roldan Cuenya, F. Besenbacher, *ACS nano*, 6, **2012**, 10743-10749.
[85] J.A. Wang, T. López, X. Bokhimi, O. Novaro, *J. Mol. Catal. A*, 239, **2005**, 249-256.
[86] C. Berger-Karin, J. Radnik, E.V. Kondratenko, *J. Catal.*, 280, **2011**, 116-124.
[87] M.P. Conley, M.F. Delley, F. Núñez-Zarur, A. Comas-Vives, C. Copéret, *Inorg. Chem.*, 54, **2015**, 5065-5078.
[88] M.F. Delley, M.-C. Silaghi, F. Nuñez-Zarur, K.V. Kovtunov, O.G. Salnikov, D.P. Estes, I.V. Koptyug, A. Comas-Vives, C. Copéret, *Organometallics*, 36, **2017**, 234-244.
[89] H.-Y.T. Chen, S. Tosoni, G. Pacchioni, *Surf. Sci.*, 652, **2016**, 163-171.
[90] X. Guo, T. Schober, *J. Am. Ceram. Soc.*, 87, **2004**, 746-748.
[91] D. Eder, R. Kramer, *Phys. Chem. Chem. Phys.*, 8, **2006**, 4476-4483.
[92] M.V. Ganduglia-Pirovano, A. Hofmann, J. Sauer, *Surf. Sci. Rep.*, 62, **2007**, 219-270.
[93] M. Occhiuzzi, D. Cordischi, R. Dragone, *J. Phys. Chem. B*, 106, **2002**, 12464-12469.
[94] A. Martinez-Arias, M. Fernandez-Garcia, C. Belver, J.C. Conesa, J. Soria, *Catal. Lett.*, 65, **2000**, 197-204.
[95] J.T. Gleaves, G. Yablonsky, X. Zheng, R. Fushimi, P.L. Mills, *J. Mol. Catal. A*, 315, **2010**, 108-134.
[96] C. Gionco, M.C. Paganini, E. Giamello, R. Burgess, C. Di Valentin, G. Pacchioni, *Chem. Mater.*, 25, **2013**, 2243-2253.
[97] D. Eder, R. Kramer, *Phys. Chem. Chem. Phys.*, 4, **2002**, 795-801.

[98] A. Trovarelli, *Catal. Rev.*, 38, **1996**, 439-520.
[99] I.D. González, R.M. Navarro, W. Wen, N. Marinkovic, J.A. Rodriguéz, F. Rosa, J.L.G. Fierro, *Catal. Today*, 149, **2010**, 372-379.
[100] S. Damyanova, J. Bueno, *Appl. Catal. A*, 253, **2003**, 135-150.
[101] L. Pino, A. Vita, M. Cordaro, V. Recupero, M.S. Hegde, *Appl. Catal. A*, 243, **2003**, 135-146.
[102] E.V. Kondratenko, Y. Sakamoto, K. Okumura, H. Shinjoh, *Appl. Catal. B*, 89, **2009**, 476-483.
[103] M.T. Elm, J.D. Hofmann, C. Suchomski, J. Janek, T. Brezesinski, *ACS Appl. Mat. Interf.*, 7, **2015**, 11792-11801.
[104] R.J.D. Tilley, *Defects in Solids*, Wiley, **2008**.
[105] Y. Han, J. Zhu, *Topics Catal.*, 56, **2013**, 1525-1541.
[106] S. Shukla, S. Seal, *Int. Mat. Rev.*, 50, **2005**, 45-64.
[107] A. Sinhamahapatra, J.P. Jeon, J. Kang, B. Han, J.S. Yu, *Scientific Reports*, 6, **2016**.
[108] S. Jaenicke, G.K. Chuah, V. Raju, Y.T. Nie, *Catal. Surv. Asia*, 12, **2008**, 153-169.
[109] T. Yamaguchi, *Catal. Today*, 20, **1994**, 199-217.
[110] R. Srinivasan, R.J. De Angelis, G. Ice, B.H. Davis, *J. Mater. Res.*, 6, **1991**, 1287-1292.
[111] C.G. Kontoyannis, M. Orkoula, *J. Mater. Sci.*, 29, **1994**, 5316-5320.
[112] A. Sekulic, K. Furic, A. Tonejc, A. Tonejc, M. Stubicar, *J. Mater. Sci. Lett.*, 16, **1997**, 260-262.
[113] S.P.S. Badwal, *Solid State Ion.*, 52, **1992**, 23-32.
[114] R. Barthos, F. Lónyi, G. Onyestyák, J. Valyon, *J. Phys. Chem. B*, 104, **2000**, 7311-7319.
[115] S. Kouva, K. Honkala, L. Lefferts, J. Kanervo, *Catal. Sci. Tech.*, 5, **2015**, 3473-3490.
[116] L.A. Gribov, I.A. Novakov, A.I. Pavlyuchko, I.O. Kulago, B.S. Orlinson, *J. Struct. Chem.*, 44, **2003**, 961-969.
[117] B. Meredig, C. Wolverton, *Chem. Mater.*, 26, **2014**, 1985-1991.
[118] J.W. Fergus, *J. Mater. Sci.*, 38, **2003**, 4259-4270.
[119] G.K. Boreskov, *Heterogeneous catalysis*, Nova Science Publishers, **2003**.
[120] S. De Rossi, M. Pia Casaletto, G. Ferraris, A. Cimino, G. Minelli, *Appl. Catal. A*, 167, **1998**, 257-270.
[121] T. Bugrova, N. Litvyakova, G. Mamontov, *Kinet. Catal.*, 56, **2015**, 758-763.
[122] M.G. Cutrufello, S. De Rossi, I. Ferino, R. Monaci, E. Rombi, V. Solinas, *Thermochim. Acta*, 434, **2005**, 62-68.
[123] S. Derossi, G. Ferraris, S. Fremiotti, E. Garrone, G. Ghiotti, M.C. Campa, V. Indovina, *J. Catal.*, 148, **1994**, 36-46.
[124] R. Wu, P. Xie, Y. Cheng, Y. Yue, S. Gu, W. Yang, C. Miao, W. Hua, Z. Gao, *Catal.Commun.*, 39, **2013**, 20-23.
[125] A. Trunschke, D.L. Hoang, J. Radnik, H. Lieske, *J. Catal.*, 191, **2000**, 456-466.
[126] M.F.M. Zwinkels, O. Haussner, P. Govind Menon, S.G. Järås, *Catal. Today*, 47, **1999**, 73-82.
[127] C. Morterra, G. Cerrato, L. Ferroni, A. Negro, L. Montanaro, *Appl. Surf. Sci.*, 65, **1993**, 257-264.
[128] Y. Zhao, W. Li, M. Zhang, K. Tao, *Catal.Commun.*, 3, **2002**, 239-245.
[129] S. Wang, K. Murata, T. Hayakawa, S. Hamakawa, K. Suzuki, *Energy Fuels*, 15, **2001**, 384-388.
[130] D. Hoang, H. Lieske, *Thermochim. Acta*, 345, **2000**, 93-99.

[131] Y. Ramesh, P. Thirumala Bai, B. Hari Babu, N. Lingaiah, K.S. Rama Rao, P.S.S. Prasad, *Appl. Petrochem. Res.*, 4, **2014**, 247-252.
[132] J.J.H.B. Sattler, A.M. Beale, B.M. Weckhuysen, *Phys. Chem. Chem. Phys.*, 15, **2013**, 12095-12103.
[133] S. Galvagno, J. Schwank, G. Gubitosa, G.R. Tauszik, *J. Chem. Soc., Faraday Trans.1*, 78, **1982**, 2509-2520.
[134] C.J. Machiels, R.B. Anderson, *J. Catal.*, 58, **1979**, 253-259.

Appendix

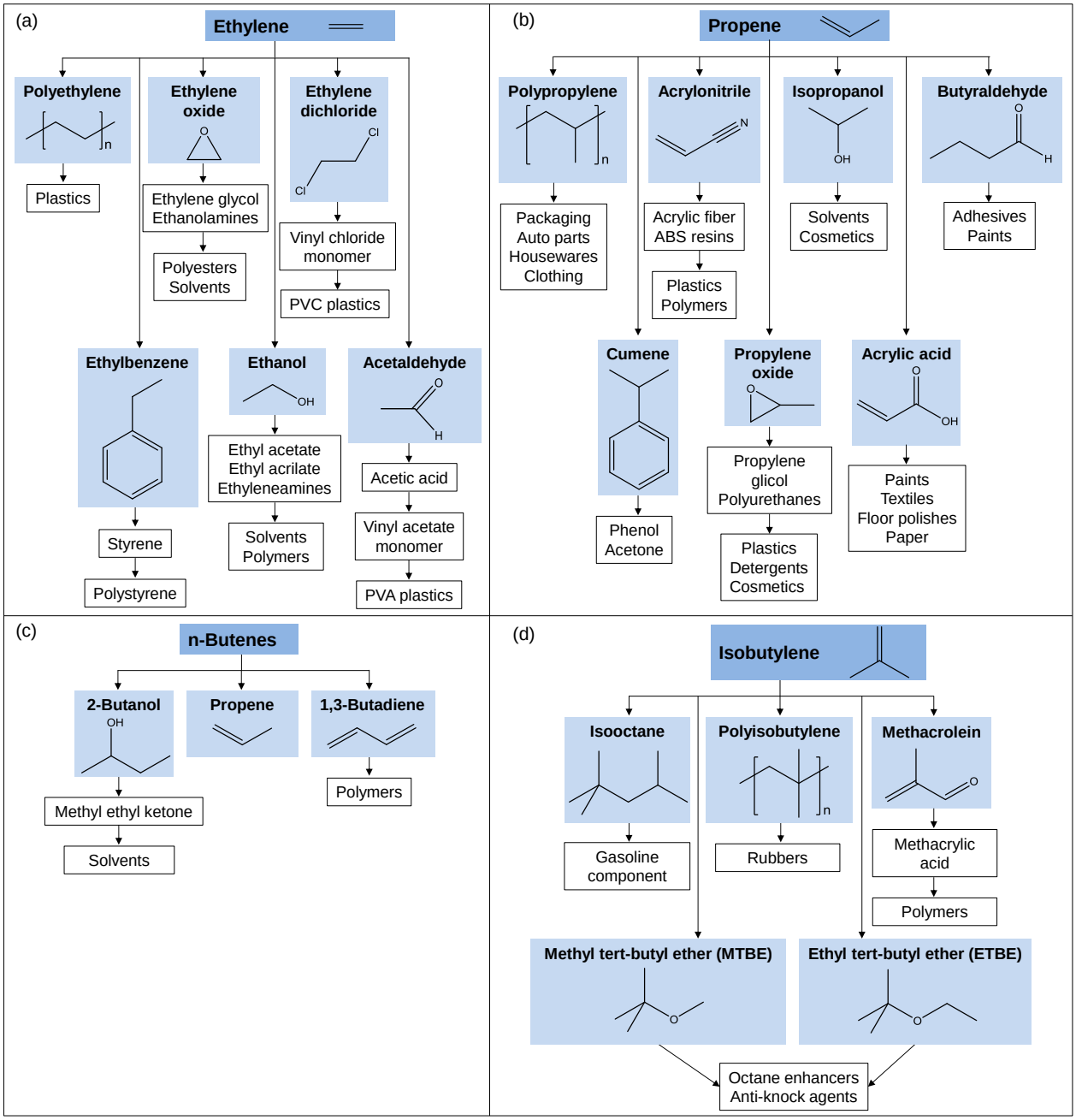

Figure A-1. Ethylene (a), propene (b), n-butenes (c) and isobutylene (d) products chains.[3-5, 37, 41]

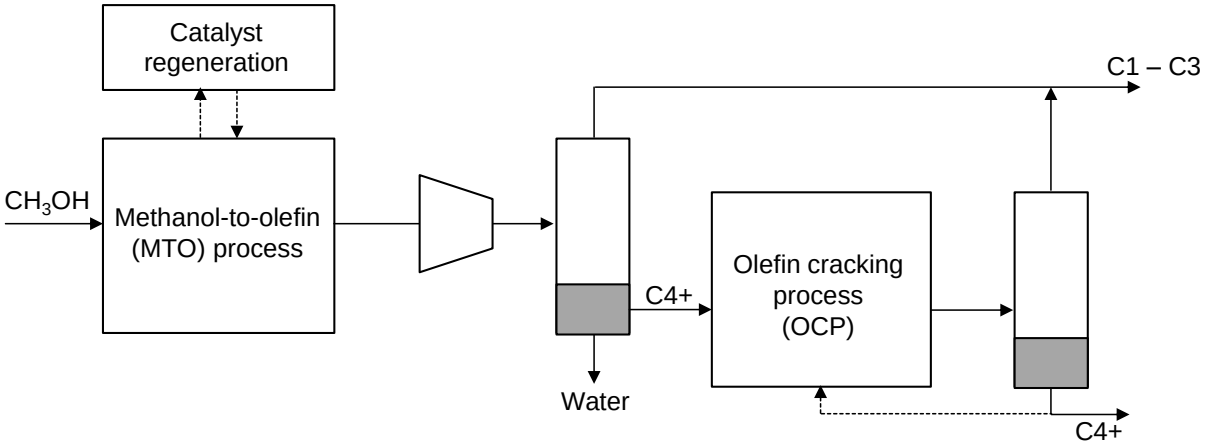

Figure A-2. Schematic illustration of the MTO fluidized-bed process combined with olefin cracking process.[20]

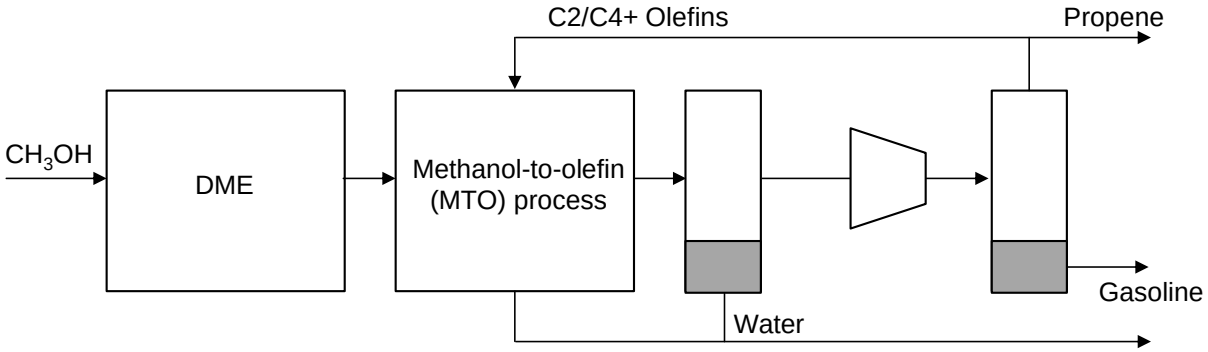

Figure A-3. Schematic illustration of Lurgi MTP process: adiabatic dehydration reactor for DME (DME = dimethyl ether) synthesis and parallel adiabatic reactors with interstage feed (quench) addition and recycle of process condensate and C_2 and C_{4+} olefins.[20]

$C_nH_{2n+2} \leftrightarrow C_nH_{2n} + H_2$ (A.1)

$$K_p = \frac{p(C_nH_{2n}) \times p(H_2)}{p(C_nH_{2n+2})} \quad (A.2)$$

$$p(H_2) = x(H_2) \times P \quad (A.3)$$

$$x(H_2) = \frac{n(H_2)}{n(C_nH_{2n+2}) + n(C_nH_{2n}) + n(H_2) + n^0(inert\ gas)} =$$

$$\frac{n^0(C_nH_{2n+2}) \times X + n^0(H_2)}{n^0(C_nH_{2n+2}) \times (1-X) + n^0(C_nH_{2n+2}) \times X + n^0(C_nH_{2n+2}) \times X + n^0(H_2) + n^0(inert\ gas)} = \frac{X + H}{1 + X + H + I} \quad (A.4)$$

$$H = \frac{n^0(H_2)}{n^0(C_nH_{2n+2})} \quad (A.5)$$

$$I = \frac{n^0(inert\ gas)}{n^0(C_nH_{2n+2})} \quad (A.6)$$

$$p(C_nH_{2n}) = x(C_nH_{2n}) \times P \quad (A.7)$$

$$x(C_nH_{2n}) = \frac{X}{1 + X + H + I} \quad (A.8)$$

$$p(C_nH_{2n+2}) = x(C_nH_{2n}) \times P \quad (A.9)$$

$$x(C_nH_{2n+2}) = \frac{1 - X}{1 + X + H + I} \quad (A.10)$$

$$K_p = \frac{(X + H) \times P \times X \times P \times (1 + X + H + I)}{(1 + X + H + I) \times (1 + X + H + I) \times (1 - X) \times P} = \frac{X \times (X + H) \times P}{(1 - X) \times (1 + X + H + I)} \quad (A.11)$$

Here, K_p is the equilibrium constant, X is the equilibrium conversion, p(i) is a partial pressure of component i, x(i) is molar fraction of component i, P is the total pressure, n(i) is a current number of moles of component i, n^0(i) is initial number of moles of component i in a feed.

$$K_p = e^{-\frac{\Delta G_r^T}{RT}} \quad \text{(A.12)}$$

$$\Delta G_r^T = \Delta H_r^T - T \times \Delta S_r^T \quad \text{(A.13)}$$

$$\Delta H_r^T = \sum \Delta H_f^{298}(product) - \sum \Delta H_f^{298}(reagent) + \sum \int_{298}^{T} c_p(product)dT - \sum \int_{298}^{T} c_p(reagent)dT + \sum \Delta H_{p.t.}(product) - \sum \Delta H_{p.t.}(reagent) \quad \text{(A.14)}$$

$$\Delta S_r^T = \sum \Delta S_f^{298}(product) - \sum \Delta S_f^{298}(reagent) + \sum \int_{298}^{T} \frac{c_p(product)}{T} dT - \sum \int_{298}^{T} \frac{c_p(reagent)}{T} dT + \sum \Delta S_{p.t.}(product) - \sum \Delta S_{p.t.}(reagent) \quad \text{(A.15)}$$

Here, K_p is the equilibrium constant, T is actual temperature (in K), ΔG_r^T is Gibbs energy of the reaction at temperature T, ΔH_r^T is enthalpy of the reaction at temperature T, ΔS_r^T is entropy of the reaction at temperature T, ΔH_f^{298} is standard enthalpy of formation, $\Delta H_{p.t.}$ is enthalpy of phase transition which occurs in temperature range from 298 till T, c_p is heat capacity, ΔS_f^{298} is standard entropy of formation, $\Delta S_{p.t.}$ is entropy of phase transition which occurs in temperature range from 298 till T.

Table A-1. Standard enthalpy and entropy of formation and heat capacity coefficients for selected hydrocarbons and H_2.

	ΔH_f^{298}, J·mol^{-1}	ΔS_f^{298}, J·K^{-1}·mol^{-1}	$c_p\ (J/K/mol) = A + B \times T + C \times T^2 + D \times T^3$			
			A	B	C	D
H_2	0	130.6	27.14	$9.274 \cdot 10^{-3}$	$-1.381 \cdot 10^{-5}$	$7.645 \cdot 10^{-9}$
C_2H_4	52340	219.56	3.806	$1.566 \cdot 10^{-1}$	$-8.348 \cdot 10^{-5}$	$1.755 \cdot 10^{-8}$
C_2H_6	-84740	229.6	5.409	$1.781 \cdot 10^{-1}$	$-6.938 \cdot 10^{-5}$	$8.713 \cdot 10^{-9}$
C_3H_6	20340	267	3.710	$2.345 \cdot 10^{-1}$	$-1.160 \cdot 10^{-4}$	$2.205 \cdot 10^{-8}$
C_3H_8	-103900	270	-4.224	$3.063 \cdot 10^{-1}$	$-1.586 \cdot 10^{-4}$	$3.215 \cdot 10^{-8}$
iso-C_4H_8	-16910	294	16.05	$2.804 \cdot 10^{-1}$	$-1.091 \cdot 10^{-4}$	$9.098 \cdot 10^{-9}$
iso-C_4H_{10}	-134600	295	-1.390	$3.847 \cdot 10^{-1}$	$-1.846 \cdot 10^{-4}$	$2.895 \cdot 10^{-8}$

Table A-2. Main features of the Oleflex and Catofin commercial dehydrogenation processes.[40, 43]

	Oleflex	Catofin
Catalyst	Pt-Sn on alumina	Chromia on alumina
Process license holder	UOP (Honeywell)	CB&I Lummus
Reaction system	Fluidized-bed system consisting of several radial-flow adiabatic reactors in series, catalyst regeneration section and product recovery section	Fixed-bed system consisting of a number of axial-flow adiabatic reactors connected in series
Main source of heat supply	Preheating of the starting and intermediate products before each reactor	Heating the catalyst during regeneration
Operating mode	Continuous (5 – 10 days catalyst cycle time)	Discontinious (15 – 30 min reaction cycle)
Operating conditions	525 – 705°C at 1 – 3 bar	575°C at 0.2 – 0.5 bar
Per-pass conversion of propane	35%	48 – 65%
Selectivity to propene	89 – 91 mol. %	88 mol. %
Per-pass conversion of isobutane	35%	50 – 60%
Selectivity to isobutylene	91 – 93 mol. %	88 – 94 mol. %
Catalyst lifetime	1 – 3 years, new catalyst being continuously added to the reactor system and dust formed due to catalyst attrition being continuously removed	2 – 3 years before the reactor is shut down and the catalyst is replaced; catalyst lifetime is prolonged by the increasing the temperature

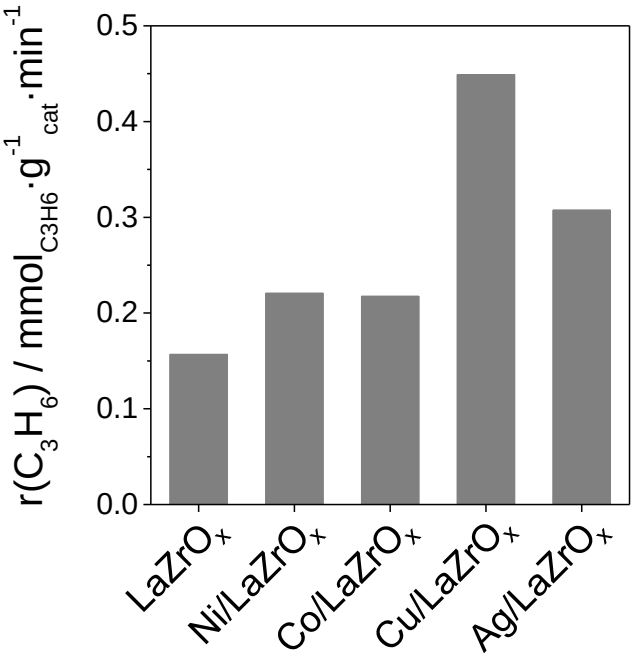

Figure A-4. Rates of propene formation over bare $LaZrO_x$ and that with 0.05 wt.% of supported Ni, Co and Cu or with 0.2 wt.% of supported Ag. Test conditions: 550°C, C_3H_8:N_2 = 40:60, WHSV of 23.6 h^{-1}. The catalysts were pre-reduced at 550°C in a flow of H_2 (57 vol.% H_2 in N_2) for 1 hour.

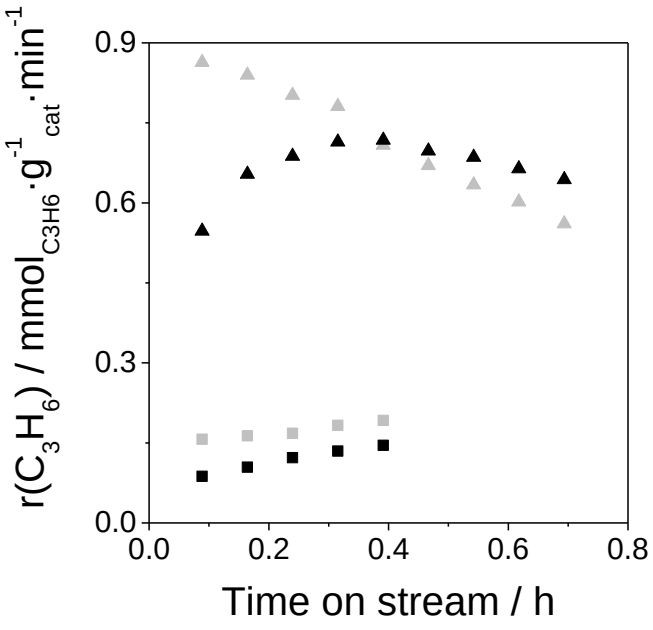

Figure A-5. Time-on stream evolution of the rate of propene formation over pre-reduced (■, ▲) and oxidized (■, ▲) $LaZrO_x$ (squares) and 0.05Ru/$LaZrO_x$ (triangles). Test conditions: 550 °C, C_3H_8:N_2 = 40:60, WHSV of 23.6 h^{-1}.

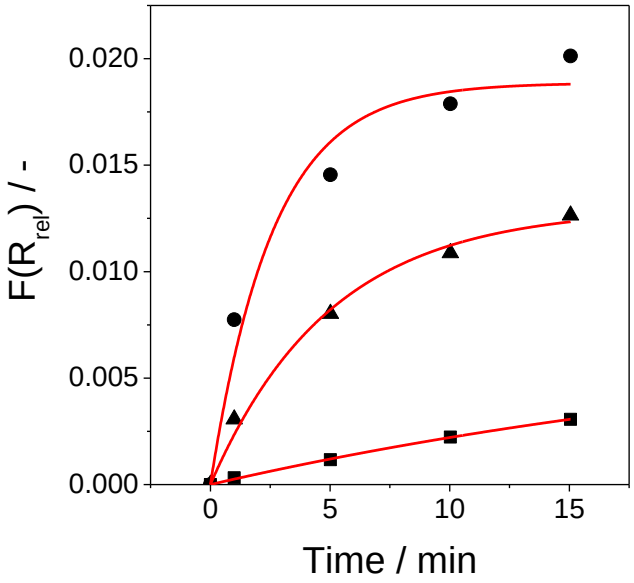

Figure A-6. Temporal changes in $F(R_{rel})$ at 450 nm during H_2 treatment of ■ $LaZrO_x$, ▲ 0.002Ru/$LaZrO_x$, and ● 0.005Ru/$LaZrO_x$ at 550°C. Red lines are related to the fitting results.

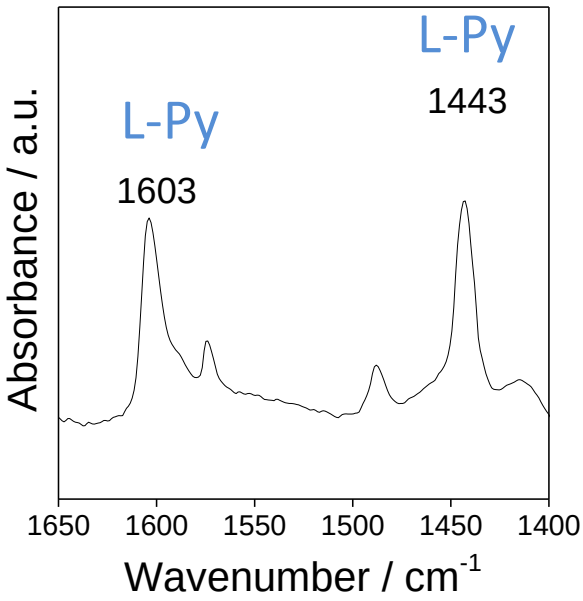

Figure A-7. The infrared spectrum of pyridine adsorbed on reduced $YZrO_x$. The bands at 1603 and 1443 cm^{-1} are related to Lewis acidic sites.

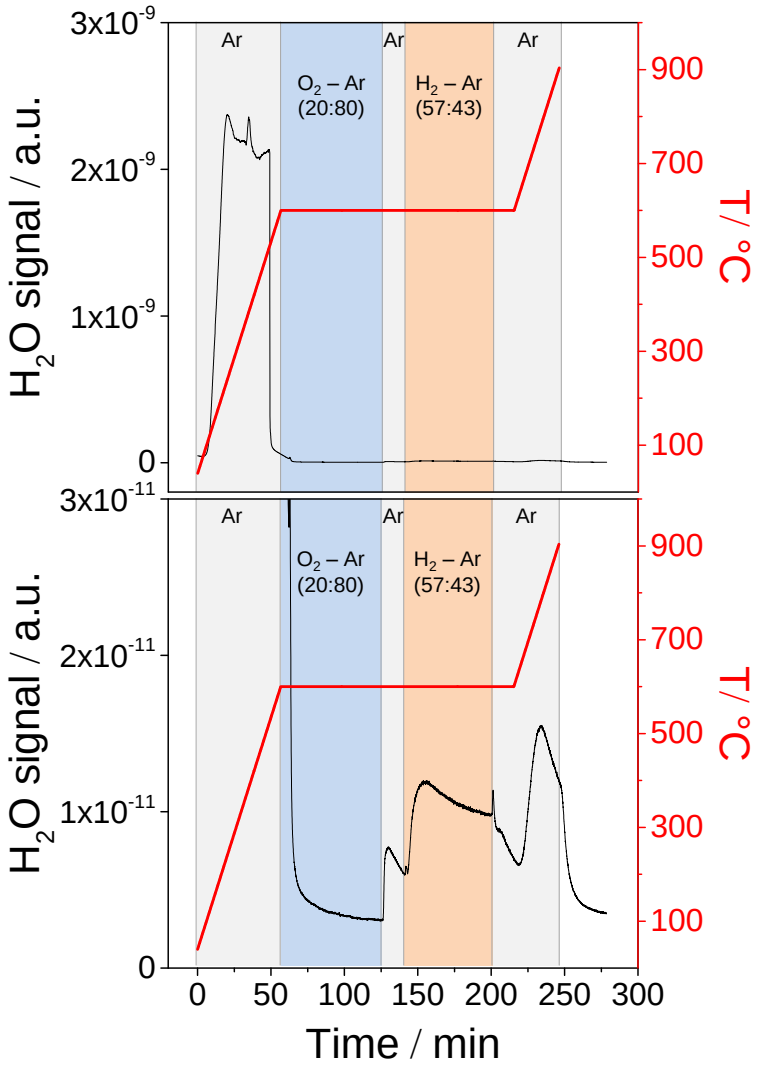

Figure A-8. Water release upon thermal treatment of $LaZrO_x$ in different feeds (Ar, 20 vol.% O_2 in Ar, or 57 vol.% H_2 in Ar). The axis Y in the bottom figure is zoomed for clear illustration of H_2O formation upon catalyst reduction and heating to 900°C.

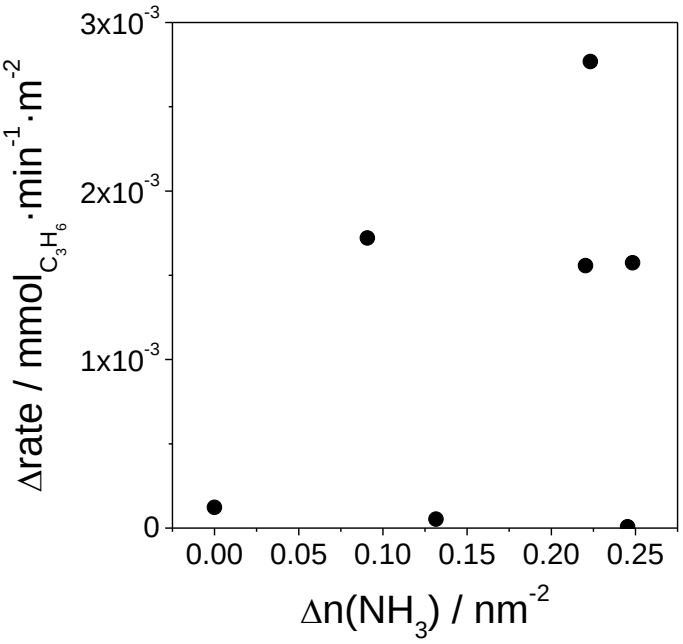

Figure A-9. Relationship between the difference in rates of alkene formation obtained for oxidized and reduced catalysts and corresponding difference in numbers of acidic sites determined from NH_3-TPD.

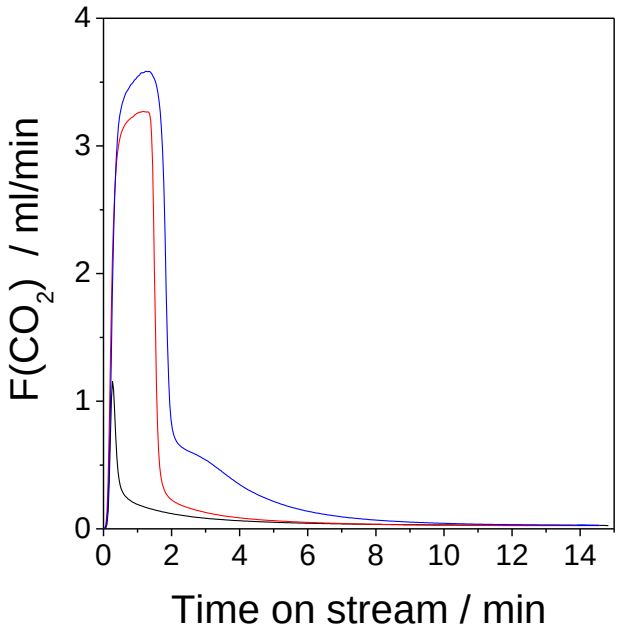

Figure A-10. CO_2 release during regeneration stage performed after 40 min of PDH stage at 550°C for $LaZrO_x$ (–), $YZrO_x$ (–) and $Ru/LaZrO_x$ (–).

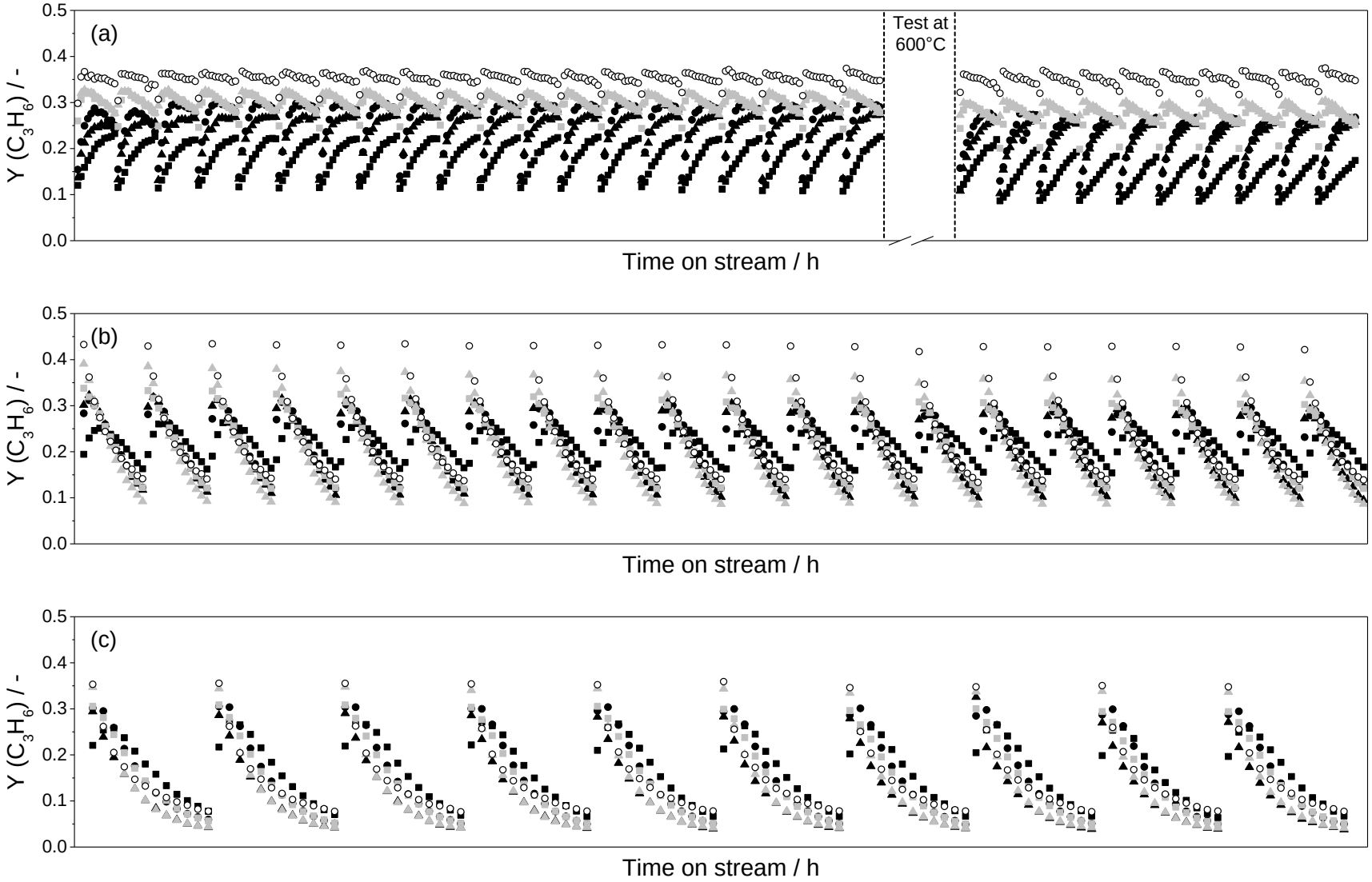

Figure A-11. Temporal change of propene yield for each cycle at (a) 550°C, (b) 600°C and (c) 625°C for ■ $LaZrO_x$, ● $Cu/LaZrO_x$, ▲ $Ru/LaZrO_x$, ● $YZrO_x$, ▲ $Ru/YZrO_x$, and ○ $K\text{-}CrO_x/Al_2O_3$. Each PDH cycle continued for 38 min.

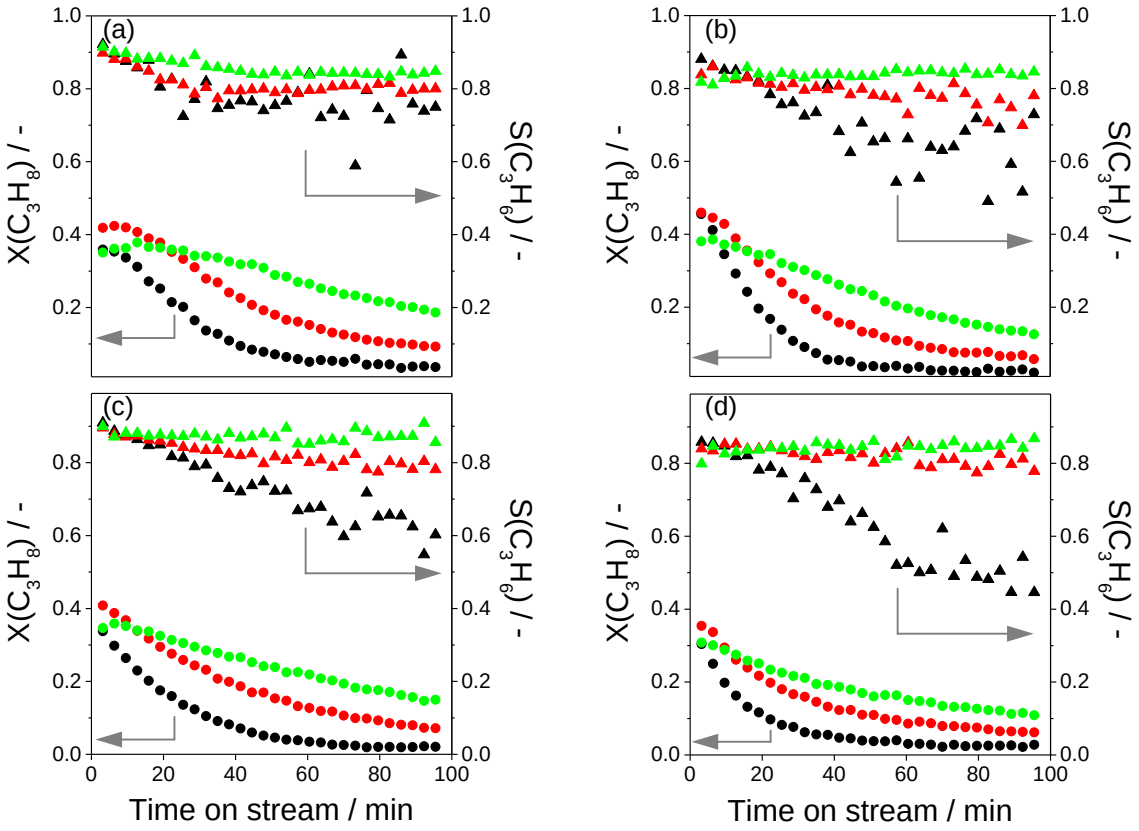

Figure A-12. Temporal change of propane conversion (circles) and propene selectivity (triangles) for (a) Cu/LaZrO$_x$, (b) 0.05Ru(imp.)/LaZrO$_x$, (c) 0.005Ru(imp.)/YZrO$_x$_NorPro, and (d) 0.05Ru(imp.)/YZrO$_x$_NorPro obtained at 600°C by using different composition of reaction mixture: ●, ▲ – 40 vol.% C_3H_8 , ●, ▲ – 40 vol.% C_3H_8-10 vol.% H_2, ●, ▲ – 40 vol.% C_3H_8-30 vol.% H_2, N_2 was a balance in all cases.

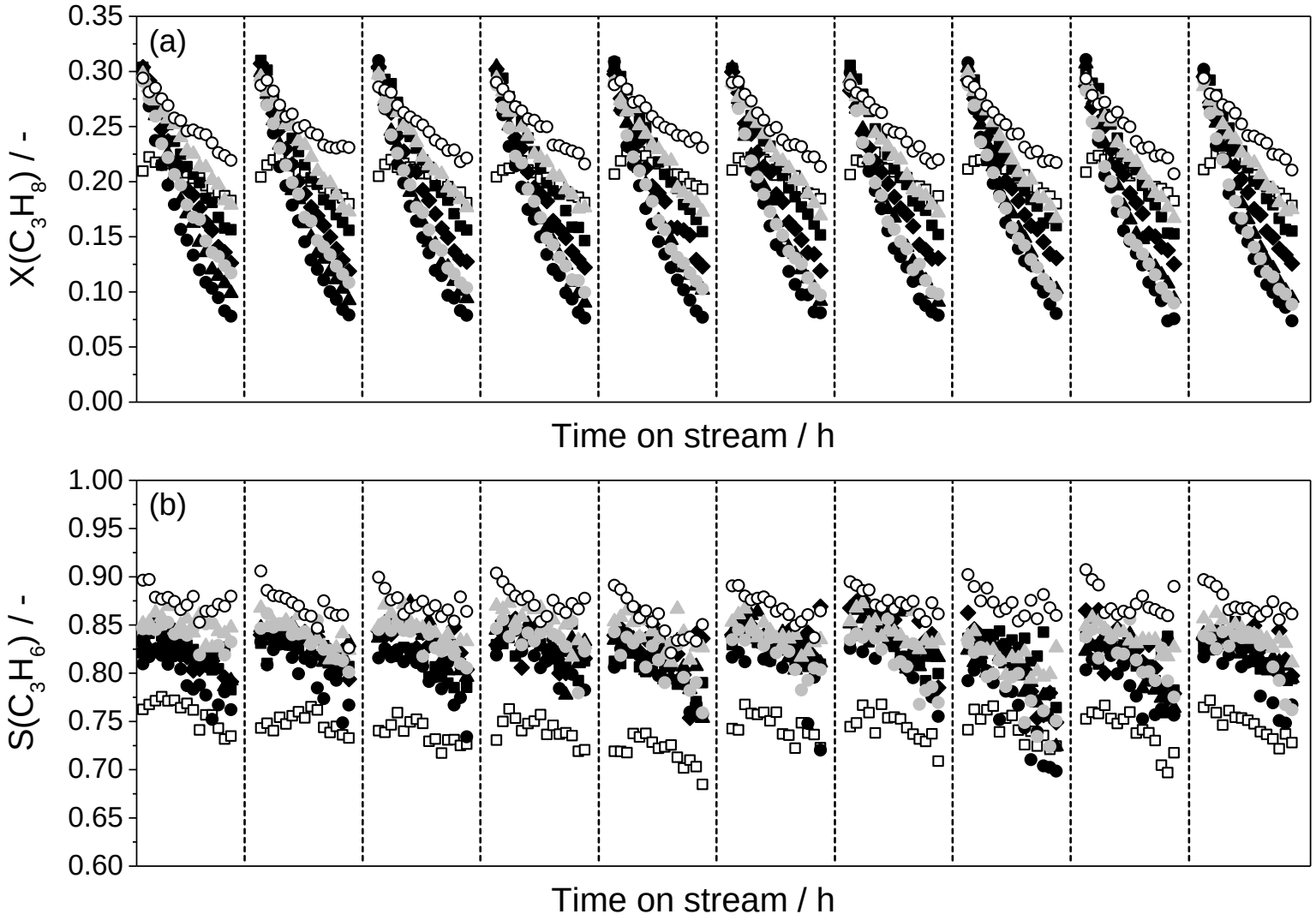

Figure A-13. Temporal change of (a) propane conversion and (b) propene selectivity for □ ZrO_2, ■ $Zr_{99.5}Cr_{0.5}O_x$, ♦ $Zr_{98}Cr_2O_x$, ▲ $Zr_{95}Cr_5O_x$, ● $Zr_{90}Cr_{10}O_x$, ▲ $0.5Cr_2O_3/LaZrO_x$, ● $3.2Cr_2O_3/LaZrO_x$, and ○ K-CrO_x/Al_2O_3 obtained in each catalytic cycle from a series of 10 PDH/regeneration cycles performed at 550°C.

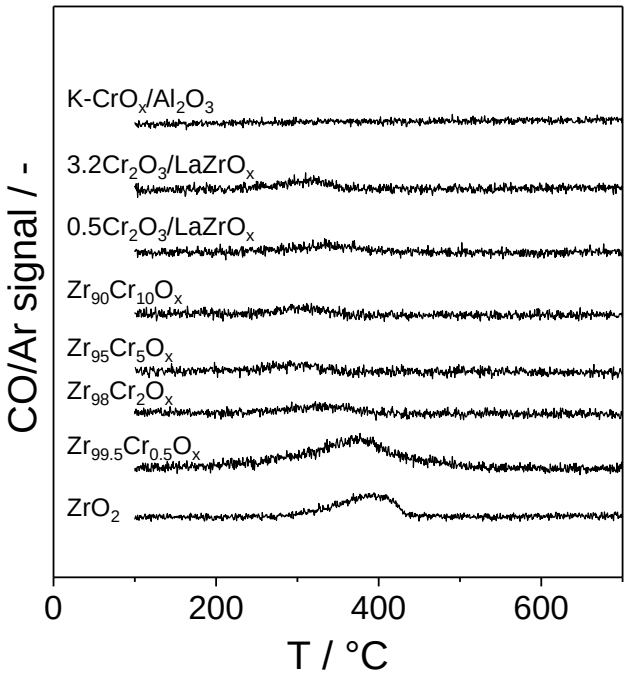

Figure A-14. TPO profiles of the spent ZrO_2 and Cr-containing catalysts: dependence of CO/Ar signal on temperature.

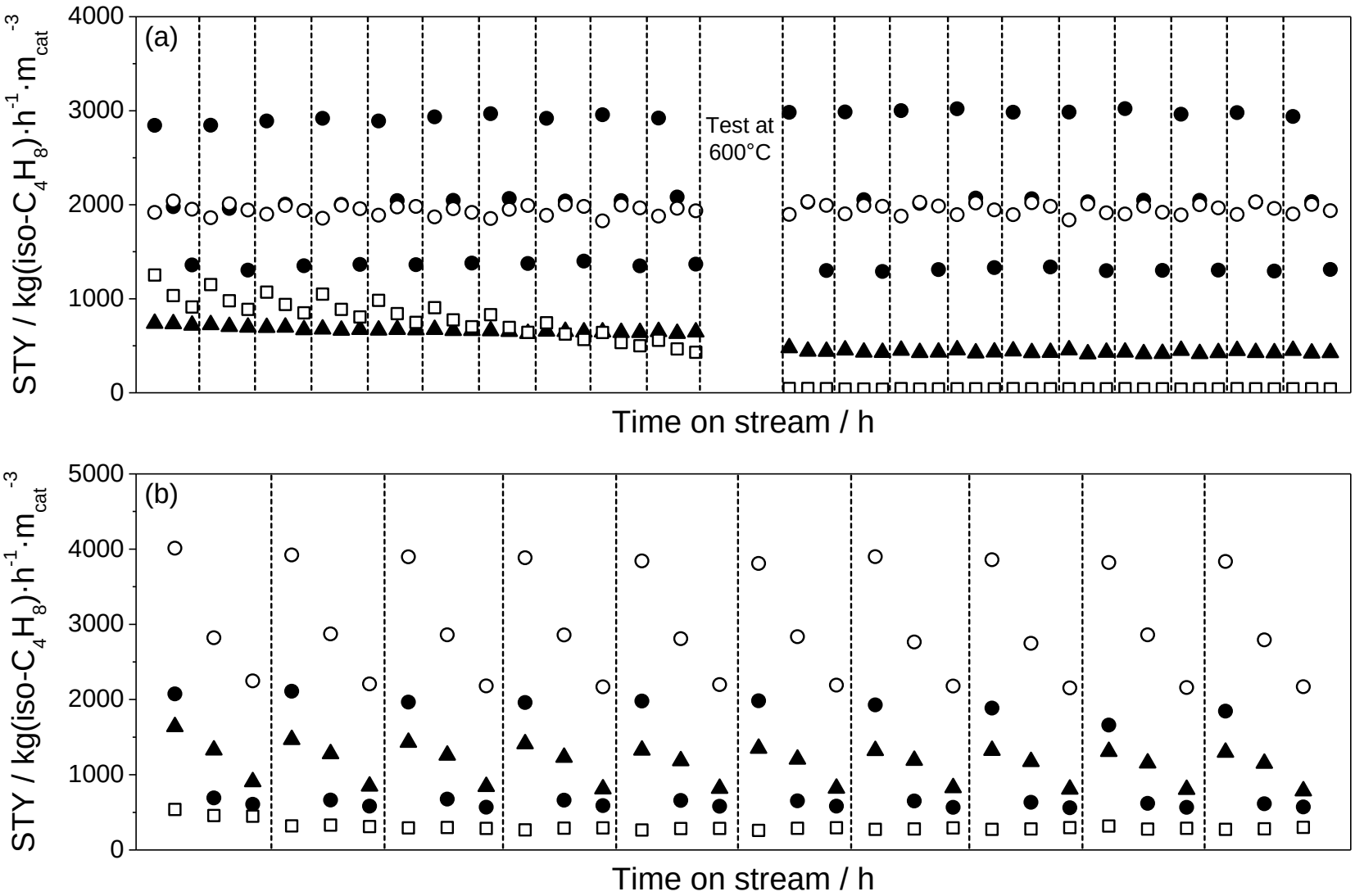

Figure A-15. Temporal change of STY of isobutylene for each DH stage at (a) 550°C and (b) 600°C for ▲ $YZrO_x$, ● $Zr_{90}Cr_{10}O_x$, ○ K-CrO_x/Al_2O_3, and □ Pt-Sn/Al_2O_3. Each DH stage continued for 27 min.

Liste der Publikationen

1. T.P. Otroshchenko, V.A. Kondratenko, U. Rodemerck, D. Linke, E.V. Kondratenko, *Non-oxidative dehydrogenation of propane, n-butane, and isobutane over bulk ZrO2-based catalysts: effect of dopant on the active site and pathways of product formation*, Catal. Sci. Tech. **2017**.
   DOI: 10.1039/C7CY01583F.

2. T. Otroshchenko, V.A. Kondratenko, U. Rodemerck, D. Linke, E.V. Kondratenko, *ZrO_2-based unconventional catalysts for non-oxidative propane dehydrogenation: Factors determining catalytic activity*, J. Catal. **2017**, 348, 282–290.
   DOI: 10.1016/j.jcat.2017.02.016.

3. U. Rodemerck, E.V. Kondratenko, T. Otroshchenko, D. Linke, *Unexpectedly high activity of bare alumina for non-oxidative isobutane dehydrogenation*, Chem. Commun., **2016**, 52, 12222-12225.
   DOI: 10.1039/C6CC06442F.

4. T. Otroshchenko, J. Radnik, M. Schneider, U. Rodemerck, D. Linke, E.V. Kondratenko, *Bulk binary ZrO_2-based oxides as highly active alternative-type catalysts for non-oxidative isobutane dehydrogenation*, Chem. Commun., **2016**, 52, 8164-8167.
   DOI: 10.1039/C6CC02813F.

5. E. Kondratenko, U. Rodemerck, T. Otroshchenko, S. Sokolov, M. Stoyanova, D. Linke, Patent 102015112612.5, Verfahren zur Herstellung von Olefinen sowie Katalysator, Germany, **2015**.

6. T. Otroshchenko, S. Sokolov, M. Stoyanova, V.A. Kondratenko, U. Rodemerck, D. Linke, E. V. Kondratenko, *ZrO_2-Based Alternatives to Conventional Propane Dehydrogenation Catalysts: Active Sites, Design, and Performance*, Angew. Chem., Int. Ed. **2015**, 54, 15880-15883.
   DOI: 10.1002/anie.201508731.

7. T. Otroshchenko, A. Turakulova, E. Lokteva, E. Golubina, V. Lunin, *Catalysts based on PdO_ZrO_2 in the hydrodechlorination reaction of chlorobenzene*, Russ. J. Phys. Chem. A. **2015**, 89, 1163–1172.
   DOI: 10.1134/S0036024415070262.

8. T. Otroshchenko, A. Turakulova, V. Voblikova, L. Sabitova, S. Kutsev, V. Lunin, *NiO and ZrO_2-Based Catalysts in the Reaction of Complete Methane Oxidation*, Russ. J. Phys. Chem. A. **2013**, 87, 1804-1808.
   DOI: 10.1134/S0036024413110162.

Wissenschaftliche Beiträge

Vorträge

1. T. Otroshchenko, U. Rodemerck, D. Linke, E.V. Kondratenko, *Efficient bulk binary $ZrCrO_x$ catalysts with low Cr content for non-oxidative dehydrogenation of low alkanes: synergy effect of Cr and Zr_{cus} sites*, 13th European Congress on Catalysis – EuropaCat-2017, Florence, Italy, 27. – 31. August **2017**.

2. T. Otroshchenko, M. Stoyanova, U. Rodemerck, S. Sokolov, D. Linke, E.V. Kondratenko, *Design and performance of alternative-type ZrO_2-based catalysts for non-oxidative dehydrogenation of light alkanes*, 11th Natural Gas Conversion Symposium, Tromsø, Norway, 6. – 9. June **2016**.

3. T. Otroshchenko, M. Stoyanova, U. Rodemerck, S. Sokolov, D. Linke, E.V. Kondratenko, *Non-oxidative propane dehydrogenation over novel ZrO_2-based catalysts: effect of dopant and reduction pre-treatment*, 49. Jahrestreffen Deutscher Katalytiker, Weimar, Germany, 16. – 18. March **2016**.

4. T. Otroshchenko, M. Stoyanova, U. Rodemerck, S. Sokolov, D. Linke, E.V. Kondratenko, *Activity control of supported catalysts with tailored Ru nanoparticles for non-oxidative propane dehydrogenation*, 12th European Congress on Catalysis – EuropaCat-2015, Kazan, Russia, 1. – 4. September **2015**.

Poster

1. T. Otroshchenko, U. Rodemerck, J. Radnik, M. Schneider, D. Linke, E.V. Kondratenko, *Highly active binary ZrO_2-CrO_x catalysts for non-oxidative propane dehydrogenation*, 50. Jahrestreffen Deutscher Katalytiker, Weimar, Germany, 15. – 17. March **2017**.

2. T. Otroshchenko, M. Stoyanova, U. Karimova, U. Rodemerck, S. Sokolov, D. Linke, E.V. Kondratenko, *Effect of support and metal on propane dehydrogenation over catalysts with tailored Pt, Rh and Ru nanoparticles*, 48. Jahrestreffen Deutscher Katalytiker, Weimar, Germany, 11. – 13. March **2015**.

3. T. Otroshchenko, A. Turakulova, E. Golubina, E. Lokteva, V. Lunin, *Biomorphic binary oxide of palladium and zirconium as catalyst precursor for hydrodechlorination reaction*, International Conference on Materials and Technologies for Green Chemistry, Tallinn, Estonia, 5. – 9. September **2011**.

Curriculum vitae

Lebenslauf

Tatiana Petrovna Otroshchenko

Geboren am 9. Juni 1990 in Nikolaew

russische Staatsangehörigkeit

Promotion

11/2014 – 01/2017	Doktorarbeit am Leibniz-Institut für Katalyse e.V. an der Universität Rostock Betreuer: Herr PD Dr. habil. E.V. Kondratenko Titel der Arbeit: *„Design, active sites and performance of unconventional ZrO_2-based catalysts for non-oxidative dehydrogenation of C_3 – C_4 alkanes“*

Studium

09/2007 – 06/2012	Chemiestudium an der Staatlichen Lomonosov Universität Moskau, Diplom mit Auszeichnung Titel der Arbeit: *„Property of catalysts based on Pd-Zr-O and Ni-Zr-O binary oxides in hydrodechlorination of chlorobenzene and methane oxidation“*

Schule

2007	Erlangung der Allgemeinen Hochschulreife in Elizowo, Russland Ausgezeichnet mit der Goldmedaille „Für besondere Lernerfolge“

Kurse

2017	Deutsch als Fremdsprache – Deutsch B2.1, Universität Rostock
2017	E-Kurs „Projektmanagement“, eNANO
2016	E-Kurse „Risikomanagement“ und „Business Process Management”, eNANO

Auszeichnungen und weitere Tätigkeiten

Dezember 2015	Sieg im Wettbewerb „Eureka! Konzept“ im Bereich „Oil & Gas“
2015 – 2016	Stipendium des Präsidenten der Russischen Föderation für das Studium im Ausland
2014 – 2015	Forschungsstipendium des DAAD

Die Teilnahme an Schulwettbewerben

2006 – 2007 Gesamtrussische Schüler-Olympiade in Chemie:
- Mitglied der letzten, fünften Etappe (Ufa, Russland)
- Diplom des 3. Grades in der Federal District (vierte Etappe)(Blagoweschtschensk, Fernost Federal District)
- 1. Platz in der Region Kamtschatka (dritte Etappe)
- 1. Platz in der Gemeinde Elizowo (zweite Etappe)

Diplom des 2. Grades in der Internationalen Mathematik-Olympiade „Third Millennium“

1. Platz in der Gemeinde Elizowo (zweite Etappe) der Gesamtrussischen Schüler-Olympiade in Mathematik

1. Platz in der Gemeinde Elizowo (zweite Etappe) der Gesamtrussischen Schüler-Olympiade in Physik

2005 – 2006 Gesamtrussische Schüler-Olympiade in Chemie:
- Mitglied der Federal District (vierte Etappe) (Yakutsk, Fernost Federal District)
- 1. Platz in der Region Kamtschatka (dritte Etappe)
- 1. Platz in der Gemeinde Elizowo(zweite Etappe)

1. Platz in der Gemeinde Elizowo (zweite Etappe) der Gesamtrussischen Schüler-Olympiade in Mathematik

1. Platz in der Gemeinde Elizowo (zweite Etappe) der Gesamtrussischen Schüler-Olympiade in Physik

3. Platz in der Gemeinde Elizowo (zweite Etappe) der Gesamtrussischen Schüler-Olympiade in Biologie

3. Platz in der Gemeinde Elizowo (zweite Etappe) der Gesamtrussischen Schüler-Olympiade in Russisch

2004 – 2005 3. Platz in der Gemeinde Elizowo (zweite Etappe) der Gesamtrussischen Schüler-Olympiade in Chemie

Sport

2009 – 2014 Rennen über 10 km:
- „Green Marathon“, Veranstalter – Sberbank (Moskau)
- „We run Moscow“, Veranstalter – Nike (Moskau)
- „Semyon Rzhischins Gedächtnislauf“ (Lobnya)

Teilnahme an der Sommer Polyathlon-Meisterschaft der Staatlichen Moskauer Universität für das Team der chemischen Fakultät

Teilnahme an der Leichtathletik-Meisterschaft der Staatlichen Moskauer Universität